TRANSPORT PHENOMENA IN DRINKING WATER SYSTEMS

by

Pedro Romero-Gomez

A Dissertation Submitted to the Faculty of the

DEPARTMENT OF AGRICULTURAL AND BIOSYSTEMS ENGINEERING

In Partial Fulfillment of the Requirements
For the Degree of

DOCTOR OF PHILOSOPHY

In the Graduate College

THE UNIVERSITY OF ARIZONA

2010

THE UNIVERSITY OF ARIZONA
GRADUATE COLLEGE

As members of the Dissertation Committee, we certify that we have read the dissertation prepared by Pedro Romero-Gomez

entitled TRANSPORT PHENOMENA IN DRINKING WATER SYSTEMS

and recommend that it be accepted as fulfilling the dissertation requirement for the Degree of Doctor of Philosophy

_____ Date: 12/16/2009
Dr. Christopher Y. Choi

_____ Date: 12/16/2009
Dr. Mark R. Riley

_____ Date: 12/16/2009
Dr. Murat Kacira

_____ Date: 12/16/2009
Dr. Ian L. Pepper

_____ Date: 12/16/2009
Dr. Kevin E. Lansey

Final approval and acceptance of this dissertation is contingent upon the candidate's submission of the final copies of the dissertation to the Graduate College.

I hereby certify that I have read this dissertation prepared under my direction and recommend that it be accepted as fulfilling the dissertation requirement.

_____ Date: 12/16/2009
Dissertation Director: Dr. Christopher Y. Choi

STATEMENT BY AUTHOR

This dissertation has been submitted in partial fulfillment of requirements for an advanced degree at the University of Arizona and is deposited in the University Library to be made available to borrowers under rules of the Library.

Brief quotations from this dissertation are allowable without special permission, provided that accurate acknowledgment of source is made. Requests for permission for extended quotation from or reproduction of this manuscript in whole or in part may be granted by the head of the major department or the Dean of the Graduate College when in his or her judgment the proposed use of the material is in the interests of scholarship. In all other instances, however, permission must be obtained from the author.

SIGNED: Pedro Romero-Gomez

ACKNOWLEDGMENTS

It is usually said that there are two kinds of people: those who let things happen and those who make things happen. I understand that the tremendous toils of my dear advisor and *jefe*, Dr. Christopher Y. Choi, on my education were all intended to take my person from the former kind to the latter kind. Only time will tell how much (or how little) his aspirations were fulfilled, but meanwhile I will do likewise whenever I have the chance to positively influence somebody else's life.

I am indebted to my committee members for their valuable advices throughout my PhD studies and for the extensive revisions on my dissertation document: Dr. Mark Riley, Dr. Murat Kacira, Dr. Kevin Lansey and Dr. Ian Pepper.

I want to acknowledge several researchers from whom I received significant feedback to improve the quality of the research work: Dr. Cliff Ho from Sandia National Labs, as well as Dr. Buchberger and Dr. Li from the University of Cincinnati.

My lab colleagues were always prompted and willing to collaborate in such a way that they turned this learning process into an exciting experience: Ryan Austin, Jerry Shen, Fernando Rojano, Alex Andrade, Inhong Song, Ryan Sinclair, Levi Johnson, Gretchen Hawkins, Kyana Young, Malorie Teich, and Mario Mondaca. I am sure you would find tiny little pieces of your efforts throughout this work.

I want to acknowledge my parents (Carmen *y* Pascual) and my siblings (Caro, Laura, Gera, Nico and Sergio) for always giving me so much encouragement and inspiration to achieve my goals, personal and academic. I know my occupations have cost a lot of time away from you and your little ones, but soon I will be back to make up for it.

DEDICATION

Natürlich für Claudia. Nur Gott weiß, wie sehr ich dich liebe.

Y también para David, que me cuenta sus historias aun cuando no las entienda.

TABLE OF CONTENTS

ABSTRACT

The current computer models used for simulating water quality in potable water distribution systems assume perfect mixing at pipe junctions and non-dispersive solute transport in pipe flows. To improve the prediction accuracy, the present study examines and expands these modeling assumptions using transport phenomena analyses. Whereas the level of solute mixing at a cross-type junction is evaluated numerically via Computational Fluid Dynamics (CFD), the axial transport in laminar flows is investigated with both CFD simulations and corresponding experimental runs in a single pipe. The findings show that solute mixing at junctions is rather incomplete owing to the limited spatio-temporal interaction that occurs between incoming flows with different qualities. Incomplete mixing shifts the expected propagation patterns of a chemical or microbial constituent from widely-spread to narrowly-concentrated over the service area. On the other hand, solute dispersion is found to prevail over advective transport in laminar pipe flows. Thus, this work develops axial dispersion rates through parameter optimization techniques. By accounting for axial dispersive effects, the patterns of solute delivery shifted from high concentrations over short time periods to lower doses at prolonged exposure times. In addition, the present study integrates the incomplete mixing model into the optimal placement of water quality monitoring stations aimed at detecting contaminant intrusions.

Keywords: drinking water, model, quality, axial dispersion, mixing, sensor location.

1. INTRODUCTION

1.1 Hydraulic and water quality modeling engines

The mission of municipal water utilities is to deliver a sufficient amount of safe potable water to all the served population. To accomplish this, utility administrators use software tools designed to manage large-scale distribution systems with multiple components, complex geometries and transient conditions. Such tools must be computationally efficient and, at the same time, sufficiently accurate and reliable to yield rigorous outcomes that can be used to support technical decision-making that concerns the needs of water utilities. For instance, water security decisions are related to the deployment of early warning monitoring systems and to the assessment of the health risks associated with potential contaminations. The primary engines of these computational packages are mathematical models that describe the underlying transport phenomena of water and its constituents within the piping networks. As a general rule, a tool of this kind is classified as either a hydraulic model or as a water quality model. A hydraulic model represents some or all the pipes, tanks, valves, pumps and other physical components in a system, as well as the operational controls. A water quality model describes disinfectant and/or microbial transport, tracer paths and water age by using information generated by hydraulic model simulations (e.g., flow rates, flow paths and velocities) and mass transfer relations (e.g. mixing, growth and decay rates).

The initial formulations for steady-state water quality modeling were proposed in the early 1980's by Don Wood at the University of Kentucky, and other researchers at the

U.S. Environmental Protection Agency (U.S. EPA) in Cincinnati, OH (Walski, 2003). This collaboration led to a model engine called KYPipe© (KYPipe Inc., Lexington, KY), which has since been further developed to operate in conjunction with a Graphical User Interface (GUI) that facilitates its use. Transient water quality analysis was introduced in 1986 in order to expand the application of modeling engines onto real-world distribution systems (AWWA, 1986a). In addition, a body of experience and knowledge associated to this subject accumulated during the course of various research meetings held in the late 1980s and early 1990s (AWWA, 1986a, 1986b, 1989, and 1991.) In 1993, the release of EPANET, a computer package developed by Lewis Rossman at the U.S. EPA, signified a major advancement in water quality modeling because it provided both an engine adaptable for linkage with commercial-grade software and a powerful research tool (Rossman, 2000).

Most water quality (WQ) models have been developed on the basis of two convenient but potentially erroneous simplifications associated with solute transport calculations. First, it is assumed that solutes mix with the water completely and instantaneously at the pipe junctions (the complete mixing assumption). Second, the longitudinal spread of solutes as they move along the pipe is ignored, and advective transport is assumed to prevail (the non-dispersive transport assumption).

This study primarily investigates the validity of the two aforementioned assumptions. Knowing beforehand of their limited applicability, this study also examines the appropriate corrections and expansions via transport phenomena analyses in order to enhance the overall capabilities of current WQ models, such as EPANET. Additionally,

this study demonstrates that an improved WQ model can provide reliable input data for methodologies applied to select the best locations for WQ monitoring stations over the piping network.

1.2 Review of the literature concerning water quality models and their outcomes

Water quality modeling of municipal distribution systems first became a major concern for utilities when the U.S. EPA promulgated rules specifying that the quality standards must be met at the user's tap rather than at the treatment plant (U.S. EPA, 2004). This spurred researchers to investigate the multiple mechanisms of transport that solutes undergo as water moves from the source to the user. Ostfeld (2005) provided a detailed review of water quality modeling in distribution systems, with emphasis on simulation, optimization, chlorine control, monitoring and water security. Modelers always face the intrinsic tradeoff between model accuracy and the simulation efficiency. Whereas various research efforts have made contributions to the field of computationally economical modeling (Clark et al. 1988; Boulos et al. 1992; Boulos and Altman, 1993; Rossman et al. 1993; Clark et al. 1994; Rossman and Boulos, 1996; Boccelli et al., 1998; Tzatchkov et al. 2002; Chung et al. 2007; Basha and Malaeb, 2007, to name a few), the present study applies transport phenomena concepts to increase the accuracy of WQ predictions by re-examining and improving the current modeling assumptions pertaining to mixing at junctions and solute transport in pipe flows.

Early hydraulic modeling tools limited the number of pipes and components that could be represented due to computer power constraints. Because of this, flows tended to

be aggregated in pipes of large diameter. Such large flows led to prevailing turbulent conditions predicted by hydraulic simulations. The turbulence at pipe junctions was assumed to be sufficient to produce a perfect and instantaneous solute mixing; i.e. two incoming and adjacent flows with different qualities at a cross junction yield outflows with the same quality. Fowler and Jones (1991) first suggested that complete mixing at junctions could potentially fail to reproduce the observed behavior in actual systems, and they also pointed out the need for further studies in this area. More than a decade passed before other researchers performed preliminary modeling and experimental runs of solute mixing at cross and double-T junctions with two adjacent inflows and two outflows (Van Bloemen Waanders et al., 2005; Ho et al., 2006; and Romero-Gomez et al., 2006.) The results showed that complete mixing did not occur at junctions in most cases, such as equal incoming flow rates with different qualities. Thus, a systematic evaluation upon various flow configurations was suggested.

In an analogous example of modeling over-simplification, dissolved solutes traveling in pipes are assumed to undergo both advective and reactive transport. The intermixing of substances among moving and adjacent water parcels is negligible owing to turbulent operating conditions that supposedly prevail in pressurized systems (Rossman, 2000). In the simplest example to illustrate this assumption, a non-reactive tracer spike injected into a pipe subject to a constant flow is predicted to travel for miles without changing its shape at all. Once again, this premise sufficed for highly skeletonized hydraulic models that were intended to represent pipes of large sizes and through which aggregated (and thus high) volumes of water travel. However, water

quality predictions of higher accuracy can be achieved by using a finer spatio-temporal system's representation, which in turn requires hydraulic models that represent all the pipes and components. In view of this refinement, Buchberger et al. (2003) determined that low speed flows dominate in the suburban and peripheral zones of service areas, and he reported that a large percentage of pipe lines convey intermittent/stagnant flows that are frequently laminar in nature.

Because laminar conditions induce a strong longitudinal spread of solutes, several research studies have centered on expanding the present advection-reaction model into an advection-dispersion-reaction transport equation in conjunction with expedient schemes for its numerical solution (Islam and Chaudry, 1998; Tzatchkov et al., 2002; Basha and Malaeb, 2007). Another collection of studies relevant to this field is concerned with the axial dispersion coefficients required in the dispersion term (Taylor, 1953; Gill and Sankarasubramanian, 1970; Lee, 2004; Li, 2006); however, these studies showed a large bias with respect to experimental observations (Romero-Gomez et al., 2008) and numerical simulations using CFD (Romero-Gomez et al., 2009). The present work examines solute transport phenomena in pipe flows, develops dispersion rates for laminar flows, and corroborates the developed modeling relations through experiments.

At present, most water utilities routinely use hydraulic models to analyze fire flow and to design, plan and implement operational strategies. In contrast, using water quality models to improve water security is a relatively new application, although more and more utilities are adopting it in recent years. Such tasks as the vulnerability assessment, the design of monitoring networks, the contaminant source identification, the real-time

emergency response and the remediation planning, all once considered exploratory tasks, are now thought of as urgent needs. Grayman (2006) summarized the recent research and developments that benefited from the ability of WQ models to predict the behavior of contaminants through the system.

Documented contamination events occurring within potable water infrastructures have demonstrated the adverse effects such incidents can have on the public health of large communities (Clark et al., 1996; MacKenzie et al., 1994). In response, one active area of research now seeks to develop warning systems that can detect contamination events as soon after they occur as is practically possible. The major fronts of this effort aims at (i) developing hardware that can quickly detect indicator parameters of chemical and biological agents (e.g. pH, temperature, turbidity and indicator organisms) or the agent itself, (ii) developing software solutions that can appropriately interpret sensor data, and (iii) developing methodologies that can most effectively lay out monitoring stations at representative locations throughout the entire piping network. Up to now, there has been no established measure of the "representativeness" of a monitoring location, although ongoing research has produced technical guidelines that help determine feasible sensor placement.

Lee and Deininger (1992) designed an optimal set of monitoring stations that detected any contamination event (100 % coverage) when all network nodes are equally likely to be the intrusion point. On the other hand, Kumar et al. (1997) defined a number of stations and maximized the coverage via a hydraulic analysis of the water network. Kessler et al. (1998) introduced a methodology for detecting accidental contaminations as

a function of the volume of contaminated water that was consumed prior to detection. Because contaminants in drinking water have a Minimum Hazard Level (MHL) that serves as a threshold for safe consumption, Ostfeld et al. (2004) developed a methodology for designing an early warning detection system as a function of the MHL when solutes dilute as they move through the water network. Ostfeld and Salomons (2004) introduced a methodology for optimal sensor placement by considering both the detection likelihood and the detection redundancy (i.e., an intrusion may be detected by more than one sensor) as a function of the number of stations to be installed. A methodology proposed by Berry et al. (2005) aimed at minimizing the expected percentage of the population that would be placed at risk. Preis and Ostfeld (2008) used Non-Dominated Genetic Algorithms to incorporate multiple objectives (detection likelihood, redundancy, and time) and thereby to optimize sensor placements. All of the aforementioned advances were developed without taking into account the recent improvements in WQ modeling accuracy. The present work seeks to merge both fields in order to improve water security and better safeguard the consumers and the infrastructure.

1.3 Research Objectives

The present work undertakes a quantitative investigation on the role of solute transport phenomena in water infrastructures. The overall objective is to produce appropriate redefinitions of, and expansions to, the conventional modeling assumptions associated with solute mixing at junctions and axial transport in pipe flows in order to

predict water quality behavior of potable water distribution systems with higher accuracy. The specific objectives are as follows:

1) Determine the level of solute mixing at cross junctions as a function of the flow configurations (Appendix A)
2) Obtain the axial dispersion rates of solutes in laminar pipe flows and to experimentally validate the developed relations (Appendix B)
3) Assess the impact of solute mixing at junctions on the size and layout of contaminant early warning systems over drinking water distribution systems (Appendix C).

2. PRESENT STUDY

2.1 Overall summary

The present work utilized computational fluid dynamics tools to quantify the level of mixing at junctions and the dispersion of solute in pipe flows (Appendix A and B, respectively). Computational Fluid Dynamics (CFD) consists of numerically solving the conservation equations that describe the velocity field and the solute distribution over a prescribed geometry. Among other relevant factors, two dimensionless variables are central in characterizing the transport phenomena analyzed in both appendices A and B: (i) the Reynolds number (Re) that determines the ratio of inertial forces to viscous forces and (ii) the Schmidt number (Sc) that gives a ratio of momentum (or eddy) diffusivity to mass (or eddy mass) diffusivity.

$$Re = \frac{du_m}{\upsilon}; \quad Sc = \frac{\upsilon}{D_{AB}}$$

Where d is the pipe diameter, u_m is the mean flow velocity, υ is the fluid kinematic viscosity and D_{AB} is the species molecular diffusivity.

The analysis of solute mixing focuses on a cross-type single junction with four pipe legs (Appendix A). All the examined cases involved two adjacent inflows and two outflows. One inflow provided clean water while the other contained a tracer. Because the flow regime was turbulent (Re > 10,000), the numerical study also determined the turbulent Schmidt number (Sc_t) which turned out to be a critical modeling parameter for representing solute transport between the two incoming jets. The outflow concentrations ranged from a dimensionless value of zero that corresponded to the clean water

concentration, to a value of one that corresponded to the tracer water concentration. If complete mixing were assumed, both outflow concentrations would be the same; however, the study revealed that tracer concentrations were unequal at the outlet pipe legs as a result of the limited spatio-temporal interaction occurring between the incoming flows. Thus, solute mixing was redefined as incomplete and dependent on the combinations of flow rates. Associated research works corroborated the incomplete mixing results via experiments at single junctions (Austin et al., 2008) and over a laboratory-scale piping network (Song et al., 2009).

The aforementioned outcomes were integrated into the layout of water quality sensors aimed at detecting contaminant intrusions within potable water distribution systems (Appendix C). The sensor network design involved two major steps. First, the incomplete solute mixing at multiple types of junctions was incorporated into EPANET as part of a collaborative research effort (Choi et al., 2008). Second, the methodology proposed by Ostfeld et al. (2004) was used to provide the framework for optimal sensor placement in conjunction with the improved water quality model. Such methodology first involved the construction of a pollution matrix which summarizes the WQ outcomes given a battery of contamination scenarios. Next, an optimization algorithm was run on the pollution matrix in order to determine the number and location of monitoring stations needed for full detection coverage. The pollution matrix was constructed by means of a series of simulations using both the conventional and improved EPANET versions. In this way, the study aimed at quantifying the impact of the incomplete mixing model on the optimal locations of monitoring stations. The results indicated that solute mixing

influenced, from a greater to a lesser extent, the sensor network design in (i) the number of monitoring units needed for full detection, (ii) the layout of sensors over the water system, and (iii) the detection domain of the monitoring stations, correspondingly.

The examination of solute transport in laminar pipe flows was conducted using CFD tools and corresponding experimental runs (Appendix B). The first step in this section was to evaluate the occurrence of laminar flows over an actual potable water system. Next, a series of experimental runs conducted with a tracer injection in constant flows through a single pipe provided input data for the CFD simulations. The verified CFD results became the baseline for developing axial dispersion rates as a function of dimensionless travel time. This relation was further verified by another set of laboratory experiments. The outcomes demonstrated an improvement in WQ prediction accuracy when the axial dispersion term and coefficients were integrated into the conventional solute transport model in pipe flows.

2.2 Overall conclusions and recommendations

Because potable water distribution systems are typically large, models must be simplified in order to expedite the evaluation of water quality behavior over the entire service area. However, this study demonstrates that the current assumptions used for solute mixing at junctions and for axial solute migration in laminar pipe flows, overlook detailed transport phenomena that become quantitatively significant when the system's components in hydraulic models are thoroughly represented. The modeling and experimental findings substantiate the improvements made in modeling outcomes upon

considering both the incomplete mixing at junctions and the bi-directional dispersive transport in pipe flows. The use of the re-defined assumptions renders water quality solvers capable of satisfying the future modeling demands related to water security, e.g. sensor network designs. Sensor network designs certainly become more reliable when input data are supplied by a water quality model that can more accurately represent the transport phenomena that solutes undergo as they travel through the piping network.

The results of this study should lead to more reliable and more accurate predictions of the spatial and temporal propagation of both beneficial and hazardous agents in the public water supply. The expanded assumptions result in changes in the expected concentration patterns and exposure times, with respect to the conventional assumptions. Whereas the incomplete mixing at junctions tends to concentrate substances over a narrow zone rather than to spread them over a large area, the axial transport in pipe flows tends to prolong the delivery of lower doses to the exposed population. This immediately calls for a quantitative reassessment of the water utility's vulnerability and of the health risks associated with chemical and microbial contamination events.

Regarding some research recommendations, the assumptions examined in this study must be fully embedded into the commercial software packages currently used for quality analysis of potable water. It is essential to extend the axial transport research to include transitional and turbulent regimes in order to attain a full description of dispersive effects over all the flow conditions that are likely to be found within a piping network. The expanded capabilities should often be ascertained via field verifications in order to confirm the usability of such enhanced water quality models.

REFERENCES

Austin, R. G., van Bloemen Waanders, B., McKenna, S., and Choi, C. Y. (2008). "Mixing at cross junctions in water distribution systems. II: Experimental study." *J. Water Resour. Plann. Manage.*, 134(3), 295-302.

AWWA, (1986a), *Proc., Seminar on Water Quality Concerns in the Distribution System*, Denver, CO.

AWWA, (1986b), *Proc., Water Quality Technology Conference*, Portland, OR.

AWWA, (1989), *Proc., Computers and Automation in the Water Industry*, Reno, NV.

AWWA, (1991), *Proc., Water Quality Modeling in Distribution Systems Conference*, Cincinnati, OH.

Basha, H.A. and Malaeb, L.N. (2007). "Eularian-Lagrangian method for constituent transport in water distribution networks." *J. Hydraul. Eng.*, 133(10), 1155-1166.

Berry, J.W., Fleischer, L., Hart, W.E., Phillips, C.A., and Watson, J.P. (2005). "Sensor placement in municipal water networks." *J. Water Resour. Plann. Manage.*, 131(3), 237-243.

Boccelli, D.L., Tryby, M.E., Uber, J.G., Rossman, L.A., Zierolf, M.L., Polycarpou, M.M. (1998). "Optimal scheduling of booster disinfection in water distribution systems." *J. Water Resour. Plann. Manage.*, 124(2), 99-111.

Boulos, P.F., and Altman, T. (1993). "Explicit calculation of water quality parameters in pipe distribution systems." *Civ. Eng. Syst.,* 10, 187-206.

Boulos, P.F., Altman, T., and Sadhal K.S. (1992). "Computer modeling of water quality in large multiple-source networks." *Appl. Math. Modelling*, 16(8), 439-445.

Buchberger, S.G., Carter, J.T., Lee, Y., and Schade, T.G. (2003). "*Random demands, travel times and water quality in deadends*." AWWA Research Foundation, Denver, CO.

Choi, C.Y., Shen, J. Y., Austin, R. G. (2008). "Development of a comprehensive solute mixing model (AZRED) for double-tee, cross, and wye junctions." *Proc. 10th Water Distribution System Analysis Symp.*, Kruger National Park, South Africa.

Chung, G., Lansey K.E., and Boulos, P.F. (2007). "Steady-state water quality analysis for pipe network systems." *J. Environ. Eng.*, 133(7), 777-782.

Clark, R.M., Geldreich, E.E., Fox, K.R., Rice, E.W., Johnson, C.H., Goodrich, J.A., Barnick, J.A., Abdesaken, F., Hill, J.E., and Angulo, F.J. (1996). "A waterborne *Salmonella typhimurium* outbreak in Gideon, Missouri: results from a field investigation." *Int. J. Environ. Health Res.*, 6, 187-193.

Clark, R.M., Grayman, W., Goodrich, J.A., Deininger R.A., and Skov, K. (1994). "Measuring and modeling chlorine propagation in water distribution systems." *J. Water Resour. Plann. Manage.*, 120(6), 871-887.

Clark, R.M., Grayman, W., and Males, R.M. (1988). "Contaminant propagation in distribution systems." *J. Environ. Eng.,* 114(4), 929-943.

Fowler, A. G., and Jones, P. (1991). "Simulation of water quality in water distribution systems." *Proc. Water Quality Modeling in Distribution Systems*, AwwaRF/EPA, Cincinnati, OH.

Gill, W. N. and Sankarasubramanian, R. (1970). "Exact analysis of unsteady convective diffusion." *Proc. R. Soc. London, Ser. A*, 316, 341-350.

Grayman, W.M. (2006). "Use of distribution system water quality models in support of water security" in *Security of water supply systems: from source to tap*, Springer, Netherlands, p. 39-50.

Ho, C. K., Orear, L., Wright, J. L., and McKenna, S. A. (2006). "Contaminant mixing at pipe joints: Comparison between laboratory flow experiments and computational fluid dynamics models." *Proc. 8th Annual Water Distribution System Analysis Symp.*, Cincinnati, OH.

Islam, M.K. and Chaudhry, M.H. (1998). "Modeling of constituent transport in unsteady flows in pipe networks." *J. Hydraul. Eng.*, 124(11), 1115-1124.

Kessler, A., Ostfeld, A., and Sinai, G. (1998). "Detecting accidental contaminations in municipal water networks." *J. Water Resour. Plann. Manage.*, 124(4), 192-198.

Kumar, A., Kansal, M.L., and Arora, G. (1997). "Identification of monitoring stations in water distribution system." *J. Environ. Eng.*, 123(8), 746-752.

Lee, Y. (2004). Mass Dispersion in Intermittent Laminar Flow. *PhD Dissertation,* University of Cincinnati, Cincinnati, OH.

Lee, B.H. and Deininger R.A. (1992). "Optimal locations of monitoring stations in water distribution system." *J. Environ. Eng.*, 118(1), 4-16.

Li, Z. (2006). Network water quality modeling with stochastic water demands and mass dispersion. *PhD Dissertation,* University of Cincinnati, Cincinnati, OH.

MacKenzie, W., Neil, M., Hoxie, N., Proctor, M., Gradus, M., Blair, K., Peterson, D., Kazmierczak, J., Addiss, D., Fox, K., Rose, J., and Davis, J. (1994). "A massive outbreak in Milwaukee of *Cryptosporidium* infection transmitted through the public water supply." *N. Eng. J. Med.*, 331, 161-167.

Ostfeld, A. (2005). "A review of modeling water quality in distribution systems." *Urban Water J.*, 2(2), 107-114.

Ostfeld, A., Kessler, A., and Goldberg, I. (2004). "A contaminant detection system for early warning in water distribution networks." *Eng. Optim.*, 36(5), 525-538.

Ostfeld, A., and Salomons, E. (2004). "Optimal layout of early warning detection stations for water distribution systems security." *J. Water Resour. Plann. Manage.*, 130(5), 377-385.

Preis, A., and Ostfeld, A. (2008). "Multiobjective contaminant sensor network design for water distribution systems." *J. Water Resour. Plann. Manage*, 134(4), 366-377.

Romero-Gomez, P., Choi, C.Y., van Bloemen Waanders, B., and McKenna, S. A. (2006). "Transport phenomena at intersections of pressurized pipe systems." *Proc. 8th Annual Water Distribution System Analysis Symp.*, Cincinnati, OH.

Romero-Gomez, P., Li, Z., Choi, C.Y., and Buchberger, S.G. (2009). "Axial dispersion coefficients for laminar flows in water distribution systems." *World Environmental and Water Resources Congress*, Kansas City, MO.

Romero-Gomez, P., Li, Z., Choi, C. Y., Buchberger, S.G., Lansey, K.E., and Tzatchkov, V.T. (2008). "Axial dispersion in pressurized pipes under various flow conditions." *10th Annual Water Distribution Systems Analysis Symposium*, Kruger National Park, South Africa.

Rossman, L. A. (2000). EPANET users' manual, US Environmental Protection Agency (EPA), Cincinnati, OH.

Rossman, L.A., and Boulos, P.F. (1996). "Numerical methods for modeling water quality in distribution systems: a comparison." *J. Water Resour. Plann. Manage.*, 122(2), 137-146.

Rossman, L.A., Boulos, P.F., and Altman, T. (1993). "Discrete volume-element method for network water-quality models."*J. Water Resour. Plann. Manage.*, 119(5), 505-517.

Song, I., Romero-Gomez, P., and Choi, C.Y. (2009). "Experimental verification of incomplete solute mixing in a pressurized pipe network with multiple cross junctions." *J. Hydraul. Eng.*, 135(11), 1005-10011.

Taylor, G. (1953). "Dispersion of soluble matter in solvent flowing slowly through a tube." *Proc. R. Soc. London, Ser. A,* 219, 186-203.

Tzatchkov, V.G., Aldama, A.A., and Arreguin, F.I. (2002). "Advection-dispersion-reaction modeling in water distribution networks." *J. Water Resour. Plann. Manage.*, 128(5), 334-342.

U.S. EPA. (2004). "Understanding the safe drinking water act", EPA Fact Sheet, EPA 816-F-04-030. Cincinnati, OH.

van Bloemen Waanders, B., Hammond, G., Shadid, J., Collis, S., and Murray, R. (2005). "A comparison of Navier-Stokes and network models to predict chemical transport in municipal water distribution systems." *Proc., World Water and Environmental Resources Congress*, Anchorage, AK.

Walski, T.M., Chase, D.V., Savic, D.A., Grayman, W., Beckwith, S., and Koelle, E. (2003). "*Advanced water distribution modeling and management*." Haestead Press, Watertown, CT.

APPENDIX A

MIXING AT CROSS JUNCTIONS IN WATER DISTRIBUTION SYSTEMS – PART I. A NUMERICAL STUDY

Pedro Romero-Gomez[1], Clifford K. Ho[2], and Christopher Y. Choi[3]

Published in the ASCE Journal of Water Resources Planning and Management, 2008, Vol. 134, No. 3, Pages 285-294.

With Permission from ASCE

[1] Graduate Research Assistant, Department of Agricultural and Biosystems Engineering, The University of Arizona, Tucson, AZ, 85721 U.S.A. E-mail: pedromer@email.arizona.edu
[2] Research Scientist, Sandia National Laboratories, P.O. Box 5800, MS-0735, Albuquerque, NM, 87185-0735 U.S.A. E-mail: ckho@sandia.gov
[3] Professor, Agricultural and Biosystems Engineering, The University of Arizona, Tucson, AZ, 85721 U.S.A. E-mail: cchoi@arizona.edu

Abstract

The present study investigates solute mixing phenomena at various flow rates within a cross junction, which is commonly found in municipal drinking water distribution systems. Simulations using Computational Fluid Dynamics (CFD) are employed to model the solute concentrations leaving the junction when one inlet is comprised of clean water while the other inlet carries a solute at $Re > 10{,}000$. For a few exemplary cases, the resulting velocity vectors and contours of dimensionless concentration are presented to explain the detailed mixing mechanisms at the impinging interface. The turbulent Schmidt number (Sc_t), an important scaling parameter, is also evaluated. Experimental results were used to assess values of Sc_t for various flow conditions that accurately captured the detailed mixing processes within the junction. The present study clearly indicates that mixing at pipe cross junctions is far from "perfect". Incomplete mixing results from bifurcating inlet flows that reflect off one another with minimal contact time. Improving the existing water quality model based on accurate mixing data and simulations is important not only to predict concentrations of chemical species such as chlorine in water distribution systems, but also to prepare for potential intentional and accidental contamination events.

Keywords: Computational Fluid Dynamics (CFD), NaCl mixing, cross junctions, dimensionless concentration

Introduction

As water utilities evolve from having the single mission of supplying high quality water to consumers to also ensuring water security, the computer modeling tools used for network analysis will also need to evolve to better simulate transport of chemicals and biological agents. Solute mixing behavior at nodes in modeling tools will impact a wide variety of network analyses, including prediction of disinfectant residuals, optimal locations for water quality sensors, prediction models for early warning systems, numerical schemes for inverse source identification, and quantitative risk assessment. Therefore, accurate modeling of water quality has become an increasingly significant issue in managing water distribution systems.

Due to the complexity of municipal water networks, new computer modeling packages have been developed to simulate the potential hydraulic scenarios in a drinking water system. These packages are capable of performing both steady and extended-period (time-varying) simulations of pressurized pipe network systems. They are composed of two model engines: the hydraulic and the water quality models. Hydraulic models generally meet the needs for water network design through years of development, application, and validation, while water quality models have yet to prove their performance, especially in highly interconnected networks. Water quality analysis is always coupled with the outcomes from hydraulic simulations because all chemical or biological species are transported throughout the network by advection and diffusion processes. This conceptual approach is widely used for developing most software tools aimed at modeling and managing drinking water systems. Among the many assumptions made regarding water quality engine codes, Mays (2004) stated that perfect and instantaneous mixing of incoming water occurs at all intersections, such as cross and tee junctions.

Fowler and Jones (1991) first questioned the assumption that “perfect” mixing occurs at various intersections in water distribution systems. Among several other concerns about water quality modeling, the assumption of perfect mixing was regarded as a potentially significant cause of discrepancies between model predictions and actual

measurements. Even though no quantification of inaccuracies or corrections were performed, they addressed the need for further studies on this assumption and its role in overall water quality in water networks.

Van Bloemen Waanders et al. (2005) examined chemical transport in network models for pressurized flows at a cross junction. In this study, two adjacent incoming flows with the same Reynolds numbers (Re = 44,000) were mixed at a cross junction and discharged at the same Reynolds numbers. Sodium chloride was introduced as a tracer in one of the inlets while tap water entered the other inlet. Furthermore, Computational Fluid Dynamics (CFD) simulations were conducted for this flow configuration. If complete mixing were to occur, each outlet would carry 50 % of the incoming NaCl mass rate. However, both experimental and numerical tools showed that complete mixing did not occur; instead, 85 % and 15 % of the total incoming NaCl mass rate was discharged to the outlets adjacent and opposite to the inlet with the tracer, respectively. Thus, the conclusions drawn from their findings suggested that the simplified assumption of perfect and instantaneous mixing at cross interactions may lead to significant inaccuracies.

Ho et al. (2006) investigated various junction geometries (*e.g.,* cross and double-tee junctions) as well as a 3 x 3-node network with two sources of water with different NaCl concentrations. Three-dimensional CFD simulations based on the finite-element method were carried out. Reynolds (*Re*) numbers ranging from 5,000 to 80,000 were simulated and validated experimentally. The *Re* numbers for all incoming and outgoing flows were the same at all pipe legs in the single-junction studies, but the *Re* numbers were variable in the network studies. In the CFD simulations, the turbulent Schmidt number (Sc_t) was modified to determine if the resulting turbulent eddy diffusivity could be used to adequately represent mixing at the cross junction. The turbulent Schmidt number (Sc_t) was adjusted to values in the range of $10^{-3} < Sc_t < 10^{-1}$ in order to account for enhanced mixing caused by instabilities and vortical structures along the interface of impinging flows. Reynolds-Averaged Navier-Stokes (RANS) results were also compared with those based on Large Eddy Simulations (LES) (Webb and van Bloemen Waanders, 2006). Results from high-fidelity LES models revealed the highly transient nature of the

mixing behavior at the intersections, unlike the steady interface simulated with RANS models.

Romero-Gomez et al. (2006) studied a wide range of Reynolds numbers to further generalize these earlier findings. The Reynolds number ratios were defined as the significant dimensionless parameters to determine the mixing ratio at a cross junction under turbulent flow conditions ($Re > 10^4$). They further integrated CFD results into the EPANET water quality model as an exemplary case. EPANET is a freeware program developed by the Water Supply and Water Resources Division of the U.S. EPA's National Risk Management Research Laboratory (Rossman, 2000) which is widely used for research on, and management of, drinking water systems. A 5 x 4-node water network with three demand points was simulated under steady-state conditions with both the original and corrected EPANET water quality model. Contour plots of NaCl concentration throughout the network showed that spatial concentration patterns were greatly changed upon the implementation of mixing ratios at each junction based on CFD results.

The present work extends the aforementioned study by Romero-Gomez et al. (2006) and investigates the solute mixing phenomena at a cross junction at various flow rate combinations. The primary emphasis here is on the underlying physical principles that govern the transport phenomena of the mixing mechanisms as well as their mathematical modeling and computational simulations. Because the water quality model runs on solutions for the velocity field at the cross junction, the generalization of an important scaling parameter, the turbulent Schmidt number (Sc_t), is also investigated. It should be noted that Austin et al. (2007) further focus on the experimental verification of the present study.

Formulation

Dimensionless Parameters and Scenarios

As shown in Figure 1a, cross junctions (Figure 1b) are common in modern water distribution network grids. The cross junctions can be simplified to two- and three-

dimensional shapes as illustrated in Figures 1c and 1d. In all the cases analyzed in this study, the flow configuration consisted of two adjacent inlets and two outlets, as depicted in Figure 2. The pipes were labeled as *W* (west inlet, low concentration water), *S* (south inlet, high concentration inlet), *E* (east outlet), and *N* (north outlet). Sodium chloride (NaCl) was used as a tracer for examining solute mixing. CFD simulations provided highly-detailed information of NaCl concentrations throughout the analyzed computational domain. Thus, a weighted-average concentration at the outlets was calculated for each CFD simulation performed. Because varying background tracer concentration can be expected, NaCl concentration was expressed in terms of its dimensionless concentration.

$$C^* = \frac{C - C_W}{C_S - C_W} \tag{1a}$$

It should be noted that C_W corresponds to the background concentration. The above equation was further defined for the north and east outlets.

$$C_N^* = \frac{C_N - C_W}{C_S - C_W} \text{ and } C_E^* = \frac{C_E - C_W}{C_S - C_W} \tag{1b}$$

It was noted that if "perfect" mixing occurred with equal flows in the four pipe legs, *C** at either outlet automatically would equal 0.5. However, the premise of this research is that dimensionless concentrations can range from 0 to 1 due to the "incomplete" or "split" mixing. It is hypothesized that Reynolds numbers (*Re*) are the primary dimensionless parameters driving the mixing at junctions for the given geometry. This suggests that there are an infinite number of combinations of Re_S, Re_W, Re_N, and Re_E to describe flow configurations at cross junctions. Therefore, the *Re* ratio of inlet flows ($Re_{S/W}$) and the *Re* ratio of outlet flows ($Re_{E/N}$) were introduced and used in this work. These provided a generalized application of our findings.

$$\mathrm{Re}_{S/W} = \frac{\mathrm{Re}_S}{\mathrm{Re}_W} \quad \text{and} \quad \mathrm{Re}_{E/N} = \frac{\mathrm{Re}_E}{\mathrm{Re}_N} \tag{2}$$

Three simplified scenarios were first introduced and the generalized case follows:

- Scenario 1: Equal inflows and outflows ($Re_S = Re_W = Re_N = Re_E$)
- Scenario 2: Equal outflows, varying inflows ($Re_S \neq Re_W$, $Re_N = Re_E$)
- Scenario 3: Equal inflows, varying outflows ($Re_S = Re_W$, $Re_N \neq Re_E$)
- Generalized case: Varying inflows and varying outflows ($Re_S \neq Re_W \neq Re_N \neq Re_E$)

There are several reasons to define and investigate both the three proposed scenarios and the generalized case. Scenario I with the same Reynolds numbers at all pipes provides a clear and simplified view of the mixing process at the interface between the two incoming sources of water. Scenarios 2 and 3 were formulated in order to examine broader generalizations of the dimensionless parameters involved in the mixing process. The three scenarios are expected to provide foundations for understanding the generalized case, which defines any real-world flow combinations at cross junctions.

Mathematical formulation

The steady-state continuity and momentum equations were used to calculate the flow field. The conservation equations are shown in Eq. (3) and Eq. (4), in which $\bar{\bar{\tau}}$ is the stress tensor that accounts for the effects of viscosity and volume dilation. No mass or momentum sources were considered and gravity effects were neglected.

$$\nabla \cdot \bar{u} = 0 \tag{3}$$

$$\left(\nabla \cdot \bar{\bar{u}}\bar{u}\right) = \frac{1}{\rho}\left[-\nabla P + \nabla \cdot (\bar{\bar{\tau}}) \right] \tag{4}$$

The nature of water flow throughout the network is a function of space and time, it is therefore complex and difficult to predict. Laminar flows (and even stagnant waters) occur in dead-end pipes that connect to households or other withdrawal points

(Buchberger and Wu, 1995). However, turbulent flows generally prevail in most locations, where *Re* > 10,000. Turbulence is characterized by random and chaotic changes in the velocity field and flow patterns.

Despite these difficulties, numerous investigative projects have focused on proposing mathematical models to describe turbulence as well as analyzing the performance of such models in specific applications. Thakre and Joshi (2000) compared fourteen versions of k-ε and Reynolds stress turbulence models to experimental data from heat transfer in pipe flows. They found that outcomes from k-ε turbulence models agreed better with experimental observations. Similar conclusions were drawn by Ekambara and Joshi (2003), who analyzed axial mixing in single pipe flows under turbulent conditions. In this work, the turbulence field was calculated using the k-ε model, which was composed of two equations that account for the turbulence kinetic energy (k, Eq. 5a) and its rate of dissipation (ε, Eq. 5b):

$$\frac{\partial}{\partial x_i}\left(\rho k u_i\right) = \frac{\partial}{\partial x_j}\left[\left(\mu + \frac{\mu_t}{\sigma_k}\right)\frac{\partial k}{\partial x_j}\right] + G_k - \rho\varepsilon \tag{5a}$$

$$\frac{\partial}{\partial x_i}\left(\rho \varepsilon u_i\right) = \frac{\partial}{\partial x_j}\left[\left(\mu + \frac{\mu_t}{\sigma_\varepsilon}\right)\frac{\partial \varepsilon}{\partial x_j}\right] + C_{1\varepsilon}\frac{\varepsilon}{k}G_k - C_{2\varepsilon}\rho\frac{\varepsilon^2}{k} \tag{5b}$$

where the dimensionless constants for the turbulent model are: $C_{1\varepsilon}$ = 1.44, $C_{2\varepsilon}$ = 1.92, C_μ = 0.09, σ_k = 1.0, and σ_ε = 1.3. After the velocity and turbulence fields on the computational domain were obtained, the concentrations of NaCl were calculated using the species transport equation (Eq. 6). In steady-state, incompressible flows, the species transport equation is composed of two mechanisms: convective transport (due to bulk flow, left-hand side of Eq. 6) and diffusion (due to concentration gradients, right-hand side of Eq. 6).

$$\rho\,\nabla\cdot\left(\bar{u}\,C_i\right) = \nabla\cdot\left(\rho D_{AB} + \frac{\mu_t}{Sc_t}\right)\nabla C_i \tag{6}$$

The diffusion of species throughout the simulated region is modeled as the superposition of both molecular and eddy diffusivity; the latter is commonly known as dispersion. Molecular diffusion is a natural, dynamic process that tends to equilibrate the concentration of species. Even though D_{AB} (molecular diffusivity of species A into medium B) depends on temperature and aggregation of solute, among other factors, its value is known for typical solutions such as NaCl in water. On the other hand, eddy diffusivity depends on flow turbulence rather than the chemistry of species. Under fully turbulent flows, eddy diffusivity overwhelms molecular diffusivity by several orders of magnitude. Thus, NaCl mixing at cross intersections is mostly driven by diffusion caused by turbulence. In the CFD simulations presented here, the prediction of NaCl concentrations was dictated by the turbulent Schmidt number (Sc_t), which established the relationship between the turbulent transfer of momentum (μ_t) and the eddy diffusivity (D_t) as follows:

$$Sc_t = \frac{\mu_t}{\rho D_t} \tag{7}$$

Numerical setup

Numerical simulations of flows at cross junctions were performed using FLUENT® (Fluent Inc., 2005), a commercial CFD package based on the finite volume technique. This package uses GAMBIT (Fluent Inc., 2005) as the pre-processor to create the geometries and meshes of the simulated physical space. Next, the conservation equations from Eq. (3) to Eq. (7) are discretized over the mesh computational domain, for which boundary conditions and material properties must be defined. The two inlets were defined as "velocity inlets" with uniform NaCl concentration profiles at each inlet. Flow rates at the two outlets were assigned based on $Re_{E/N}$. A list of the set boundary conditions and their mathematical definitions is provided in Table 1. The material was set as a mixture composed of two constituent species: water (ρ = *997 kg m*$^{-3}$, molecular weight = *18.01 kg kgmol*$^{-1}$) and NaCl (ρ = *2170 kg m*$^{-3}$, molecular weight = *58.45 kg kgmol*$^{-1}$). The varying mixture function depended upon the concentration of sodium

chloride in water (volume-weighted-mixing-law) and the dynamic viscosity was $\mu = 1 \times 10^{-3}$ kg m^{-1} s^{-1}. The molecular diffusion of NaCl in water was set equal to 1.5×10^{-9} m^2 s^{-1}. These material properties remained the same for all the simulations.

Because several parameters of the numerical setup significantly affect the CFD outcomes even under the same flow and water quality configurations, careful analyses of these parameters are needed in order to ensure that they do not become a source of error. Such parameters include convergence criteria, mesh size, distribution of non-uniform mesh, discretization schemes, etc.

Convergence criteria are prescribed error tolerances for the scaled residuals of the conservation equations. The discretization of the conservation equation for any modeled variable ϕ (x-, y-velocity, species, kinetic energy, etc.) results in an algebraic equation, as expressed in Eq. (8). In this equation, a_P and ϕ_P are the coefficient and value of the variable φ at the cell center, respectively, whereas a_{nb} and ϕ_{nb} come from the influencing neighbor cells and b is mostly influenced by the boundary conditions and source terms.

$$a_P \phi_P = \sum_{nb} a_{nb} \phi_{nb} + b \tag{8}$$

For every iteration, the solver provides a solution for the resulting set of algebraic equations for all the conservation variables ϕ. From such a solution, Eq. (8) does not hold true; instead, there is an imbalance that has to be quantified by subtracting the left-hand side from the right-hand side of Eq. (8). The imbalances from all the mesh cells are then added up and scaled, as expressed in Eq. (9). The iteration process stops when the scaled residual of the variable ϕ satisfies the prescribed convergence criteria. In order to test the optimal value that was used for further simulations, the convergence criteria were set equal for all the conservation equations; these ranged from 10^{-2} to 10^{-7}.

$$R^{\phi} = \frac{\sum_{cells\ P} \left| \sum_{nb} a_{nb} \phi_{nb} + b - a_P \phi_P \right|}{\sum_{cells\ P} \left| a_P \phi_P \right|} \leq \textit{Convergence criterion} \tag{9}$$

Among the characteristics of the computational mesh, the shape and number of elements are the most relevant parameters for accuracy. In this work, several mesh sizes were tested in order to define their influence on the numerical solution. The mesh size ranged from 2,064 elements (the mesh size used by van Bloemen Waanders et al. (2005) with MP Salsa based on the Finite Element Method) up to 80,064 for 2D problems. An optimal mesh size produces no noticeable change in the outcomes corresponding to increased elements. Because the geometry of the pipes was very regular, quadrilateral elements were used over the entire computational domain and finer cells were drawn adjacent to the wall, with gradual enlargement at locations far from the wall (Romero-Gomez et al., 2006).

Numerical methods applied to the conservation equations are based on several discretization techniques. A particular technique has a set of corresponding solutions. Whereas in some applications, CFD simulations exhibit the same solution regardless of the set discretization technique, in other applications the CFD outcomes are markedly influenced by this setting. Therefore four schemes, First-order Upwind, Second-order Upwind, Quick, and Power Law schemes (Fluent Inc., 2005), were tested when the Reynolds number was equal to 44,000 at all inlets and outlets. This particular Reynolds number (44,000) was chosen because of the experimental data (van Bloemen Waanders et al., 2005) available at the beginning of the present study. The aim was to quantify the effect of each scheme on the dimensionless concentration at both outlets as well as to select one to be used in further simulations.

Most physical processes occur naturally in 3D spaces; however, a recurring question in numerical modeling is whether 2D CFD simulations produce outcomes that are essentially equal to those obtained on 3D discretizations. Dropping one independent spatial variable not only simplifies the conservation equations to be manipulated, but also dramatically reduces the computational time spent to obtain the solution. Thus, a 3D mesh of the computational domain with 109,824 elements was created and simulations were performed in order to compare the outcomes to analogous 2D CFD results (Romero-Gomez et al., 2006). For this purpose, Scenario 1 (recall, equal inflows and

outflows, $Re_S = Re_W = Re_N = Re_E$) was tested when the Reynolds number ranged from 11,000 to 88,000. The 3D boundary conditions remained the same as for the two-dimensional scheme.

Turbulent flow at cross junctions is induced by different means. The ratio of wall roughness to pipe diameter contributes to increased turbulence intensity, mainly for long pipes. Because wall surfaces were assumed to be smooth throughout this study and the computational domain did not allow for the development of high turbulence due to wall roughness, this turbulence source was not relevant. On the other hand, because fittings create changes in geometry by creating either gaps or bumps that change turbulence intensity and the corresponding NaCl mixing ratio, fittings are localized sources of turbulence present at cross junctions. For this reason, the following sizes of bumps were examined by creating a geometrical shape as depicted in Figure 2 (see the inset): D_b/D = 0.84, 0.92, 0.96 and 0.98. Furthermore, the following locations (L_b/D) of a bump of size D_b/D = 0.96 were tested: 1.5, 1, 0.5 and 0.25 for Scenario 1. For all these simulations, the dimensionless concentration at both outlets was computed and plotted in order to determine whether the location and size of bumps had any effect on NaCl mixing. The width of the bump (W_b/D) was also considered as one of the parameters. The CFD package has several physical models available, and the users can examine or select a model depending on the specific modeling needs. For this reason, a thorough study was conducted to examine the accuracy of solutions for four benchmark problems with known analytical solutions and/or experimental data (Romero-Gomez et al., 2006). For instance, enhanced wall treatment was used instead of wall functions because enhanced wall treatment performed better when analyzing turbulent boundary layers, and based on the benchmarking results, its application proved to be more generalized than wall functions.

An analysis of dimensionless concentration based on the number of cells at the east outlet indicated that the optimal number of cells on the two-dimensional simulation was about 60,000 cells (Romero-Gomez et al., 2006). The 2D results were compared with those for a three dimensional geometry with 110,000 cells, as shown in Figure 1c. The 2D and 3D simulation outcomes remained nearly the same, and the computational time is

drastically reduced when 2D geometry is used. Thus, all the simulations in the present study are conducted with 60,000 control volumes for the two dimensional geometry. A non-uniform mesh was carefully constructed and finer cells were used near the walls and the mixing zone due to larger gradients of the velocity, turbulence, and species fields. Approximately 30 % of the cells were defined as "boundary layer cells", on which enhanced treatment of the conservation equations was applied.

Numerical simulations

Scenario 1 is the most idealized case; all the inlet and outlet pipes have the same Reynolds number. Simulations were performed for the following Reynolds numbers to examine the effect of the flow speed on the mixing phenomena: 11,000 (u_o = 0.218 m s^{-1}), 22,000 (u_o = 0.436 m s^{-1}), 44,000 (u_o = 0.874 m s^{-1}), and 88,000 (u_o = 1.743 m s^{-1}). The 'split' mixing ratio remains approximately constant based on numerical and experimental test runs in this Re range (i.e., Re > 11,000, the turbulent regime). The range of Reynolds number for the present study (Re ≥ 11,000) is justified, since the majority of water distribution systems operate in the turbulent regime.

Scenario II (recall equal outflows and varying inflows, $Re_S \neq Re_W$, $Re_N = Re_E$) examines the Reynolds number ratios at the inlets while maintaining the same Reynolds numbers for both outlets. In all cases the flows were turbulent, and the specific Reynolds numbers set at the pipes are given in Table 2. Scenario III (equal inflows and varying outflows, $Re_S = Re_W$, $Re_N \neq Re_E$) was set up in a similar manner based on equal inflow and varying outflow conditions.

Thus far, species transport simulations were uncoupled with the momentum and mass conservation models. Physically, this approach means that the species concentrations do not affect the flow patterns; i.e., the species of study (NaCl) is considered a passive scalar. In the species transport model defined in Eq. (6), the total diffusivity is composed of the molecular and eddy diffusivities. Eddy diffusivity is calculated through the turbulent Schmidt number and the definition is given in Eq. (7). Therefore, eddy diffusivity is directly proportional to the eddy viscosity computed at each

node and inversely proportional to the Sc_t. The aforementioned simulations were performed using the default value assigned to the turbulent Schmidt number (Sc_t = 0.7). However, no universal relationship between turbulent momentum and species diffusivity exists. Therefore, comparisons of CFD outcomes to experimental data from Austin et al. (2007) helped to find the Sc_t numbers that governed the mixing process under investigation. This was completed by iterative processes based on experimental data for the generalized case ($Re_S \neq Re_W \neq Re_N \neq Re_E$). For each experimental data point, the actual Reynolds numbers for the four pipes and their corresponding velocities were extracted and set at the boundary conditions. After a CFD simulation was performed, the dimensionless concentrations at both outlets were obtained. If the simulated NaCl concentrations differed largely from experimental measurements, the Sc_t was updated and the simulation was run again. This update of Sc_t continued until the difference was less than the tolerance error (0.02).

Results and Discussion

Numerical Analysis

The required computational time is estimated based on the convergence criteria set. Any decrease in the convergence criteria conveys a significant increase in the time needed to obtain the results. Consequently, after a set of convergence criteria were tested, the results indicated that the minimum value of R^{ϕ} (Eq. (9)) to be used was 10^{-3} for all the conservation equations, as further decreases did not produce any significant changes in the results. The four tested discretization methods produced no substantial differences in dimensionless concentration at the outlets (less than 3 %). The first order scheme produced higher mixing while the second order and Quick schemes both produced similar outcomes that indicated less mixing. Because a scheme that provides higher-order accuracy is preferable, the second order scheme was used for all subsequent simulations; this resulted in lowered computational time to perform simulations as compared to the Quick scheme.

The implementation of a bump due to fittings induced no significant increased mixing at the junction. Even when the diameter was reduced by 16 % (D_b/D = 0.84, L_b/D=1, and W_b/D = 0.1), C_E* did not change significantly (about 2 %). Thus, it is assumed that the influence of fittings on the mixing is relatively small when the flow rates are nearly equal (Scenario 1).

Flow patterns and concentration contours

A major advantage of the CFD approach is that it enabled us to analyze and visualize flow and mass transport phenomena in detail. For instance, Figure 3a and 3b show the velocity vectors and NaCl concentration contours (C*), respectively, when the Re_S= Re_W= Re_E= Re_N= 44,000 (i.e., Scenario 1), and D = 2 in (5.08 cm). The NaCl dimensionless concentration ranges from 0 to 1 throughout the domain and the largest gradients occur where the two incoming flows merge along the line AB in Figure 3b, where the actual mixing of the two sources of water occurs. The water at high concentrations (south inlet) interacts over a very narrow mixing interface, the "impinging interface" (Ho et al., 2006), with the incoming pure water (left inlet), as if two impinging jets reflected off of the interface AB as shown in Figure 3a. The velocity vectors in the computational domain are nearly symmetrical with respect to line AB because the hydraulic conditions at the inlets and outlets are the same for this particular case (Scenario 1). However, dynamic boundary conditions and/or other turbulence modeling approaches produce non-symmetrical velocity vectors, as presented by Webb and van Bloemen Waanders (2006). It is evident that the limited instantaneous interaction between the two sources of water is the reason why the complete mixing assumption fails to represent the actual transport phenomena occurring at the cross junction. Another fundamental reason comes from the scaling factor (the turbulent Schmidt number, Sc_t) that links the velocity and turbulent numerical fields with the species transport in this limited mixing zone. As expressed in Eq. (7), decreasing the turbulent Schmidt number (Sc_t) or increasing eddy viscosity (μ_t) is one way to enhance turbulent eddies.

Figure 3c depicts the resulting contours of the NaCl dimensionless concentration (C^*) with an adjusted Sc_t based on the experimental data. In this case, the turbulent Schmidt number was modified iteratively until the CFD outcomes matched the experimental results obtained for that case (Scenario 1) by Austin et al. (2007). This scaling parameter does not modify the velocity field obtained previously and shown in Figure 3a. However, the contours in Figure 3c show a wider strip that implies enhanced eddy diffusivity, and the enhanced mixing results in greater interaction between the two water sources.

Four illustrated scenarios

The dimensionless concentrations under the same *Re* numbers at the inlets and outlets (Scenario 1) are depicted in Figure 4a. Again, the default value of the Schmidt number (Sc_t = 0.7) is used to observe the overall trend. This trend is the result of two effects that act at the intersection of both incoming flows. On the one hand, higher *Re* numbers produced larger velocities, which consequently induced higher eddy diffusivity at the interface. But unexpectedly, no monotonic decrease in dimensionless concentration is observed in Figure 4a. Instead, the curve increases steadily until it gradually approaches an asymptote ($C^*_E \rightarrow 0.96$) when Re > 40,000, revealing the relevance of the interaction time spent by both incoming flows of water at the interface. This interaction time was lower at higher Re numbers, reducing the capacity for eddies to induce higher mixing between the high and low concentrations of water. This finding along with the observations from Figure 3 clearly shows that both the interaction time and space have a significant effect on mixing at the junction.

It should be noted that the difference in dimensionless concentrations was only about 2 % over the studied *Re* number range ($11{,}000 \leq Re \leq 88{,}000$). From a research standpoint, the variation of dimensionless concentration with respect to the Reynolds number must be analyzed in order to obtain a better understanding of the physical models used in transport phenomena within pressurized pipe systems. From a practical standpoint, however, considering the uncertainties in real distribution systems, this

difference may be ignored in order to simplify modeling. The dimensionless concentration can be assumed to be constant at 0.95 when $Re \geq 10{,}000$. This assumption is not valid in laminar and transitional regimes, and further investigations are necessary over broader Re number ranges.

After simulations of Scenario 2 (Table 2), different Reynolds numbers at two inlets (south and west) were used to plot a series of curves of the dimensionless concentration at the east outlet, as depicted in Figure 4b. For each curve, the amount of low concentration water was held constant while the flow of high concentration water was increased. As a consequence, dimensionless concentrations were higher as Re_S increased. The data points (A, B, C, and D) that correspond to Figure 4a are circled in Figure 4b to demonstrate that Scenario 1 is a specific case of Scenario 2. It is clear that the Reynolds number ratio of two inlets is the dominant factor of the solute concentration split at the cross junction. Therefore, the general trend in Figure 4b can be better summarized using the *Re* ratio of the inlets ($Re_{S/W}$) and the dimensionless concentration to the east outlet (C_E^*) at various Re_W, the results of which are presented in Figure 5, again with $Sc_t = 0.7$.

The curves are nearly overlapping each other. Slight differences are observed at $Re_{S/W} = 1$ at various Re_W, particularly at the lower limits (11,000 and 22,000). The largest difference can be observed between the curves for Re_W = 11,000 to 22,000, whereas the curves remain essentially the same in the transition from Re_W = 44,000 to 88,000. For Scenario 1 ($Re_{S/W}$ = 1, a special case of Scenario 2), the trend was clearly shown in Figure 4a. No change is expected if curves of $Re_W > 88{,}000$ were plotted. From the results obtained outside of the range $0.7 < Re_{S/N} < 1.7$, mixing at cross junctions is mainly driven by ratios of Reynolds numbers, rather than Reynolds numbers explicitly. For the entire $Re_{S/W}$ of the given scenario, it is likely that the difference is negligible for real-world water quality modeling practices as long as Re_W remains greater than 10,000. A similar exemplary case can be described for Scenario 3, though for brevity, the case is not presented here.

In Figure 5, point α corresponds to the instance when Re_S = 10,478 and Re_W = 52,393 ($Re_{S/N}$ = 0.25), whereas point β corresponds to the case when Re_S = 47,154 and Re_W = 15,718 ($Re_{S/N}$ = 3). The visualization of NaCl dimensionless concentration contours and velocity vectors for both cases are presented in Figure 6. The complete mixing assumption indicates that the water flows have enough interaction to flow out with the same concentration. However, for α, high concentration water is swept out mostly to the east outlet because the momentum of the low concentration flow is larger, and entrains the NaCl coming from the South inlet (Figures 6a and 6b, Sc_t = 0.0468). On the other hand, Point β represents the case when larger volumes of high concentration water sweep the low concentration water flow through the north outlet without allowing for interactions that could lower the concentration at the east outlet (Figure 6c and 6d, Sc_t = 0.125). It is clear that the flow rate ratio is the driving force that determines the mixing patterns at cross junctions.

Adjustment of the Schmidt number

It was postulated that the turbulent Schmidt number (Sc_t) has a major influence on the instantaneous mixing phenomena along the mixing zone, as discussed earlier. All the preceding simulations were performed with Sc_t = 0.7, which is the default value assigned by FLUENT® when the k-ε turbulence model is used. However, Austin et al. (2006) compared CFD and experimental NaCl dimensionless concentrations for Scenario 2 and found that CFD values were overestimated (over the analyzed range of $Re_{S/W}$), with a maximum error of about 8 % with respect to experimental measurements. Thus, this study suggests that the Sc_t should be corrected over a set of experimental data points.

The generalized case of different *Re* numbers for inlets and outlets was investigated experimentally by Austin et al. (2007). A total of 49 cases with three repetitions were carried out, and their results were used in this study to map the turbulent Schmidt number that best fit each combination of *Re* numbers tested. The contours of the fitted turbulent Schmidt numbers are shown in Figure 7. The figure also includes the locations of three example cases (α and β in Figure 5 and Scenario 1). Even though a

large range of Sc_t ($0.03 < Sc_t < 1$) produced the CFD outcomes that matched experimental data, some trends over the chart are manifest. The dimensionless concentrations have values near 1 for $Re_{E/N} \sim 0$ (bottom edge), while low values ($0.03 < Sc_t < 0.2$) are observed along the left edge ($Re_{S/W} \sim 0$) and most of the right edge ($Re_{S/W} \sim 4$, and $Re_{S/W} > 1$). Contours for low dimensionless concentrations ($0.1 < Sc_t < 0.2$) prevail over most of the central region of the area ($0.5 < Re_{S/W} < 3.5$ and $1 < Re_{E/N} < 3$).

Although experimental data were obtained for $0.25 \leq Re_{S/W} \leq 4$ and $0.25 \leq Re_{E/N} \leq 4$, actual flows in water distributions systems can reach beyond that range. General trends beyond this range can be assessed via extrapolation of the experimental results as shown in Figure 8. Scenario 1 and cases α and β used in Figure 5 are also presented for the purpose of comparison. However, flow in one of four pipe legs is likely in laminar and transitional regimes as $Re_{S/W}$ or $Re_{E/N}$ approaches the two extreme limits (0 and ∞). Thus, it is important to note that Figure 8 should be used for water quality modeling only if Re > 10,000.

In the present study, the Reynolds numbers (*Re*) is considered as the primary dimensionless parameter. However, the Reynolds number may not account for all scaling factors under various conditions. For example, with larger pipe diameters, the flow velocity will be significantly smaller than the velocities used in the experiments for the same Reynolds number. A slower velocity and larger pipe diameter would increase contact time, contact area, and potentially the amount of mixing when compared to mixing in smaller pipes with higher velocities at the same Reynolds number. A few cases were examined with several pipe diameters (ID at 12.7, 19.1, and 50.8 mm) at the same Reynolds number with a constant diffusivity (NaCl), and the mixing ratio remained the same for all cases. The outcome may change when highly diffusive solutes flow in a large water main at a low flow rate. In this case, the molecular diffusivity of a solute may play a significant role for the mixing ratio. However, it would be rare to observe low flow rates in water mains. It should be also noted that the RANS model used for the present investigation may not be able to capture potentially transient behaviors at the cross junction. To address these issues, further studies are recommended using flow

visualization and high-fidelity computational techniques such as large eddy simulation (LES) and direct numerical simulation (DNS).

Conclusions

The representation of solute mixing behavior at pipe junctions impacts a wide variety of water distribution network analyses, including prediction of disinfectant residuals, optimal locations for water quality sensors, prediction models for early warning systems, numerical schemes for inverse source identification, and quantitative risk assessment. The present study addressed solute mixing phenomena at four-pipe cross junctions, which are commonly found in municipal drinking water distribution systems. Simulations using Computational Fluid Dynamics (CFD) were employed to understand mixing mechanisms at the junction and to examine the general trend of percent solute splits. Experimental results were used to assess representative Sc_t numbers for various flow conditions. The present study indicates that mixing at pipe cross junctions is far from "perfect". Incomplete mixing results from bifurcating inlet flows that reflect off of one another with minimal contact time. Additional experiments and computational studies are necessary to understand the mixing phenomena of flows ranging from laminar to transitional to turbulent flows at cross junctions.

Acknowledgements

This work is supported by the Environmental Protection Agency/Department of Homeland Security (under Grant No. 613383D). Sandia is a multi-program laboratory operated by Sandia Corporation, a Lockheed Martin Company for the United States Department of Energy's National Nuclear Security Administration under contract DE-AC04-94AL85000. We would like to acknowledge collaborators at Tucson Water (Dan Quintanar and Dean Trammel) who have contributed their valuable time and efforts to the present work.

Notation

a_P = coefficient at cell center
a_{ab} = coefficient at influencing neighbor cell
b = coefficient influenced by boundary conditions and source terms
C = NaCl concentration, kg kg^{-1}
C^* = dimensionless concentration
C_i = NaCl concentration at *i-th* cell
D = pipe diameter, m
D_b = reduced pipe diameter, m
D_{AB} = molecular diffusivity, m^2 s
D_t = eddy diffusivity, m^2 s
G_k = generation of turbulence kinetic energy, kg m^{-1} s^{-3}
I = turbulence intensity, %
k = turbulence kinetic energy, m^2 s^{-2}
L = hydraulic diameter, m
L_b = distance of bump from pipe intersection, m
P = pressure, Pa
R^{ϕ} = residual of conservation variable ϕ
Re = Reynolds number, $\rho DU/\mu$
Sc_t = turbulent Schmidt number, $\mu_t/\rho D_t$
$\bar{u}$ = velocity vector, m s^{-1}
u = x-velocity component, m s^{-1}
v = y-velocity component, m s^{-1}
u_i = *i-th* velocity component at cell center, m s^{-1}
U = average pipe flow velocity, m s^{-1}
W_b = bump length, m

ε = turbulence dissipation rate, m^{-2} s^{-3}
μ = molecular viscosity, kg m^{-1} s^{-1}
μ_t = eddy viscosity, kg m^{-1} s^{-1}
ρ = mixture density, kg m^{-3}
$\bar{\bar{\tau}}$ = stress tensor, kg m^{-1} s^{-2}
ϕ_P = conservation variable at cell center
ϕ_{ab} = conservation variable at influencing neighbor cell

subscripts
W = west inlet
S = south inlet
E = east outlet
N = north inlet
S/W = ratio of inlets, south to west
E/N = ratio of outlets, east to north

References

Austin, R. G., van Bloemen Waanders, B., McKenna, S., and Choi, C. Y. (2007). "Mixing at cross junctions in water distribution systems – part II. an experimental study," *ASCE Journal of Water Resources Planning and Management*, 134(3), 298-302.

Buchberger, S. G., and Wu, L. (1995). "Model for instantaneous residential water demands." *Journal of Hydraulic Engineering*, 121(3), 232-246.

Ekambara K., and Joshi, J. B. (2003). "Axial mixing in pipe flows: turbulent and transition regions." *Chemical Engineering Science*, 58: 2715 – 2724.

Fluent Inc. 2005. *Fluent 6.2 User's guide*.

Fluent Inc. 2005. *Gambit 2.2 User's guide*.

Fowler, A. G. and Jones, P. (1991). "Simulation of water quality in water distribution systems." *Proc. in Water Quality Modeling in Distribution Systems,* AwwaRF/EPA, Cincinnati, OH.

Ho, C. K., Orear, L., Wright, J. L., McKenna, S. A. (2006). "Contaminant mixing at pipe joints: comparison between laboratory flow experiments and computational fluid dynamics models." *Proceedings of the 8th Annual Water Distribution System Analysis Symposium*, Cincinnati, OH.

Mays, L. W. (2004). *Water supply systems security,* McGraw-Hill Professional, New York, N.Y.

Romero-Gomez, P., Choi, C. Y., van Bloemen Waanders, B., and McKenna, S. A. (2006). "Transport phenomena at intersections of pressurized pipe systems." *Proceedings of the 8th Annual Water Distribution System Analysis Symposium*, Cincinnati, OH.

Rossman, L. (2000). *EPANET-User's Manual*, US Environmental Protection Agency (EPA), Cincinnati, OH.

Thakre, S. S. and Joshi, J. B. (2000). "*CFD modeling of heat transfer in turbulent pipe flows*." *AIChE Journal*, 46 (9), 1798–1812.

van Bloemen Waanders, B., Hammond, G., Shadid, J., Collis, S., and Murray, R. (2005). "A comparison of Navier-Stokes and network models to predict chemical transport in municipal water distribution systems." *Proc., World Water and Envi. Resour. Congress*, Anchorage, AL.

Webb, S. W. and van Bloemen Waanders, B. G. (2006). "High fidelity computational fluid dynamics for mixing in water distribution systems," *Proceedings of the 8th Annual Water Distribution System Analysis Symposium*, Cincinnati, OH.

Tables

Table 1. Boundary conditions for numerical simulation of the cross junction.

Boundary	Velocity BC	Turbulence BC	Species BC
West inlet	$u = u_O$, $v = 0$	$I = I_o$, $L = D$	$C = 0$
South inlet	$u = 0$, $v = v_O$	$I = I_o$, $L = D$	$C = C_O$
East outlet	$\frac{\partial u}{\partial x} = 0$, $\frac{\partial v}{\partial x} = 0$	$\frac{\partial k}{\partial x} = 0$, $\frac{\partial \varepsilon}{\partial x} = 0$	$\frac{\partial C_i}{\partial x} = 0$
North outlet	$\frac{\partial u}{\partial y} = 0$, $\frac{\partial v}{\partial y} = 0$	$\frac{\partial k}{\partial y} = 0$, $\frac{\partial \varepsilon}{\partial y} = 0$	$\frac{\partial C_i}{\partial y} = 0$
Walls	$u = 0$, $v = 0$	*Enhanced Wall Treatment*	$\frac{\partial C_i}{\partial n} = 0$ *

* n = normal vector to the wall

Table 2. Reynolds numbers at the inlets and outlets for Scenario 2.

$Re_{S/W}$	Re_S	Re_W	Re_E	Re_N
1	11,000	11,000	11,000	11,000
2	22,000	11,000	16,500	16,500
4	44,000	11,000	27,500	27,500
8	88,000	11,000	49,500	49,500
0.5	11,000	22,000	16,000	16,000
1	22,000	22,000	22,000	22,000
2	44,000	22,000	33,000	33,000
4	88,000	22,000	55,000	55,000
0.25	11,000	44,000	27,500	27,500
0.5	22,000	44,000	33,000	33,000
1	44,000	44,000	44,000	44,000
2	88,000	44,000	66,000	66,000
0.125	11,000	88,000	49,500	49,500
0.25	22,000	88,000	55,000	55,000
0.5	44,000	88,000	66,000	66,000
1	88,000	88,000	88,000	88,000

Figures

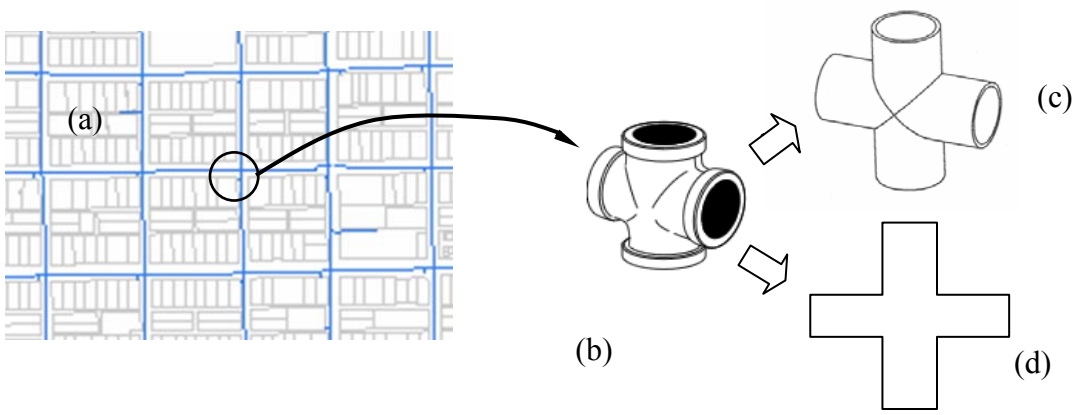

Figure 1. (a) A water distribution system featuring a cross junction in a mid-town neighborhood (Tucson, Arizona; courtesy of Tucson Water), (b) a typical cross-junction connector, (c) an idealized three-dimensional shape, and (d) a two-dimensional simplification.

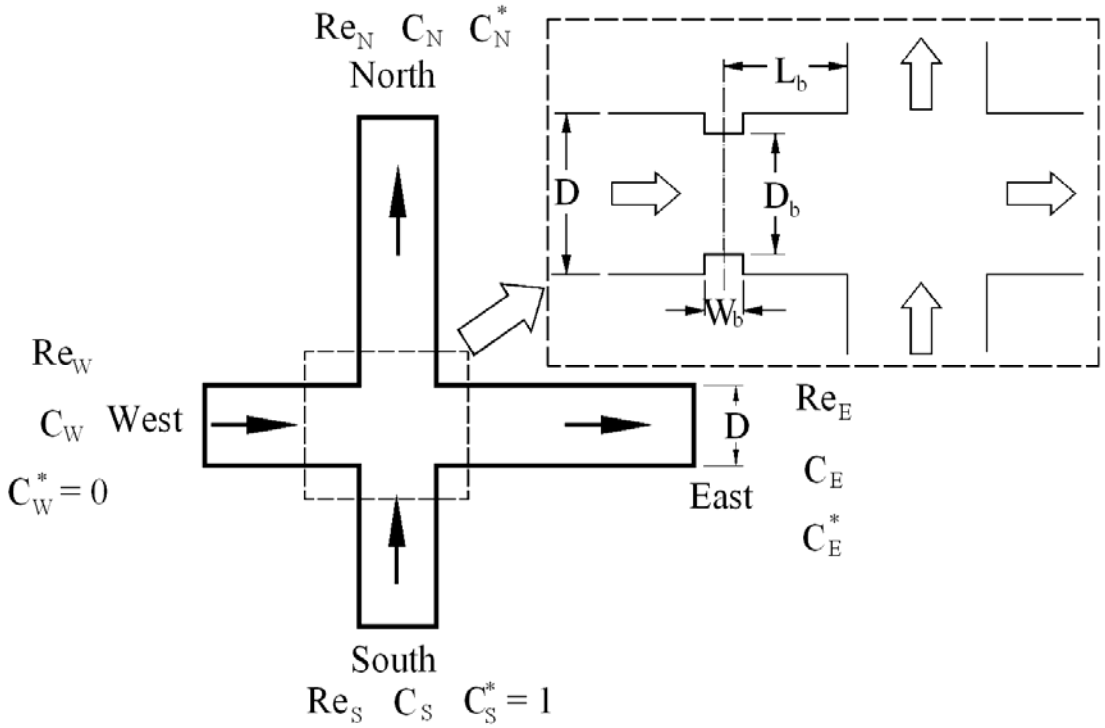

Figure 2. Hydraulic and water quality configurations of the flow at a cross junction, with detailed geometry of a generic fitting at one of the outlets.

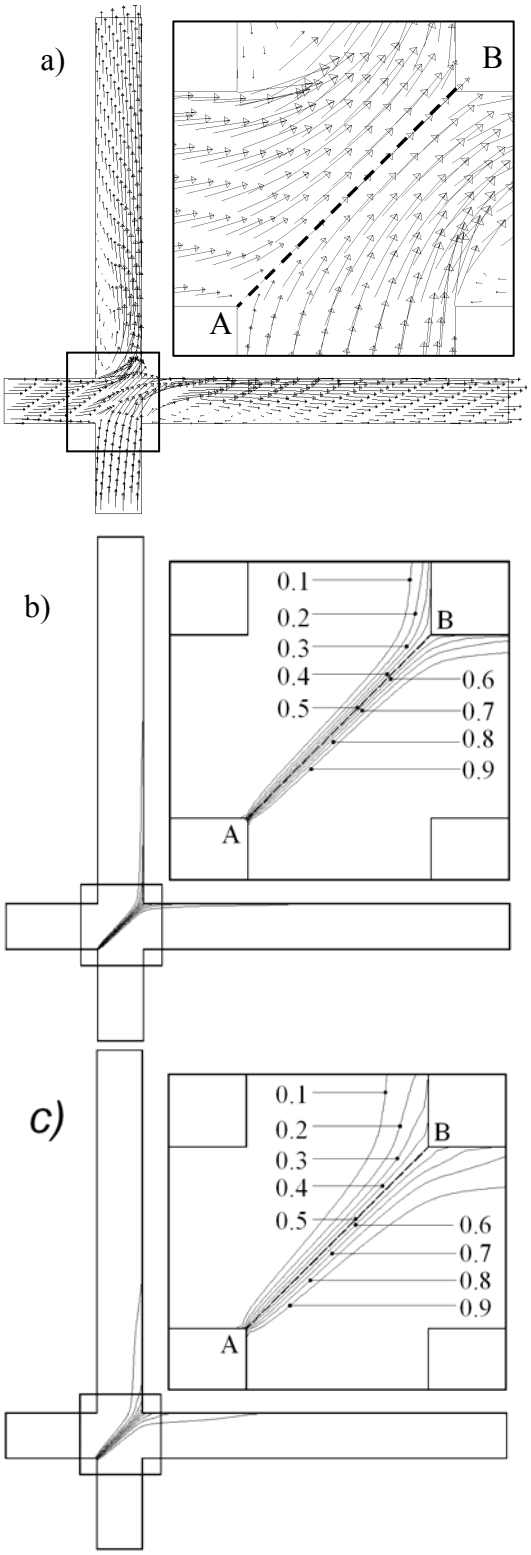

Figure 3. Flow and concentration visualization for Scenario 1 at Re = 44,000; (a) Velocity vectors, (b) Contours of NaCl dimensionless concentration with default Sc_t = 0.7, and (c) Contours of NaCl dimensionless concentration with corrected Sc_t = 0.1875.

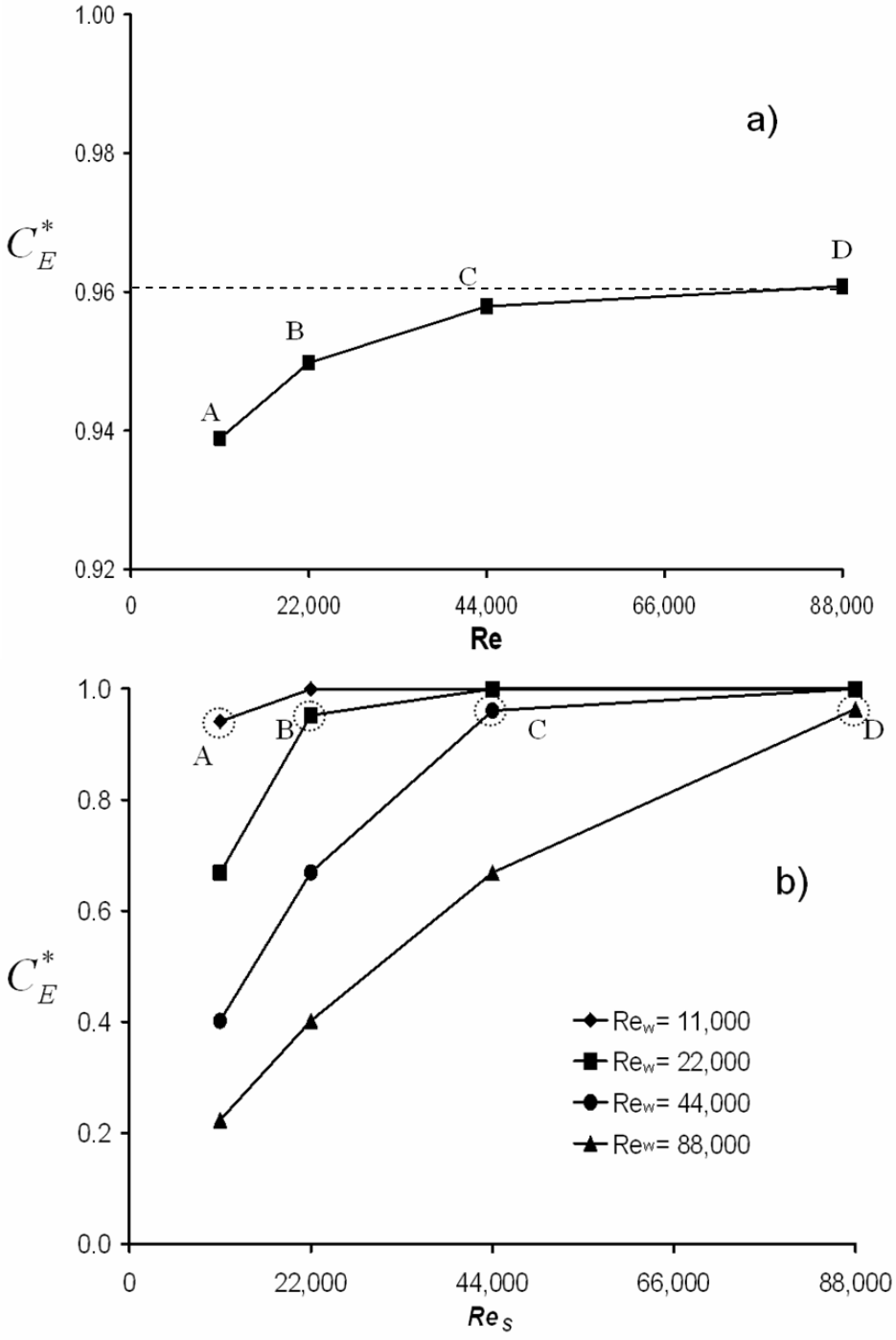

Figure 4. Effects of the Reynolds number in dimensionless concentration at the east outlet: (a) results for Scenario 1 and (b) C^*_E as a function of Reynolds number at the south inlet (Re_S) for Scenario 2. The data points (A, B, C, and D) that correspond to (a) are circled in (b).

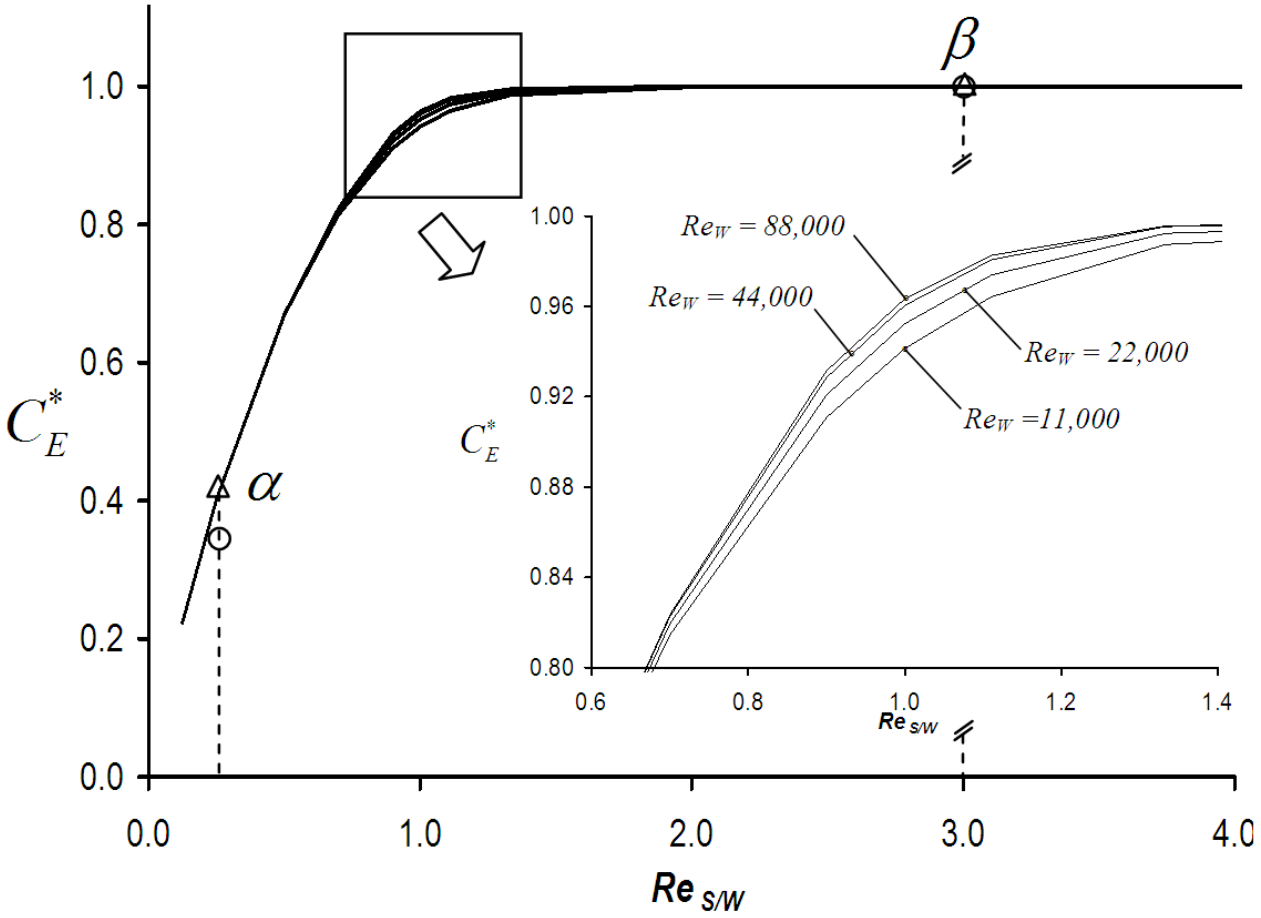

Figure 5. Dimensionless concentration at the east outlet as a function of ratio of Reynolds numbers of both inlets ($Re_{S/W}$), when $Sc_t = 0.7$. Triangle points α and β are calculated when $Re_{S/W} = 0.25$ and 3.0, respectively. Circular points are calculated with corrected Schmidt numbers based on experimental results; i.e., $Sc_t = 0.046$ and 0.125, respectively, when $Re_{S/W} = 0.25$ and 3.0.

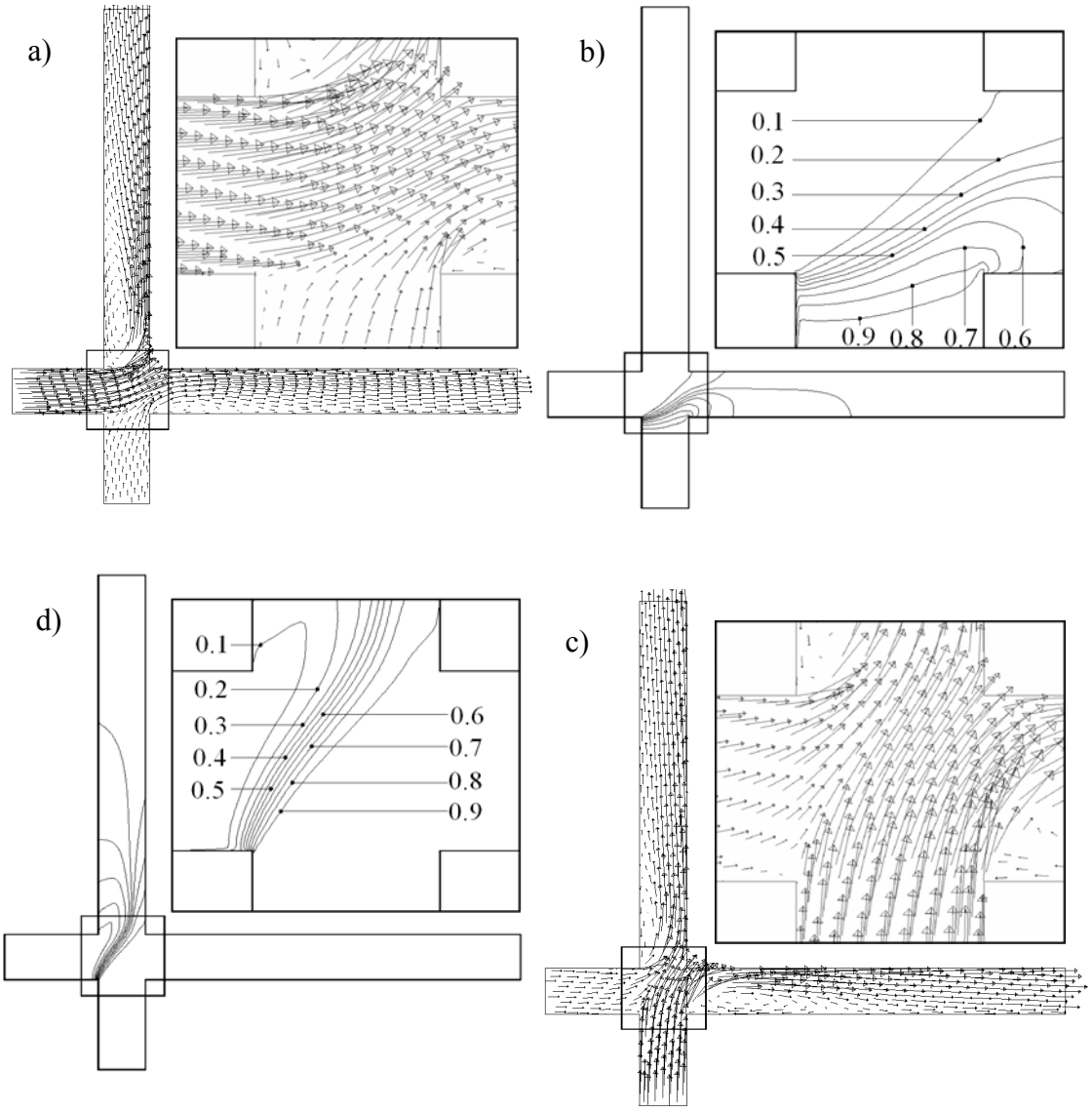

Figure 6. Flow and concentration visualization at α and β (see Figure 5) with corrected Sc_t: (a) velocity vectors at α, (b) C^* contours at α (Sc_t = 0.0468), (c) velocity vectors at β, and (d) C^* contours at β (Sc_t = 0.125).

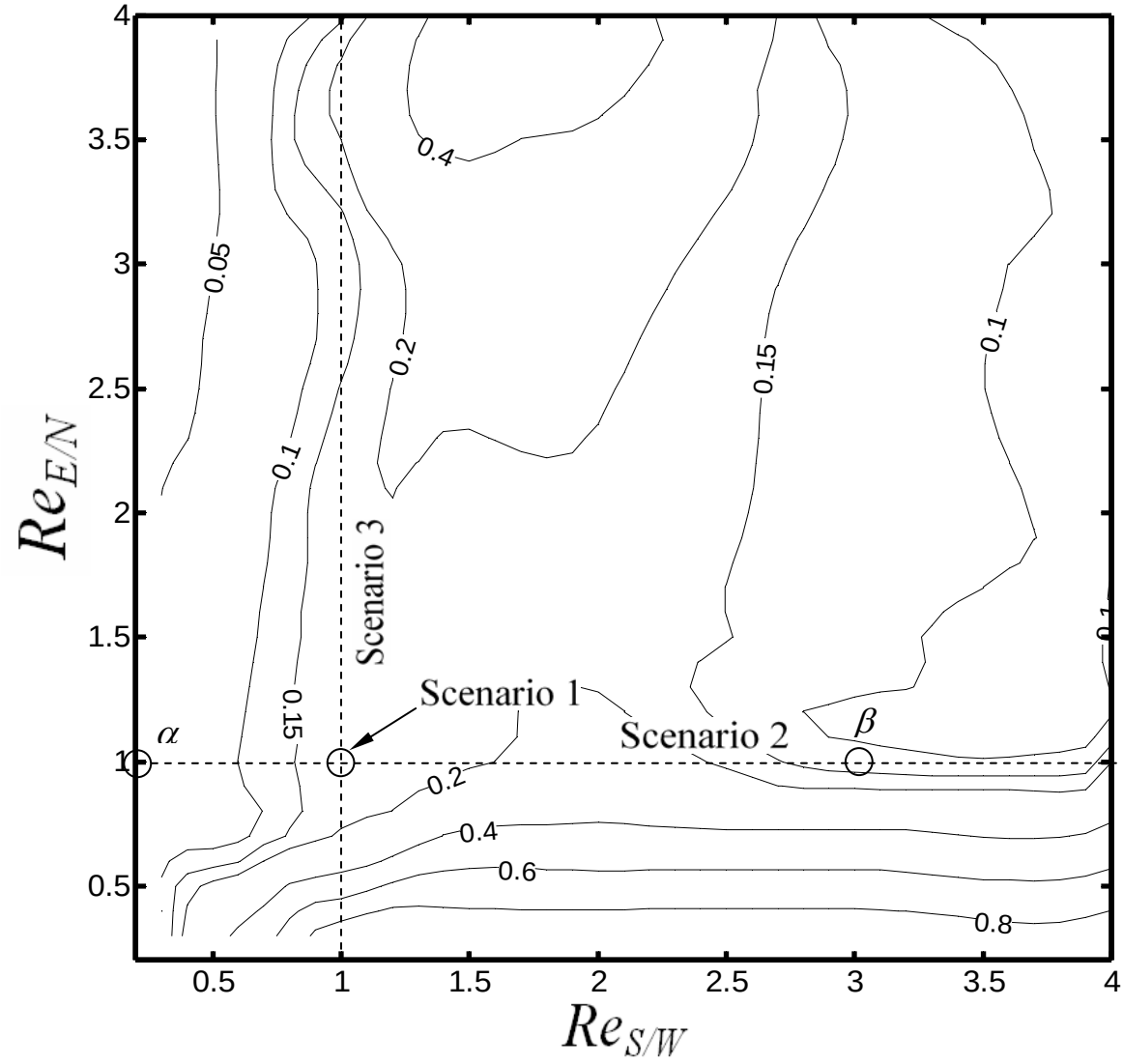

Figure 7. Contour of fitted turbulent Schmidt number (Sc_t) as a function of both $Re_{S/W}$ and $Re_{E/N}$ based on experimental results by Austin et al. (2007). See Figure 5 for α and β.

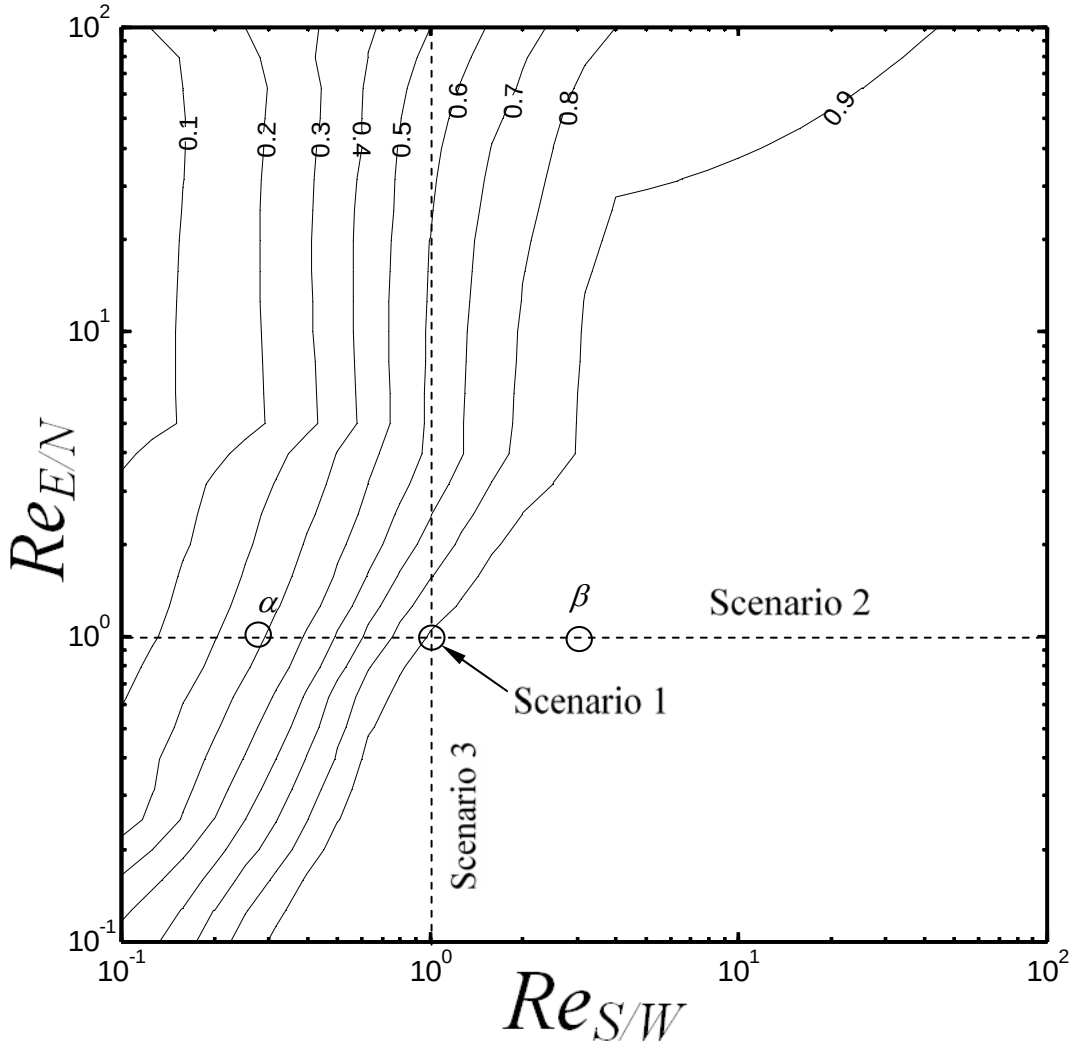

Figure 8. Contours of dimensionless concentrations at the east outlet (C^*_E) extrapolated over $Re_{S/W} > 4$ and $Re_{E/N} > 4$. See Figure 5 for α and β.

APPENDIX B

AXIAL DISPERSION COEFFICIENTS IN LAMINAR FLOWS OF WATER DISTRIBUTION SYSTEMS

Pedro Romero-Gomez[1] and Christopher Y. Choi[2]

To be submitted to the ASCE Journal of Hydraulic Engineering

[1] Graduate Research Assistant, Department of Agricultural and Biosystems Engineering, The University of Arizona, Tucson, AZ, 85721 U.S.A. E-mail: pedromer@email.arizona.edu
[2] Professor, Department of Agricultural and Biosystems Engineering, The University of Arizona, Tucson, AZ, 85721 U.S.A. E-mail: cchoi@arizona.edu

Abstract

The plug flow model has been widely used for representing solute transport in pressurized water distribution systems. Further improvements that consider axial dispersion pose a significant challenge. In particular, the dispersion coefficients relevant to the conditions commonly found in piping networks must be quantified. However, previously proposed models amplified the longitudinal spread as solutes move downstream. The present study sought to develop and to experimentally verify a modified advection-dispersion-reaction transport equation, along with formulas for the axial dispersion coefficient. The conditions in the analysis are laminar flows, constant mean velocities, and short travel times. Regarding the modified transport equation, the dispersion term was assumed to be direction-dependent. Thus, two distinct dispersion rates (forward and backward were recognized) were quantified, as opposed to the single-value needed in the conventional dispersion model. Taking the dimensionless travel time as the independent variable, the developed dispersion coefficients increased at about one-fourth of the growth rate exhibited by the conventional dispersion formula. The proposed scheme demonstrated a large improvement in the performance against experimental runs with various combinations of pipe lengths, tracer injections, mean flow velocities and solute properties. The findings could enhance the overall accuracy of water quality predictions and corresponding quantitative risk assessments, especially in pressure zones where low speed flows prevail.

Keywords: drinking water system, quality, axial dispersion, coefficient, optimization, ADR.

Introduction

Water resources managers and engineers utilize computational tools for assessing the status of hydraulic and water quality conditions over large drinking water distribution systems and for designing utility expansions. In addition, researchers on drinking water-related topics usually rely on such tools to propose and test methodologies that address the increasingly-stricter requirements imposed by customers and regulation agencies. For instance, water safety regulations mandate the reduction of hazardous byproducts produced by disinfectants and the ability to respond promptly to public health emergencies. The primary engines of these tools are the mathematical models that describe the underlying transport mechanisms that move water and solutes through the system's various components. In general, hydraulic models evaluate pressures, velocities, tank levels, etc., whereas water quality models predict concentrations of dissolved substances or water age in time and space. Currently, most quality solvers are based on the convenient but erroneous assumption that solutes do not spread as a water parcel moves along a pipe, i.e., axial dispersion is neglected. In the simplest example of such assumption, a non-reactive tracer pulse of short duration, injected at the upstream location of a long pipe, is incorrectly predicted to travel for miles without changing its shape at all. In fact, the concentration of biological and chemical tracers will change as the material disperses on the pipe's axis. Here, axial dispersion is neglected under the assumption that flows in pressurized systems are highly turbulent throughout the system and that this promotes a strong advective solute transport that prevails over longitudinal spread. However, the refinement of all-pipe hydraulic models reveals a wide range of conditions from highly-turbulent flows through mains and transmission lines, to intermittent or even stagnant flows in service lines, which are laminar in nature. To account for these phenomena, the present study aims at quantifying dispersion rates under such low flow conditions.

In view of the advancing modeling capabilities, dispersive transport has progressively been taken into consideration as a way to better describe the water quality behavior of pressurized water systems. Essentially, we aimed at expanding the one-

dimensional Advection-Reaction model (1D-AR) currently in use and turned it into a 1D-Advection-Dispersion-Reaction (1D-ADR) equation that can predict quality parameters with higher accuracy.

The numerous research efforts in this field can be divided into *(i)* those that seek a more efficient, accurate and applicable solution to the expanded equation, and *(ii)* those that seek to determine the dispersion coefficients that better represent the solute transport. Of the first type of study, one conducted by Axworthy and Karney (1996) is notable because it leads to the development of an analytical criterion to determine whether or not the 1D-AR transport model suffices in terms of quality prediction accuracy when used with a constant solute injection into pipes connected in series. Islam and Chaudhry (2008) solved for the 1D-ADR equation in two steps: the first the advection portion by applying the Warming-Kutler-Lomax scheme and next the dispersion and decay terms by using an explicit scheme. Another advance came when Tzatchkov et al. (2002) enhanced the solution's efficiency by formulating a two-stage Eularian-Lagrangian numerical scheme in conjunction with numerically-computed Green's functions. Another approach by Basha and Malaeb (2007) first discretized the dispersion term only, and then integrated the semi-analytical form of the 1D-ADR equation by using the method of characteristics.

Although the aforementioned studies introduced numerical schemes that were feasible for actual networks with a large number of pipes, they were not concerned with the dispersion coefficients to be used in their proposed formulations. Taylor (1953) quantified steady-state dispersion rates (E^*) in capillary tubes with constant flows via analytical solutions and corresponding experimental validations. If Taylor's model is scaled up to match the sizes of pipes and flows typically found in municipal water distribution systems, his formula only applies in the unlikely event that the residence time in a single pipe reaches the order of days. Yet, his methodology and findings unfolded other investigations aimed at determining dispersion rates at relatively short travel times. Gill and Sankarasubramanian (G-S, 1970), for example, derived a complex method for finding the dispersion rates following an instantaneous injection of solute in a long pipe under steady laminar flows. They demonstrated that the dispersion rate is transient,

increases with respect to travel time and asymptotically approaches the value calculated with Taylor's formula, E^*. However, the process of implementing the derived model into the 1D-ADR equation is complex and not feasible. In order to overcome this drawback, Lee (2004) provided simplified forms of G-S's equation (1970), versions that can actually be integrated into the 1D-ADR model.

Other studies have complemented the analytical formulas by using Computational Fluid Dynamics (CFD) tools to examine axial dispersion in pipe flows, an approach integrally employed in the present study. One such study, conducted by Ozdemir and Ger (1999), analyzed transient chlorine transport with decay rates via CFD and verified the model results experimentally. Ekambara and Joshi (2004) carried this work further by performing extensive CFD simulations over a wide range of the Peclet number and of the dimensionless time, with acceptable experimental/numerical confirmations. However, no simplified dispersion-rate model was produced for implementation into the 1D-ADR equation. CFD tools were also used by Romero-Gomez et al. (2008) to evaluate modeling and experimental runs at various Reynolds numbers covering the laminar, transitional and turbulent flow regimes. Romero-Gomez et al. (2009) further defined and validated the CFD setup upon which the present study is based (2009).

The objective of the present study is to develop and to experimentally validate an axial dispersion model capable of representing the spread of solute in the laminar flows of pressurized water distribution systems. Axial dispersion formulas needed in the 1D-ADR equation are developed for solutes traveling at constant laminar flows during short time spans. Such conditions constitute the foundation to further examine solute transport under more complex configurations. Axial dispersion under the low-speed, steady-state flow condition is the basis for analyzing stagnant and intermittent flows that often occur in peripheral zones of piping systems (Buchberger, 2003). It should be noted that the travel time of solutes moving along pipes in drinking water systems is considerably shorter than the time necessary to reach the steady-state dispersion rate introduced by Taylor (1954). Therefore, in order to generalize the findings in this investigation, we will perform our analysis in terms of the following dimensionless parameters: (i)

dimensionless pipe length (x*) to define the location of solute migration, L, with respect to the pipe diameter, d, (ii) Reynolds number (Re) to account for the mean flow velocity (u_m), geometric dimensions (d), and conveying fluid properties (kinematic viscosity, ν), (iii) Schmidt number (Sc) to accommodate the solute properties (solute diffusion coefficient, D_{AB}). Ultimately, the dimensionless travel time (T) combines all these parameters and dictates the extent to which the dispersion coefficient has elapsed towards reaching steady-state conditions.

$$x^* = \frac{L}{d}; \qquad \mathrm{Re} = \frac{du_m}{\nu}; \qquad Sc = \frac{\nu}{D_{AB}}; \qquad t = \frac{L}{u_m}$$

$$T = \frac{4D_{AB}t}{d^2} = 4\frac{x^*}{Sc\,\mathrm{Re}} \tag{1}$$

The present work contributes to a broader research effort aimed at expanding the capabilities of the current water quality prediction tools. Figure 1 illustrates the way such improvement will proceed from micro-scale model development toward macro-scale development with its corresponding experimental/field verifications. To make a contribution, this study began with a series of axial dispersion experimental runs in a single long pipe, which shows how the inlet concentration/flow conditions (experimental input data) give rise to a concentration pulse at the pipe outlet. Next, these same experimental input data are fed into CFD simulations in order to thoroughly map out the spatio-temporal solute distribution along the pipe. When an acceptable agreement between the two approaches exists, the CFD technique then becomes a feasible way to characterize the axial dispersion rate, E, as a function of flow, solute properties and travel time. Further verifications of the developed model determine its applicability to represent axial dispersion in laminar pipe flows.

Prevalence of laminar flows and the need for a comprehensive model

In order to assess the prevalence of low-flow conditions in water supply systems, Buchberger et al. (2003) defined the dead-ends as those pipes that have only one connection to the primary looped portion of the network. In a dead-end, water flows in

one direction only (in contrast to a loop, where bi-directional flow is possible), namely from the entrance to the user. They also established that dead-ends are very common in suburban and peripheral zones, as shown by a random sample taken from 14 service zones in Cincinnati, OH, USA, in which 23% of the total water main length could be considered dead-end. Similarly, they classified about 35% of the water distribution system in Milford, OH, USA, as dead-end mains. They found that many pipes in dead-end zones were characterized by random (even intermittent) flow rates throughout day, which in turn implied laminar-type conditions.

Blokker *et al*. (2009) conducted a tracer test in a distribution network with 10 km of mains connected to 1,000 homes, 2 hotels, and 30 commercial properties in the Dutch town of Zandvoort, near Amsterdam. The primary purpose of the study was to determine the water age at four locations in the network. The drinking water is distributed through pipe lines (Diameter > 16 cm or 6.3 in.) without any disinfectant, as is common in the Netherlands, and NaCl was used as the tracer. The Reynolds numbers estimated at several locations starting from the booster station (the tracer injection point) ranges from laminar, transitional, and turbulent flows. Consequently, their result demonstrates the difficulty of achieving reasonable prediction results based on the 'plug flow' model using the top-down and bottom-up demand allocations in an "all pipe" hydraulic model. At the downstream measurement location, the model showed a pulse of 2.5 hours (as opposed to an input pulse of 3 hours at the injection location), but the research team measured a pulse that lasted 9 hours. This discrepancy clearly demonstrates the need for a comprehensive and accurate axial dispersion model.

As part of this study, we also surveyed the percentile of pipes that conveyed laminar flows over a specific pressure zone in the distribution system of Tucson, AZ, USA. The zone spanned approximately 22 miles by 18 miles (35.4 km by 29 km) in the south-north and east-west directions, respectively. The hydraulic model was manipulated with EPANET and contained 38 reservoirs and 5 tanks, 1703 pipes and 1265 nodes with demands subject to a time-varying pattern obtained from the peak month of 2005. An EPANET toolkit/C++ routine performed hydraulic simulations (time step equal to one

hour, 96 h-simulation duration) and calculated Reynolds numbers for each pipe. The mean flow velocity through the links was computed by means of two methods: (A) all velocity values in the time series were averaged out, and (B) the velocity values below the 25th percentile were averaged out. The findings revealed that 6% and 16% of the pipes carry laminar flows ($Re \leq 2{,}100$) based on velocity averaged by methods A and B, respectively. It is important to remark that the hydraulic model was skeletonized and that the percentile can be expected to increase if all pipes were included, as confirmed by the magnitudes reported by Buchberger et al. (2003). Therefore, the present study examines solute transports under flows of such low velocities that generally exacerbate axial dispersion.

Experimental technique

The experimental setup was constructed at the Real-Time Sensor Testing Laboratory of the Water Village, an experimental facility at the University of Arizona, Tucson, AZ, USA. Figure 2 depicts the components of the water conditioning system and the main pipe section. Municipal tap water was run through five water filters connected in series in order to remove particles of sequentially decreasing sizes: 20 μm (FXWTC Carbon filter, GE Company, Louisville, KY, USA), 1 μm (Hytrex GX01-10, GE Company, Minnetonka, MN, USA), 0.65 μm, 0.2 μm and 0.04 μm (Clariflow 25-10320, Parker Hannifin Corp., Oxnard, CA, USA). Following filtration, a reverse osmosis system (GE Merlin, GE Company, Hollywood, FL, USA) removed most of the salts contained in the tap water (about 90%) and increased the efficiency of an additional two-tank deionizer unit (Culligan International Company, Northbrook, IL, USA). In this way, the water conditioning system lowered the background conductivity from a range of 500-600 μS cm^{-1} to less than 20 μS cm^{-1} so that only the salt tracer injected in the pipe section affected the conductivity sensor readings.

A frequency inverter (L100-004MFU2, Hitachi Ltd., Chiba, Japan) controlled the centrifugal pump (1MS1C5E4, ITT Corporation, Auburn, NY, USA) that delivered the main water source into a PVC pipe (15.6 mm diameter, ½" nominal diameter). A

programmable peristaltic pump (Tandem 1081, SciLog Inc., Middleton, WI, USA) injected pulses of tracer water from a beaker. The tracer injection did not increase the main flow rate significantly (1-2% increase for short time periods). A turbine-type flow sensor (FTB602B-T, Omega Corporation, Stamford, CT, USA) measured the flow rates, which were controlled with a needle valve. The flow sensor had an accuracy of ±1%, over the range of 0.3 – 9 L min^{-1}, and was calibrated before use. A static mixer (1/2-40C-4-12-2, Koflo Corp., Cary, IL, USA) homogenized the tracer's distribution over the cross-section of the pipe. The flow straightener eliminated swirls and distortions created by the mixer and induced the parabolic velocity distribution to develop more quickly. A four-ring potentiometric probe, combined with a conductivity transmitter (models CDE-1201 and CDTX1203, respectively, Omega Corporation, Stamford, CT, USA), measured the inlet conductivity data (upstream detection point). The accuracy was ±2% of the full range (0 – 1999 μS cm^{-1}). Another unit was used to measure the conductivity values of grab samples taken at the downstream detection point. These sensors were first calibrated at two points using commercially available solutions (CDSA-1500, Omega Corporation, Stamford, CT, USA). Next, sensor readings at various tracer solutions determined the relation between conductivity and salt concentration. Flow rates and upstream solute concentrations were recorded every second using a datalogger (CR23X Micrologger, Campbell Scientific, Logan, UT, USA).

The development of the axial dispersion model was based on a set of experimental runs that targeted Reynolds numbers ranging from 1,300 to 2,000 at intervals of 100, in a 6.5 m-long pipe ($x^* = 416$) and subject to 10 second-long injection pulses (Table 1). Table 2 lists the experimental runs used for verifying the developed model in both a 6.5 m- and a 12.5 m-long pipe ($x^* = 416$ and $x^* = 801$, respectively.)

Computational Fluid Dynamics (CFD) approach

The experimental runs supplied the inlet boundary conditions (flow rate and inlet concentration data) needed to simulate the solute mass transport using CFD techniques. The approach consists of numerically solving a set of conservation equations that fully

describe the velocity field and solute distribution in pipe flows under prescribed initial/boundary conditions. Although the CFD approach to solving for axial dispersion is computationally intensive for real-world applications, analyses of selected cases provide a detailed portrayal of the mass transport phenomena taking place as the solute moves along the pipe. The approach follows three steps:

(i) Pre-processing - the computational domain on which the transport equation was solved represented the pipe as a two-dimensional, axisymmetric rectangle with a height equal to the pipe radius (a) and width equal to the pipe length (L). The boundary types at the domain edges were: velocity inlet (left), outflow (right), wall (top), and axis (bottom).

(ii) Numerical setup - because a fully-developed laminar flow was assumed from the pipe entrance, a field function of the conventional parabolic velocity distribution was defined and applied over the domain. Such assumption eased the computational expense to only solving the species transport equation. The simulated model was laminar, two-dimensional, axisymmetric, and unsteady-state, as dictated by Equation 2.

$$\frac{\partial}{\partial t}(\rho C_i) + \nabla \cdot \left(\rho \bar{u} C_i\right) = \nabla \cdot (\rho D_{AB}) \nabla C_i \qquad (2)$$

This equation states that the transient change (first term, left-hand side) of solute concentration at the cell node *i* (C_i) is the result of the convection flux (second term, left-hand side) induced by local velocities ($\bar{u}$) and the diffusive solute transport resulting from concentration gradients (first term, right-hand side). Sodium chloride was assumed to be conservative (no growth or decay) with $D_{AB} = 1.2 \times 10^{-9}$ m^2 s^{-1}. The water density (ρ) setting was 998 kg m^{-3}.

(iii) Post-processing, the CFD simulations allow us obtain the time series of solute concentration at various distances, thus establishing a baseline for deriving the dispersion rates included in the 1D-ADR model. For this reason, the flow rate-weighted average (C_D) of cell center concentrations (C_k) at location x_j and time t_i was calculated as follows:

$$C_D(x_j, t_i) = \frac{2}{a^2 u_m} \sum_{k=1}^{N} u_k \, C_k \, r_k \, \Delta r_k \tag{3}$$

where u_k is the local axial velocity at the cell center, r_k is the cell center's distance from the pipe centerline, Δr_k is the cell size in the radial direction and u_m is the mean flow velocity. Furthermore, the flow rate-weighted average physically corresponded to the solute concentration of the bulk grab sample collected at the pipe outlet.

The CFD simulations of axial dispersion in pipes were performed using the finite volume technique (Fluent Inc., 2009). Preliminary runs by Romero-Gomez et al. (2008) proved that this tool can achieve an acceptable performance. In addition, Romero-Gomez et al. (2009) provided details on the pre-analysis of the numerical setup used in the present study, as well as its benchmarking against experimental data obtain by Taylor (1953). The numerical setup's pre-analysis was aimed at determining the non-uniform mesh size, the discretization scheme and the time step that have no effect on the simulated solution to axial dispersion. The goal of the benchmarking process was to minimize the likelihood of incorrect settings or erroneous assumptions. The resulting numerical setup contained 4,800 cells for every 100 diameters of pipe length simulated with a 2nd order upwind scheme (Fluent Inc., 2009) at a time interval of 0.01 s. Approximately 30% of the cells pertained to the boundary layer zone defined near the pipe wall, where large concentration gradients were expected.

One-dimensional Advection-Dispersion-Reaction (1D-ADR) model

A feasible approach for analyzing axial dispersion over large water systems requires the simplified one-dimensional Advection-Dispersion-Reaction (1D-ADR) model. The 1D-ADR model represents the unsteady mass transport process by means of the following partial differential equation:

$$\frac{\partial C_S}{\partial t} = E \frac{\partial^2 C_S}{\partial x^2} - u_m \frac{\partial C_S}{\partial x} + k C_S \tag{4}$$

This equation states that the unsteady solute distribution (C_S) at any time and at any location in the pipe (left-hand side) is the result of (i) the intermixing of mass between adjacent water volumes (dispersion, first term, right-hand side), (ii) the solute mass that the bulk flow conveys (advection, second term, right-hand side), and (iii) the growth or decay in the solute mass due to reactions within the bulk flow or along the pipe walls (reaction, third term, right-hand side). Because this study focuses on conservative constituents in water, only the first and second terms in the right-hand side of the equation are considered (no reaction term). Taylor's groundbreaking discovery of a formula (E^* in Equation 5) to quantify steady-state dispersion coefficients (for first term in right-hand side of Equation 4) at long solute travel times led to the development of transient dispersion coefficients approximated by Lee (2004) with the form indicated in Equation 6.

$$E^* = \frac{a^2 u_m^2}{48 D_{AB}} \tag{5}$$

$$E(T) = E(0)\exp(-16T) + \beta(T)E^* \tag{6}$$

where $E(0)$ is the initial value of the dispersion rate and $\beta(T) = 1 - exp(-16T)$. The existing models for E tend to amplify the dispersion effect for the special conditions in piping systems, i.e. the relatively short travel times and the strong influence of initial rates. Furthermore, the presence of solute "tailing" long after most of the mass has passed a specific location evidences that the dispersive transport tends to be stronger in the backward direction as compared to the forward dispersion rate, which also results in a sharp breakthrough curve at the downstream detection points. Thus, applying the same dispersion rate in both directions does not fully represent the actual transport phenomena. Therefore, we modified the diffusion term in the 1D-ADR equation in order to accommodate the fact that the dispersive transport is direction-dependent. Figure 3 depicts the flow of solute mass into and out of a thin pipe slice of volume $A \cdot \Delta x$, where A is the cross-sectional area and Δx is the length interval. The major assumption is that the difference in mass fluxes through the back and front boundaries (at x and $x+\Delta x$,

respectively) stems from the different dispersion rates at which the mass transports take place (E_b and E_f, respectively). Therefore, the modified 1D-ADR equation and its boundary conditions had the following form:

$$\frac{\partial C_S}{\partial t} = \frac{1}{\Delta x}\left(\phi_b - \phi_f\right) - u_m \frac{\partial C_S}{\partial x}$$

$$\begin{aligned} &\textit{Initial Condition} && C_S(x,0) = 0 && \\ &\textit{Boundary Condition } 1 && C_S(0,t) = C_0(x) && t > 0 \\ &\textit{Boundary Condition } 2 && \left.\frac{\partial C_S}{\partial x}\right|_{x\to\infty} = 0 && \end{aligned} \tag{7}$$

where:

$$\phi_b = -E_b \left.\frac{\partial C}{\partial x}\right|_b \text{ and } \phi_f = -E_f \left.\frac{\partial C}{\partial x}\right|_f .$$

As shown in Equation 6, the transient form of *E(T)* incorporates two components: an initial dispersion rate that decays exponentially in time and an increasing instantaneous rate that becomes asymptotic to Taylor's dispersion rate (E^*) at long time spans. In following such general formulation, the proposed dispersion models took the form:

$$E_f = E_f(0)\exp(-16T) + \beta_f(T)E^* \tag{8a}$$

$$E_b = E_b(0)\exp(-16T) + \beta_b(T)E^* \tag{8b}$$

Here, the second term is almost linear at short time spans ($T < 0.01$) for which the present study anticipates the coefficients β_f and β_b to be also linear.

In order to obtain a numerical solution to Equation 7, the unconditionally-stable Crank-Nicholson scheme was applied. This classical scheme is referred to as an explicit/implicit method because when the solver marches in time (Δt), it provides the transient concentration distribution based on the current values while involving the later ones as part of the solution process. The discretization in current and future times (*n* and

n+1, respectively) applied to all the derivatives as defined in Equation 9, which were then rearranged to obtain Equation 10. Because the latter equation gave rise to a tridiagonal system of equations, the Gaussian elimination was simplified by applying the widely-known Thomas algorithm and the discretized boundary condition at the pipe end (B.C. 2 in Equation 7).

$$\frac{\partial C_S}{\partial t} \approx \frac{C_S^{i,n+1} - C_S^{i,n}}{\Delta t};$$

$$\left.\frac{\partial C_S}{\partial x}\right|_i^n \approx \frac{C_S^{i+1,n} - C_S^{i-1,n}}{2\Delta x}; \qquad \left.\frac{\partial C_S}{\partial x}\right|_i^{n+1} \approx \frac{C_S^{i+1,n+1} - C_S^{i-1,n+1}}{2\Delta x}$$

$$\left.\frac{\partial C_S}{\partial x}\right|_b^n \approx \frac{C_S^{i,n} - C_S^{i-1,n}}{\Delta x}; \qquad \left.\frac{\partial C_S}{\partial x}\right|_b^n \approx \frac{C_S^{i,n+1} - C_S^{i-1,n+1}}{\Delta x} \tag{9}$$

$$\left.\frac{\partial C_S}{\partial x}\right|_f^n \approx \frac{C_S^{i+1,n} - C_S^{i,n}}{\Delta x}; \qquad \left.\frac{\partial C_S}{\partial x}\right|_f^{n+1} \approx \frac{C_S^{i+1,n+1} - C_S^{i,n+1}}{\Delta x}$$

$$\begin{aligned}&\left[\frac{u_m}{4\Delta x} - \frac{E_f}{2\Delta x^2}\right] C_S^{i+1,n} + \left[\frac{1}{\Delta t} + \frac{1}{2}\left(\frac{E_f}{\Delta x^2} + \frac{E_b}{\Delta x^2}\right)\right] C_S^{i,n} + \left[-\frac{u_m}{4\Delta x} - \frac{E_f}{2\Delta x^2}\right] C_S^{i-1,n} \\ &= \left[-\frac{u_m}{4\Delta x} + \frac{E_f}{2\Delta x^2}\right] C_S^{i+1,n} + \left[\frac{1}{\Delta t} - \frac{1}{2}\left(\frac{E_f}{\Delta x^2} + \frac{E_b}{\Delta x^2}\right)\right] C_S^{i,n} + \left[\frac{u_m}{4\Delta x} + \frac{E_f}{2\Delta x^2}\right] C_S^{i-1,n}\end{aligned} \tag{10}$$

Partial Differential Equation (PDE)-constrained parameter optimization

This work focuses on estimating the parameters (axial dispersion models, E_f and E_b) of a mass transport phenomenon that is governed by a Partial Differential Equation (PDE, Equation 7). This class of problems is called PDE-constrained parameter optimization. The optimization formulation sought to minimize an error occurring between the solute concentrations predicted by the 1D-ADR equation (C_S, Equation 7) and the results obtained by the CFD-simulation (C_D, Equation 3) upon the application of dispersion coefficients E_f and E_b, which thus became the decision variables. The two

terms in the objective function (z_j) measures the differences between CFD-generated and 1D-ADR-simulated concentrations. The objective function also expresses an emphasis on the prediction of the arrival time and maximum downstream concentration (first term, from time zero to the time when the maximum value of C_D occurs, T_{max}) while accounting for the solute mass that lags behind after the maximum value is detected (second term, past T_{max}).

$$\min \quad z_j = \sum_{i=0}^{T\max} \left[\left| C_D(x_j, t_i) - C_S(x_j, t_i) \right| \right]^3 + \sum_{i=T\max+1}^{T} \left[C_D(x_j, t_i) - C_S(x_j, t_i) \right]^2 \quad (11)$$

Newton's method was applied in order to numerically minimize the objective function (z_j) which is implicitly a function of two dispersion coefficient variables (through Equation 7) arranged in a vector, $\bar{E} = (E_f, E_b)$. The first step was to calculate the gradient of z_j (∇z_j) and to evaluate it at the initial guess values ($\bar{E}_0$). Next, the Hessian matrix of z_j, $H(z_j)$, was also evaluated at $\bar{E}_0$, where

$$\nabla z_j = \left(\frac{\partial z_j}{\partial E_f}, \frac{\partial z_j}{\partial E_b} \right) \quad (12)$$

$$H(z_j) = \begin{pmatrix} \dfrac{\partial^2 z_j}{\partial E_f^2} & \dfrac{\partial^2 z_j}{\partial E_f \partial E_b} \\ \dfrac{\partial^2 z_j}{\partial E_b \partial E_f} & \dfrac{\partial^2 z_j}{\partial E_b^2} \end{pmatrix} \quad (13)$$

Finally, the updated dispersion values were computed by subtracting the product of the gradient of z_j (by the inversed Hessian matrix) from the initially presumed value in the following equation.

$$\overline{E}_n = \overline{E}_{n-1} - \nabla z_j(\overline{E}_{n-1}) \cdot \left[H\left(z_j(\overline{E}_{n-1}) \right) \right]^{-1} \quad (14)$$

This iterative process was continued until a pre-specified error between the old (n-1) and updated (n) values was met. Newton's method typically requires a fairly accurate initial presumption of the value in order to speed up convergence. This, however, does not represent a drawback because the dispersion values were expected to monotonically

increase after an initial dispersion estimate at the pipe entrance was obtained, as prescribed by Equations 8a and 8b.

By solving this formula at subsequent pipe intervals, we could infer how much the axial dispersion coefficients would change as a function of travel time and then obtain the dimensionless parameter β_f and β_b (in Equations 8a and 8b) to further generalize the applicability to other scenarios.

Results and discussion

The first stage in the development of the axial dispersion model entailed validating the results from CFD-simulations against the experimental readings of solute concentration in a 6.5 m-long pipe ($x^* = 416$). To accomplish this, we introduced a 10 s-long injection pulse of a sodium chloride solution at a flow rate equal to 30 ml/min. A preliminary series of runs with an in-line conductivity sensor at the downstream location showed concentration curves consistently delayed with respect to the expected ones. Further examinations of CFD-simulated cross-sectional solute distributions revealed that whereas the mixer ensured consistent pulse-shape concentrations for the upstream conductivity sensor to read, the large radial gradients developed at the pipe outlet lowered the downstream sensor's ability to accurately read and average out the bulk-flow values. Grab samples, on the other hand, provided flow rate-weighted concentration values that were directly comparable to CFD results.

Another significant issue also developed at the experimental stage of this work: the spread of solute after traveling 6.5 m ($x^* = 416$) at low Re numbers ($Re < 1{,}300$) produced concentration measurements that became more strongly affected by the sensor's lower conductivity limit. Thus, although the flow meter was able to read flow velocities for Re values as low as 800, the tested Reynolds number ranged between 1,300 and 2,000 due to the combination of flow/conductivity limits of sensors. Nevertheless, because the outcomes of this analysis were non-dimensionalized, the findings directly applied to the entire laminar flow regime as demonstrated in subsequent sections. All experimental data

points presented in this work were obtained in duplicate runs, which were conducted at the same Reynolds number in order to guarantee repeatability during data collection.

Figure 4 depicts the results obtained from all the approaches when the pulse migrated to the pipe end at Re = 1,516. Although the inlet pulse lasted 10 s, the upstream readings dispersed due to the travel distance and the components (flow meter, mixer, and flow straightener) in place between the injection point and the upstream sensor. All downstream data featured lower peak values as well as a stretched curve as compared to the upstream signal. Nevertheless, such expected characteristics were quantitatively distinct, depending upon the approach. Among the four downstream curves, the CFD-simulated results and experimental results showed the highest correlation over time (R^2 = 0.96 for this Re number in Figure 5). The largest discrepancies of the CFD approach resulted from the solute's arrival to the peak value as concentrations were underestimated. They arose from the local disturbances caused by pipe fittings and other minor geometric changes along the pipe, changes that were not represented in the numerical setup. Another error occurred because collecting each sample required 4 seconds in order to attain the minimum volume required to fill the conductivity probes (at least 60 ml). Because the solute distribution in the outgoing water volume changed continuously in both time and space, the samples ultimately averaged out the concentration gradients. However, the CFD-simulated results were only spatially-averaged. The significant improvement in water quality prediction achieved by using CFD is evident when the outcomes obtained via 1D-ADR simulations using the existing dispersion model (Lee, 2004) are taken into consideration. The shorter solute arrival time, the lower peak concentration, and the more extended curve over time all indicate that the model magnifies the dispersive effect. Whereas previous evidence confirms the accuracy of this model when long travel times have elapsed, the present findings suggest a possibility of developing a more representative dispersion formula for short pipes. The 1D-AR model (only-advection) exhibited the largest deviation against experimental observations, as the outlet concentrations essentially mimic the shape of the upstream tracer injection.

The other experimental runs listed in Table 1 essentially replicated the aforementioned similarities and discrepancies between experimental and CFD-simulated results as depicted in the scattergrams in Figure 5. The x-coordinate of each data point corresponds to the concentration reading whereas its y-coordinate represents the CFD-predicted tracer concentration. Each chart also shows the squared-R value and the number of data points included in the comparison (N). The CFD technique slightly under-predicted peak concentrations for all cases excepting Re = 1,796. The squared-correlation coefficient remains high for all the instances, with the lowest value for Re being 1,796 (R^2 = 0.81) and the highest one for Re being 1,281 (R^2 = 0.97). These plots further corroborate the ability of CFD tools to accurately represent the axial dispersion transport in pipe flows. Outcomes from 1D-ADR runs conducted using the existing dispersion model (Lee, 2004) reproduced the previously-explained features for Re = 1,516 and thus are omitted in Figure 5.

The CFD simulations made concentration time series available at any location for stepwise calculations of the dispersion coefficients. The case for Re = 1,705 fell near the middle of the analyzed Re number range and was selected to carry out the parameter optimization phase of this work. The optimization formulation (Equation 11) was applied at $\Delta x^* = 32$ in the range $x^* = 0 – 960$, at $\Delta x^* = 64$ within the range $x^* = 960 – 1600$ and at $\Delta x^* = 160$ in the range $x^* = 1600 – 3200$. The length interval increased gradually because the formulation became less sensitive to Δx^* as the solute pulse migrated from the pipe inlet. Figure 6a depicts the linear evolution of optimal dispersion coefficients as a function of travel time. In all instances, the backward dispersion rate (E_b) was greater than the forward value (E_f) by a relatively constant absolute difference ($E_b - E_f$) with an average equal to 5.3×10^{-3} $m^2 s^{-1}$. The forward dispersion rate (E_f) was lower than E_b by 24% to 1%, thus decreasing monotonically from the entrance to the pipe outlet, accordingly. This finding indicates that the influence of both the initial values and the direction-dependence of dispersion rates is significantly stronger near the pipe entrance and lessens at longer travel times. The optimal coefficients did not produce a perfect agreement with the CFD-simulated concentrations at all the locations; instead, they

yielded the least possible error produced by the bi-directional dispersion model. In fact, the optimal coefficients induced slightly earlier arrival times and a longer delay to peak concentrations as compared to the CFD-simulated baseline. Nevertheless, there was a considerable improvement in comparison to the overestimated, direction-independent dispersion rates obtained by Lee (2004) and shown in Figure 6a.

The curve fitting of the optimal coefficients in Figure 6a to models in Equations 8a and 8b led to initial dispersion rates of $E_b(0) = 7.5 \times 10^{-3}$ m^2 s^{-1} and $E_f(0) = 2.1 \times 10^{-3}$ m^2 s^{-1}, whereas the β_b and β_f coefficients turned out to be alike (Equation 15) as illustrated in Figure 6b. This finding represents a substantial advance in the development of the instantaneous dispersion model for short pipes because it dictates an eventual convergence of both the backward and forward dispersion rates at long travel times. The slope in Equation 15 is 24.5% of the β-coefficient found by Lee (2003), and confirmed the earlier findings obtained by Romero-Gomez et al. (2008), in which the experimental dispersion rates calculated by the method of moments were 20-25% of those predicted by Lee's model.

$$\beta_f = \beta_b = \beta = 3.705T \tag{15}$$

The battery of experimental tests listed in Table 2 was run in order to verify the axial dispersion formula for various combinations of Reynolds number, pipe length and injection duration. All runs in Figure 7 demonstrate the applicability of the model over a range of Re values (from 1,479 to 1,750) at two different pipe lengths. The charts on the left illustrate the dispersion effect in a 6.5 m-long pipe (x* = 416) whereas the charts on the right depict the outcomes of runs at corresponding (or nearly corresponding) Reynolds numbers in a 12.5 m-long pipe (x* = 801). As expected, the inlet pulse disperses considerably more at larger x* values. With respect to the dispersion model developed in the present study, there exists an acceptable agreement between the experimental measurements and the 1D-ADR predictions. The largest discrepancies were observed at peak concentrations for runs at Re = 1,727 and at Re = 1,750. These were underestimated by the modeling approach; however, this is a consequence of the

optimization formulation in which we primarily emphasized the ability of the model to predict the solute arrival time over its ability to reproduce other features. All experimental runs were carried out in duplicates that produced downstream concentration time series that complemented each other.

Reducing the computational time needed for simulating the solute transport is another important aspect to consider when assessing enhanced modeling capabilities. Accordingly, we found that the completion of a single CFD simulation run on a personal computer (with an Intel Core 2.33 GHz, 1.99 GB of RAM) required 12 to 18 hours, whereas the corresponding 1D-ADR run took less than three seconds on average and on the same computer. It is expected that expedient numerical schemes that seek to efficiently solve the 1D-ADR equation for large piping networks (Tzatchkov et al., 2002; Basha and Malaeb, 2007) will probably require much shorter simulation times.

A close inspection of Figure 7 provides evidence that the experimental tests involving combinations of long pipe length/low Reynolds number and short pipe length/high Reynolds number may lead to large measuring errors due to sensor and sampling limitations. Specifically, the former configuration (long L/low Re) would generate very low outlet concentrations and thus produce a large conductivity sensor error. The latter (short L/high Re) makes sample collection difficult because the frequency should increase in conjunction with shorter sampling durations that may not make up for the water volume required by the conductivity probe. Therefore, the experimental verification at a low Reynolds number (Re = 1,341, Figure 8) was performed in a short pipe only (L = 6.5 m, x* = 416), whereas a high flow rate (Re = 1,976, in Figure 8) was run in long pipes (L = 12.5 m, x* = 801). As observed in previous cases, the comparisons demonstrate an acceptable agreement between the two approaches, although they also suggest that the developed dispersion model tends to overestimate the dispersion effect in water flows at Reynolds numbers that are close to the conventional limit of the laminar regime (Re ~ 2,100).

The axial dispersion coefficients formulated by Equations 8a and 8b, along with the dimensionless parameter β in Equation 15, establish that the solute intermixing from a

water parcel to the adjacent volumes becomes stronger in a quasi-linear fashion with respect to the travel time (or as a function of the reached length, upon constant mean flow velocity, u_m). This phenomenon results from the simultaneous, local mass transfers occurring at the micro-scale level, such as (i) axial diffusion transport due to large concentration gradients in the x-direction, (ii) local convective transfers occurring as bulk flow motion takes place at different, radially-distributed velocities, and (iii) radial diffusion of that solute acting at the pulse front extending from the high-velocity center region of the pipe to the low-velocity pipe wall region and occurring in the opposite direction at the back end of the pulse. Because the aforementioned processes take place irrespective of whether the solute is introduced in the main stream as a pulse or a continuous injection, we extended the experimental verification of the developed dispersion model to include both a long injection pulse (1 minute-duration) and continuous (but not constant) solute injection.

Figure 9 illustrates the evaluation of the model performance for long-injection runs (1 min) at two Reynolds numbers (Re = 1,493 and Re = 1,893) in a 12.5 m-long pipe ($x^* = 801$). Once again the model more accurately predicted downstream concentrations at lower flow rates and underestimated the peak concentrations in both instances. It is also worth pointing out that the prediction error over the curve tailing for the case Re = 1,493 was relatively larger than those of the previous runs (as shown in Figures 7 and 8). This error may arise because the optimization formula penalizes, to a lesser extent, the differences over the tailing side of the curve (differences are squared in the second term). Another meaningful aspect in these outcomes is that the 1D-ADR run made with Lee's model (2004) for Re = 1,893 falls the closest to the experimental data, considering all the cases presented in this study. This similarity may have to do with the smaller concentration gradients that were generated with a long pulse in the x-direction as opposed to a short, sharper solute injection of 10 seconds. The smaller the spatial gradients, the weaker the dispersive solute transport and the lower the effect of the overestimated dispersion rates used by Lee (2004).

The developed model was also tested upon a continuous, time-varying solute injection at the pipe inlet. The baselines for this verification run are CFD-simulated concentrations, instead of experimental readings. The upstream value was obtained from the widely-known experimental data released by the U.S. EPA as part of the EPANET computer package (Example Network 2, Cherry Hill/Brushy Plains network, Node ID 19). Although the series is given in hours at unequal time intervals in the original dataset, it was re-defined into minutes at equal intervals (through a linear interpolation tool) in order to accommodate the time span over which the developed dispersion model applies ($T < 0.01$). The inlet solute concentration is shown in Figure 10. The solute was chlorine ($D_{AB} = 1.38 \times 10^{-9}$ m^2 s^{-1}) traveling through a 5.08 cm-diameter pipe (2" nominal value) at a mean flow velocity of 2 cm s^{-1} (Re = 1,011). The concentration time series at 25 m from the pipe inlet ($x^* = 492$) was computed as flow rate-weighted, averaged values (Equation 3) from CFD results. The initial dispersion rates had values of $E_b(0) = 1.6 \times 10^{-4}$ m^2 s^{-1} and $E_f(0) = 0$ m^2 s^{-1}.

As depicted in Figure 10, the 1D-ADR runs with the developed model evidence the ability to predict concentration fluctuations after solute arrival at x = 25 m (time is approx. 800 s). On the other hand, the conventional model tends to flatten out the oscillations and predicts a rather smooth curve. The time series plotted in Figure 10 also include results obtained from simulations that only considered the advection solute transport (EPANET). They make clear that the prediction errors produced by an only-advection model are characterized by a greatly delayed arrival time and an inaccurate replication of the inlet boundary condition.

The developed dispersion model is applicable at short dimensionless travel times, $T < 0.01$. In the context of pipe diameters and the solutes of interest in drinking water distribution systems, Table 3 exhibits the pipe lengths into which the dimensionless time limit translates, assuming Reynolds numbers of 500 and 2,000. Free chlorine (Cl_2), sodium fluoride (NaF) and monochloramine (NH_2Cl) are commonly used as disinfectants in municipal water systems in the U.S., whereas sodium chloride (NaCl) is exhibited because it was used as tracer in the present work. As seen in Table 3, the pipe length over

which the model applies is inversely proportional to the molecular diffusion coefficient (D_{AB}) and directly proportional to the pipe diameter (d) and flow Reynolds number (Re).

The present work revealed that the dispersion process in short pipes is more sensitive to initial dispersion rates than in long pipes. Thus, a major challenge is to quantify the initial dispersion rates that may be strongly related to solute mixing occurring as the water flows through the network's components (flow sensor, mixer, and flow straightener) before arriving at the upstream measuring point, and also related to the distances that the solute has traveled before first being detected. The initial dispersion can be studied with respect to the experimental results and modeling assumptions. The CFD modeling of cases in Table 1 provided a guidance for the values of $E_b(0)$ and $E_f(0)$ that were used in the model verification phase of this study and that are listed in Table 2. However, a parametric analysis may be implemented in order to examine the conditions that most strongly influence the initial dispersion values. The initial dispersion rate used for Lee's model, E(0), was taken as the average of the backward and forward rates and is also listed in Table 2 for each verification run.

Conclusions

The axial dispersion of solutes traveling in laminar pipe flows was numerically examined and experimentally verified in this work. A new formula for dispersion rates was developed and implemented in a proposed direction-dependent transport equation. Such an equation is plausible for evaluating water quality parameters over drinking water distribution systems within a feasible computational time span. For short time spans, the dispersion rates behave in a quasi-linear manner as a function of travel time, with a slope that is about one fourth of that dictated by the existing formulas. Because the model was defined in terms of dimensionless variables, it can accommodate a wide variety of practically-achievable combinations of flow rates, pipe diameters and solute properties as long as the flow regime remains laminar and the dimensionless travel time is less than 0.01. The verification runs ascertained the applicability of the proposed model upon short, long and continuous upstream injections of solute. The present study also shows

that axial dispersion effects shape the overall distribution of a solute in the low-velocity pipes of water networks and therefore need be integrated into current water quality solvers, which up to now oversimplified the transport of non-reactive solutes, depicting it as an advection-only mode.

Because the behavior of hydraulic and water quality parameters in piping networks is complex and highly-transient, the developed model may also serve as the starting point for determining dispersion coefficients under unsteady, intermittent, and stagnant flow conditions in pipe systems. The methodology pursued in this study could also be used to further explore the solute dispersion characteristics occurring under transitional and turbulent flows in order to complete the spectrum of conditions that are likely to be found in drinking water distribution systems. Furthermore, future research should combine the proposed dispersion model with efficient numerical schemes for analyses over large-size networks and then verify it by means of field testing.

Acknowledgements

This work is supported by the Environmental Protection Agency/Department of Homeland Security (under Grant No. 613383D). We would like to acknowledge collaborators Dr. Steve G. Buchberger and Dr. Zhiwei Li at the University of Cincinnati, in Cincinnati, OH, as well as Mirjam Blokker at KWR in The Netherlands. The following UA students contributed their valuable time and efforts to the experimental phase of this work: Ryan G. Austin, Mario Mondaca, Malorie Teich, Fernando Rojano, and Alex Andrade.

References

Axworthy, D.H. and Karney, B.W. (1996). “Modeling low velocity/high dispersion flow in water distribution systems.” *J. Water Resour. Plann. Manage.*, 122(3), 218-221.

Basha, H.A. and Malaeb, L.N. (2007). “Eularian-Lagrangian method for constituent transport in water distribution networks.” *J. Hydraul. Eng.*, 133(10), 1155-1166.

Blokker E.J.M., Vreeburg, J.H.G., Beverloo, H., Arfman, M. K. (2009). “A bottom-up

approach of stochastic demand allocation in water quality modeling." *Proc. Computing and Control in the Water Industry (CCWI),* Sheffield, UK.

Buchberger, S.G., Carter, J.T., Lee, Y., and Schade, T.G. (2003). "*Random demands, travel times and water quality in deadends*." AWWA Research Foundation, Denver, CO.

Chang, Y.C. and Myerson, A. S. (1985). "The diffusivity of potassium chloride and sodium chloride in concentrated, saturated, and supersaturated aqueous solutions." *AIChe Journal*, 31(6), 890-894.

Cochran, W.L., McFeters, G.A., and Stewart, P.S. (2000). "Reduced susceptibility of thin Pseudomonas aeruginosa biofilms to hydrogen peroxide and monochloramine." *J. Appl. Microbiol.*, (88), 22-30.

Ekambara, K., and Joshi J.B. (2004). "Axial mixing in laminar pipe flows." *Chem. Eng. Sci.*, (59), 3929-3944.

Fluent Inc. (2005). *Fluent user's guide*, Lebanon, N.H.

Gill, W. N. and Sankarasubramanian, R. (1970). "Exact analysis of unsteady convective diffusion." *Proc. R. Soc. London, Ser. A*, 316, 341-350.

Islam, M.K. and Chaudhry, M.H. (1998). "Modeling of constituent transport in unsteady flows in pipe networks." *J. Hydraul. Eng.*, 124(11), 1115-1124.

Kau, P.M.H., Binning P.J., Hitchcock P.W., and Smith D.W. (1999). "Experimental analysis of fluoride diffusion and sorption in clays." *J. Contam.Hydrol.*, 36(1-2), 131-151.

Lee, Y. (2004). Mass Dispersion in Intermittent Laminar Flow. *PhD Dissertation,* University of Cincinnati, Cincinnati, Ohio.

Ozdemir, O.N. and Ger, A.M. (1999). "Unsteady 2-D chlorine transport in water supply pipes." *Water Res.*, 17(33), 3637-3645.

Romero-Gomez, P., Z. Li, C. Y. Choi, and Buchberger, S.G. (2009). "Axial dispersion coefficients for laminar flows in water distribution systems." *World Environmental and Water Resources Congress*, Kansas City, MO.

Romero-Gomez, P., Z. Li, C. Y. Choi, S.G. Buchberger, K.E. Lansey, and Tzatchkov, V.T. (2008). "Axial dispersion in pressurized pipes under various flow conditions." *10th Annual Water Distribution Systems Analysis Symposium*, Kruger National Park, South Africa.

Rossman, L.A. (2000). EPANET users manual, U.S. EPA. Cincinnati, OH.

Tang, A., and Sandall, O.C. (1985). "Diffusion coefficient of chorine in water at 25-60 degree C." *J. Chem. Eng. Data,* 30(2),189-191.

Taylor, G. (1953). "Dispersion of soluble matter in solvent flowing slowly through a tube." *Proc. R. Soc. London, Ser. A*, (219), 186-203.

Tzatchkov, V.G., Aldama, A.A., and Arreguin, F.I. (2002). "Advection-dispersion-reaction modeling in water distribution networks." *J. Water Resour. Plann. Manage.*, 128(5), 334-342.

Tables

Table 1. Target and measured Reynolds numbers for verification of CFD simulations. Mean flow velocities and resulting dimensionless times are calculated for a pipe diameter of 1.56 cm (½ in-nominal diameter)

Reynolds number (Target)	Reynolds number (Measured)	Mean flow velocity (U), m s^{-1}	Dimensionless time (T), 10^3
1,300	1,281	0.083	1.552
1,400	1,387	0.089	1.434
1,500	1,516	0.098	1.312
1,600	1,585	0.102	1.255
1,700	1,705	0.110	1.166
1,800	1,796	0.116	1.107
1,900	1,903	0.123	1.045
2,000	1,997	0.129	0.996

Table 2. Measured Reynolds numbers, dimensionless pipe lengths, and injection durations for experimental verifications of the developed axial dispersion model. The initial dispersion rates to simulate each case with the modified 1D-ADR equation are also listed. The outcomes are shown in the figures referred in the last column.

Reynolds number (Measured)	x*	Injection duration, s	Initial dispersion rates, 10^3 m^2 s^{-1}			Figure
			$E_b(0)$	$E_f(0)$	E(0)	
1,341	416	10	8.0	4.0	6.0	8
1,479	801	10	0.0	0.0	0.0	7
1,493	801	60	1.5	0.0	0.8	9
1,497	416	10	7.3	3.8	5.6	7
1,596	416	10	8.0	4.0	6.0	7
1,620	801	10	0.0	0.0	0.0	7
1,727	416	10	8.0	4.0	6.0	7
1,750	801	10	1.0	0.0	0.5	7
1,893	801	60	0.0	0.0	0.0	9
1,976	801	10	0.0	0.0	0.0	8

Table 3. Pipe length (in meters) where the developed dispersion formula applies upon flows of Re = 500 (bottom bound) and Re = 2,000 (top bound)

Solute	D_{AB} x 10^9, m^2 s^{-1}	Nominal pipe diameter, cm					Sc
		1.27	2.54	5.08	10.16	15.24	
Free Chlorine (Cl_2)	1.38 [1]	11.6/46.2	23.1/92.5	46.2/185.0	92.5/370.0	138.7/554.9	728.3
Sodium Fluoride (NaF)	1.39 [2]	11.5/45.9	23.0/91.8	45.9/183.6	91.8/367.3	137.7/550.9	723.0
Monochloramine (NH_2Cl)	1.88 [3]	8.5/33.9	17.0/67.9	33.9/135.8	67.9/271.6	101.8/407.3	534.6
Sodium Chloride (NaCl)	1.53 [4]	10.4/41.7	20.9/83.4	41.7/166.8	83.4/333.7	125.1/500.5	656.9
Mean flow velocity, cm s^{-1}		3.96/15.83	1.98/7.91	0.99/3.96	0.49/1.98	0.33/1.32	
Nominal pipe diameter, in		½	1	2	4	6	

[1] Chang and Myerson (1985)
[2] Kau et al. (1999)
[3] Cochran et al. (2000)
[4] Tang and Sandall (1985)

Figures

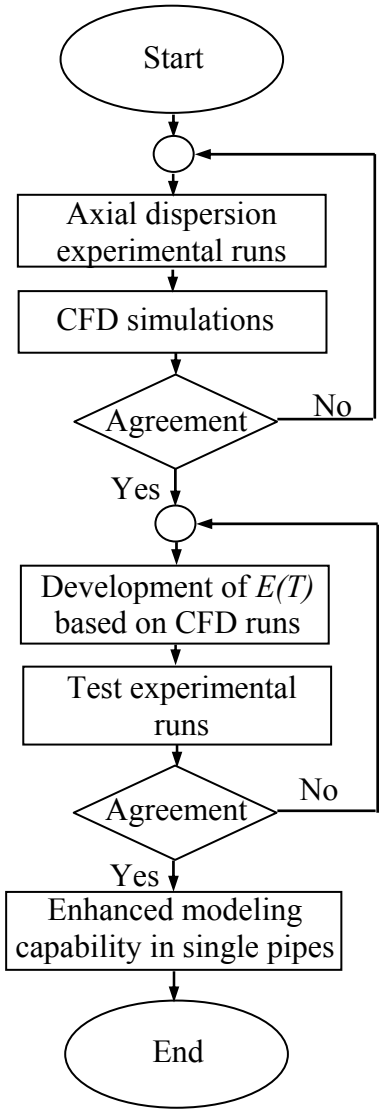

Figure 1. Flowchart of the procedure for improving axial dispersion prediction

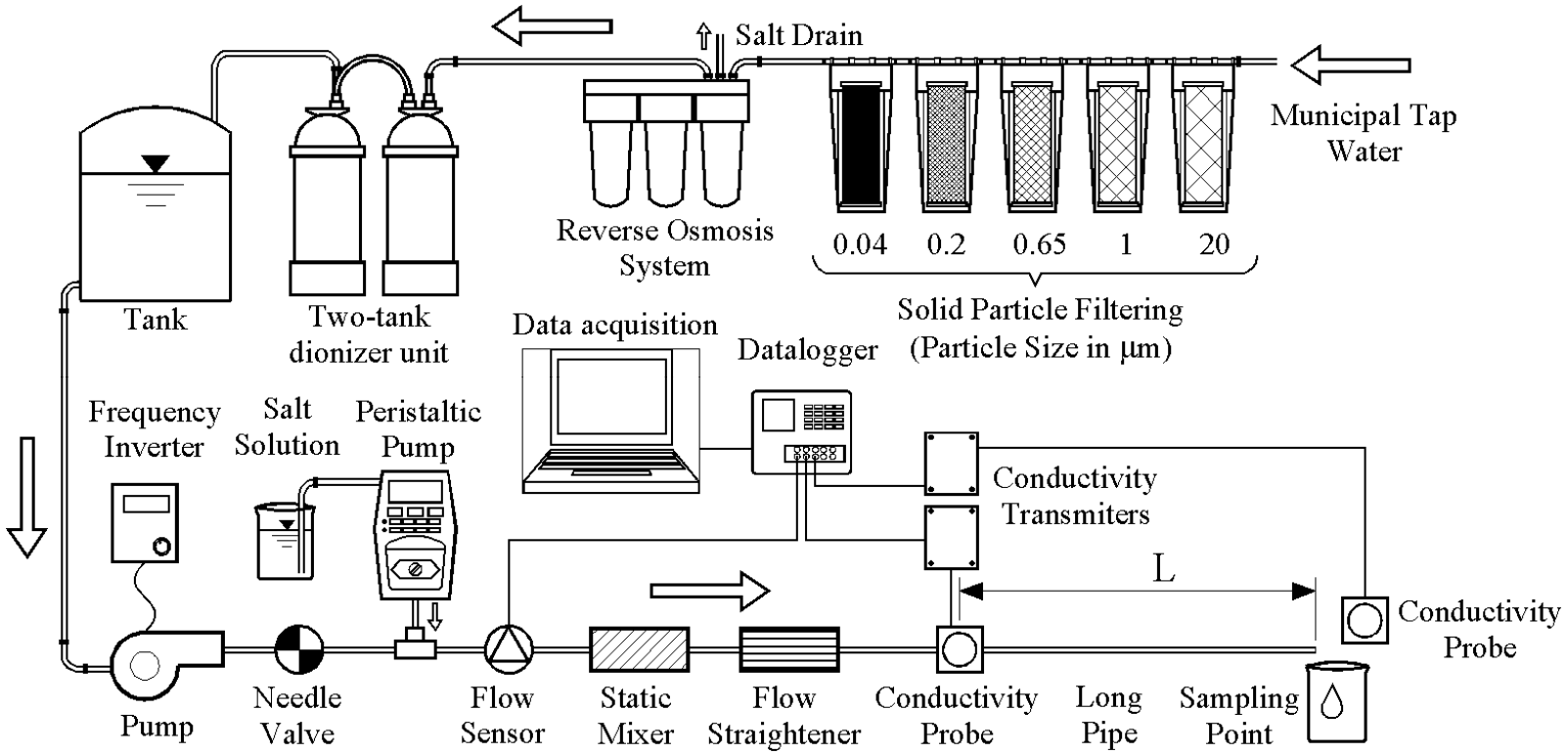

Figure 2. Experimental setup for axial dispersion experiments in laminar flow rates

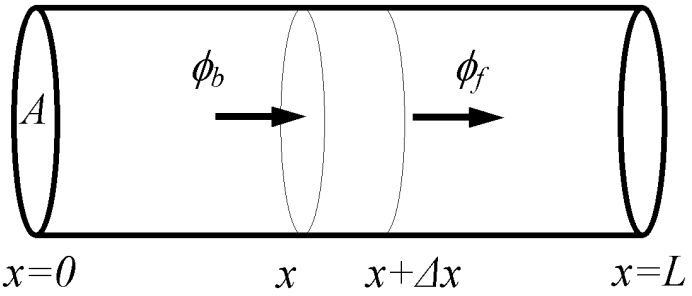

Figure 3. One-dimensional pipe with solute mass flowing into and out of a thin slice

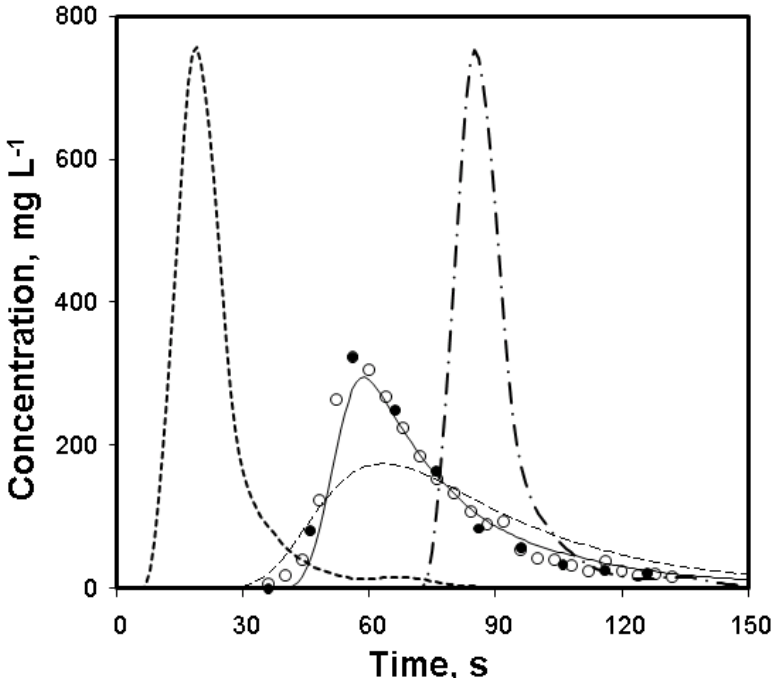

Figure 4. The inlet concentration pulse (dotted line, ·····) traveling at Re = 1,516 gives rise to downstream concentration vs. time curves at x* = 416 by several approaches: CFD simulations (continuous line, ——), 1D-AR transport model (only advection, dash-dot line, —•—), 1D-ADR runs with dispersion rates by Lee (2004) (dashed line, – – –) and experimental runs (1st run, ●; 2nd run, ○).

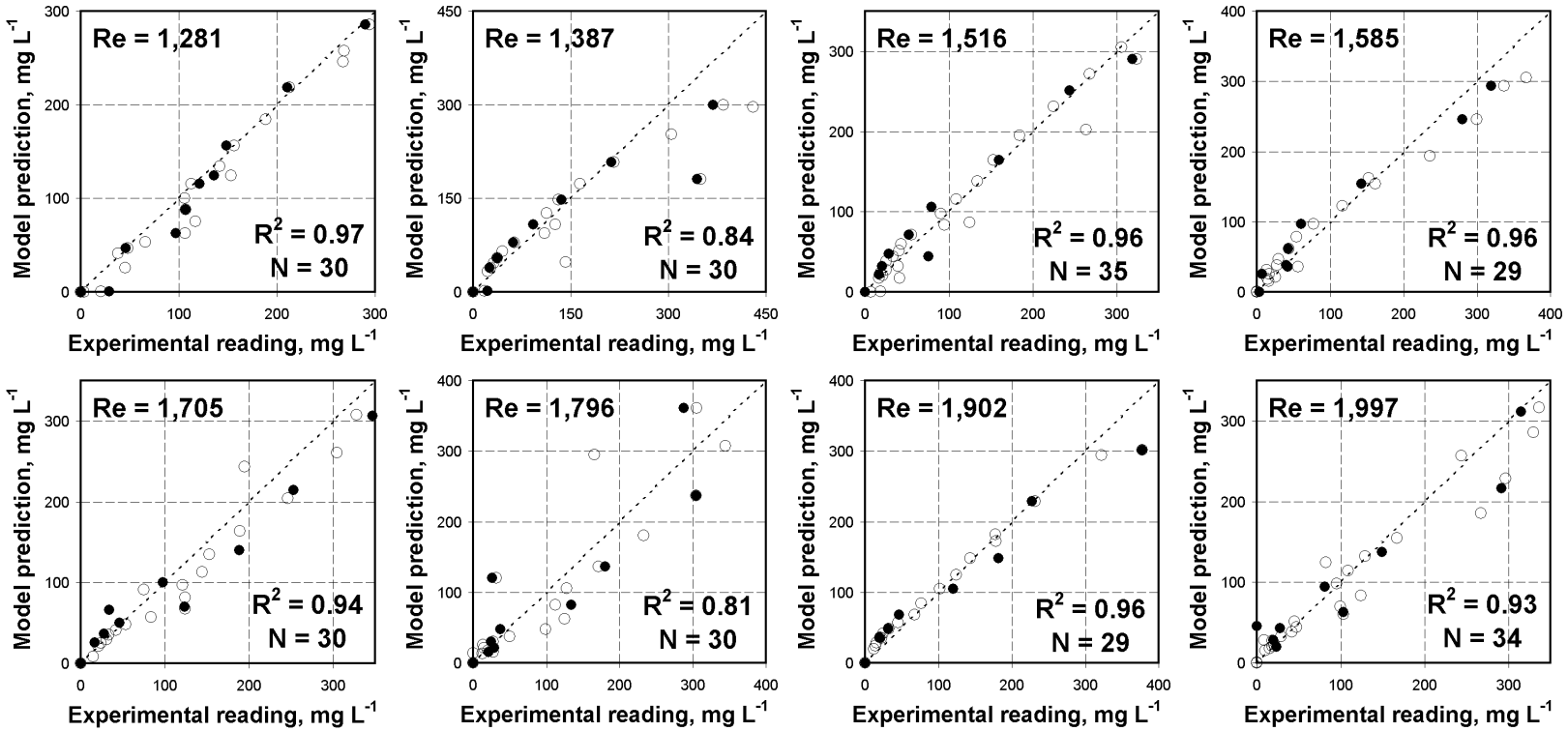

Figure 5. Comparison of experimental (1st run, ●; 2nd run, ○) vs. CFD-simulated concentrations at the downstream location (x* = 416) for all tested Reynolds numbers.

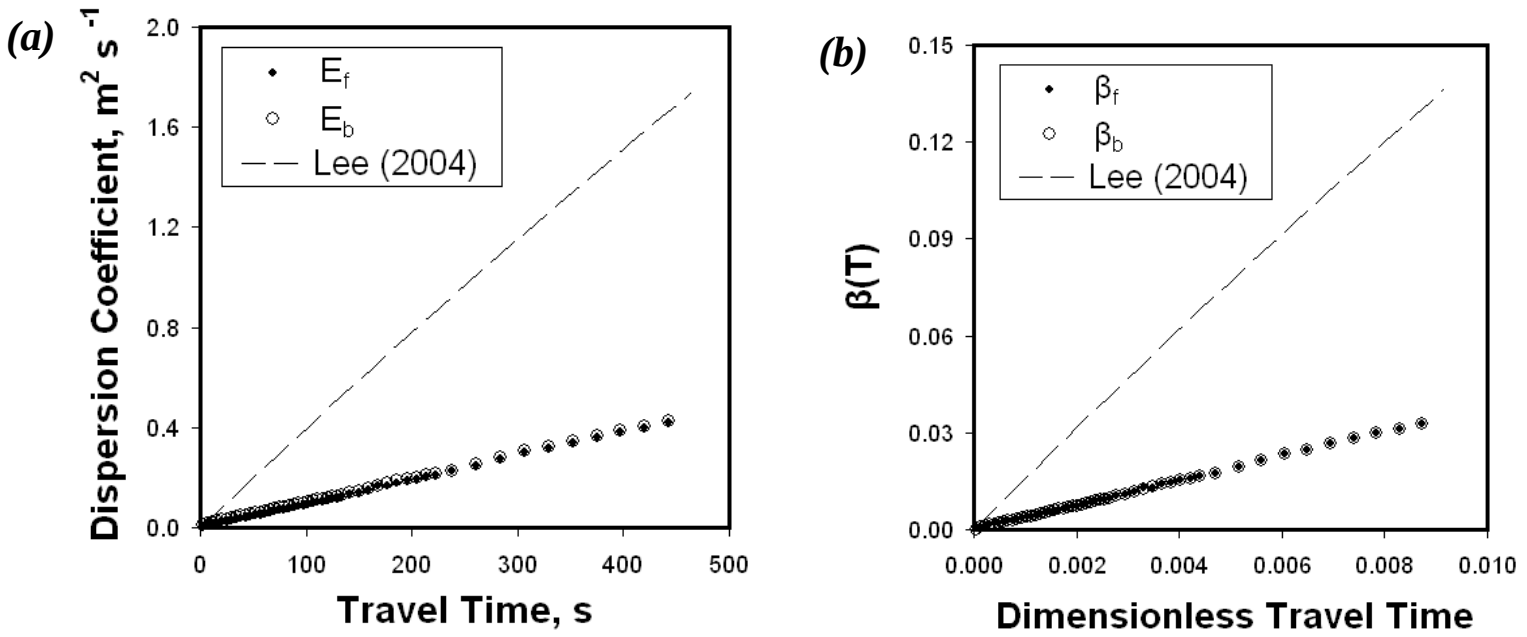

Figure 6. (a) Dimensional and (b) dimensionless axial dispersion coefficients as a function of travel time for Re = 1,705

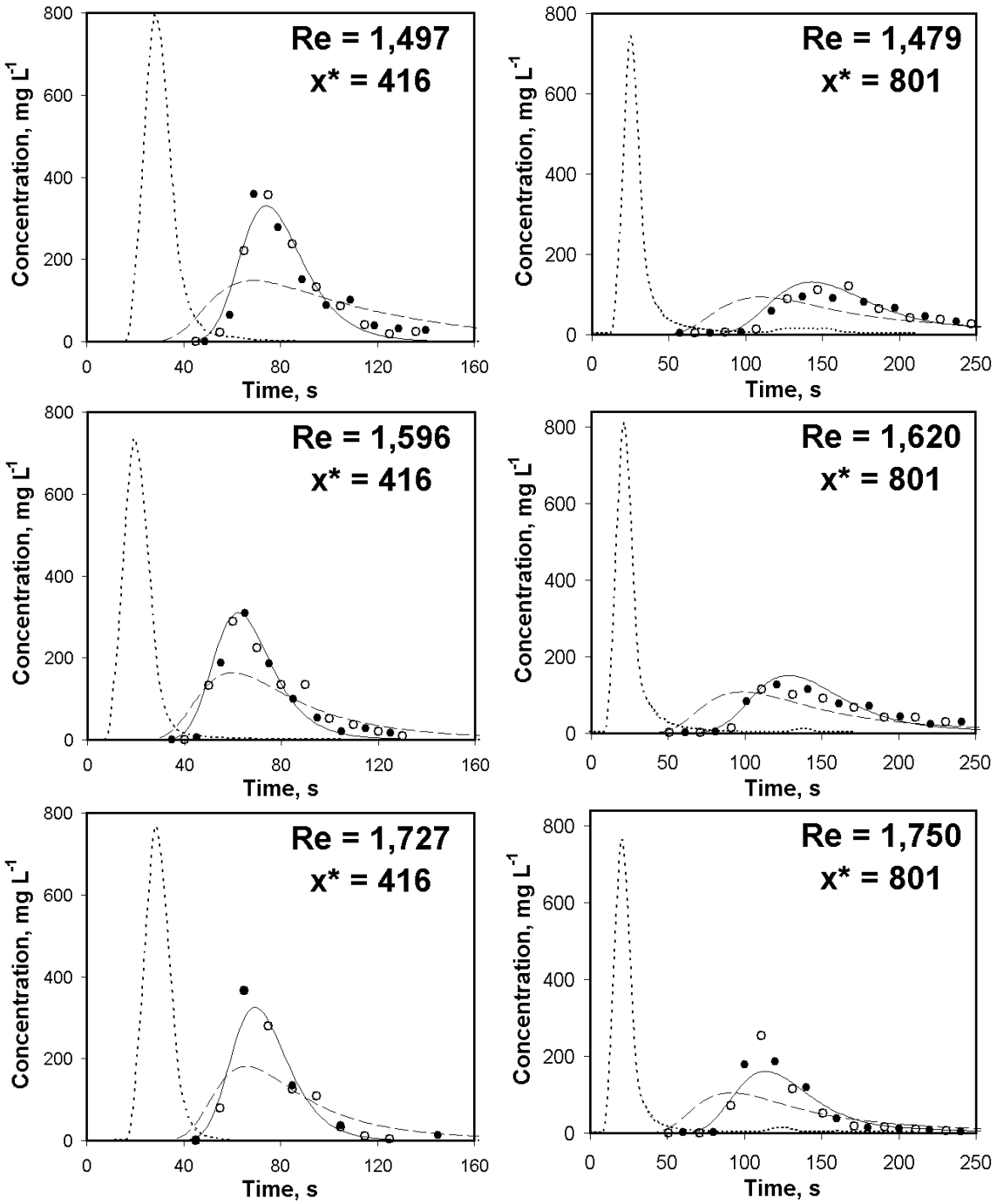

Figure 7. Experimental verification of the developed axial dispersion coefficient model at various Reynolds numbers. The inlet concentration pulse (dotted line, ·····) gives rise to downstream concentration vs. time curves at x* = 416 and x* = 801 by several approaches: 1D-ADR with dispersion rates developed in the present study (continuous line, —), 1D-ADR with dispersion rates by Lee (2004) (dashed line, – – –), and experimental measurements ((1st run, ●; 2nd run, ○).

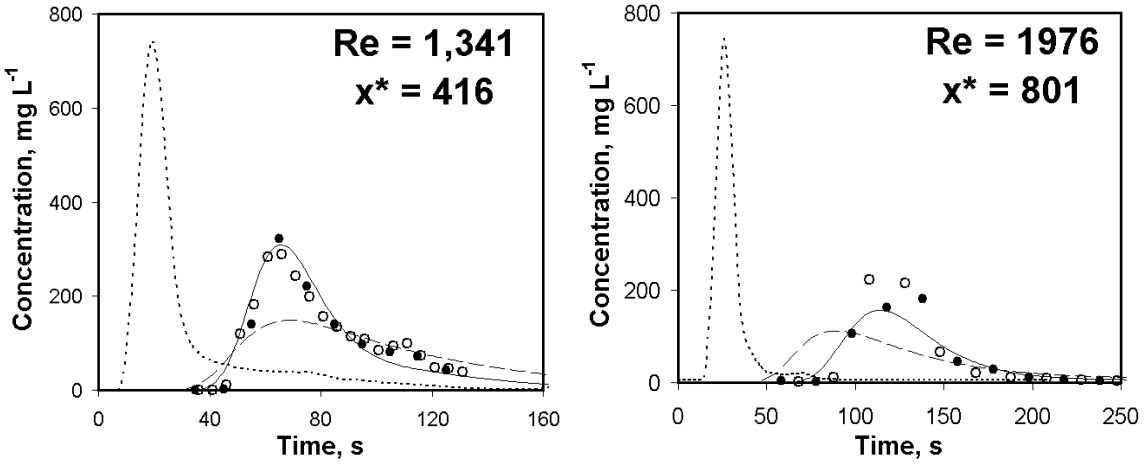

Figure 8. Experimental verification of the developed axial dispersion coefficient model at short pipe/low Re and long pipe/high Re configurations. The inlet concentration pulse (dotted line, ·····) gives rise to downstream concentration vs. time curves by several approaches: 1D-ADR with dispersion rates developed in the present study (continuous line, —), 1D-ADR with dispersion rates by Lee (2004) (dashed line, – – –), and experimental measurements ((1st run, ●; 2nd run, ○).

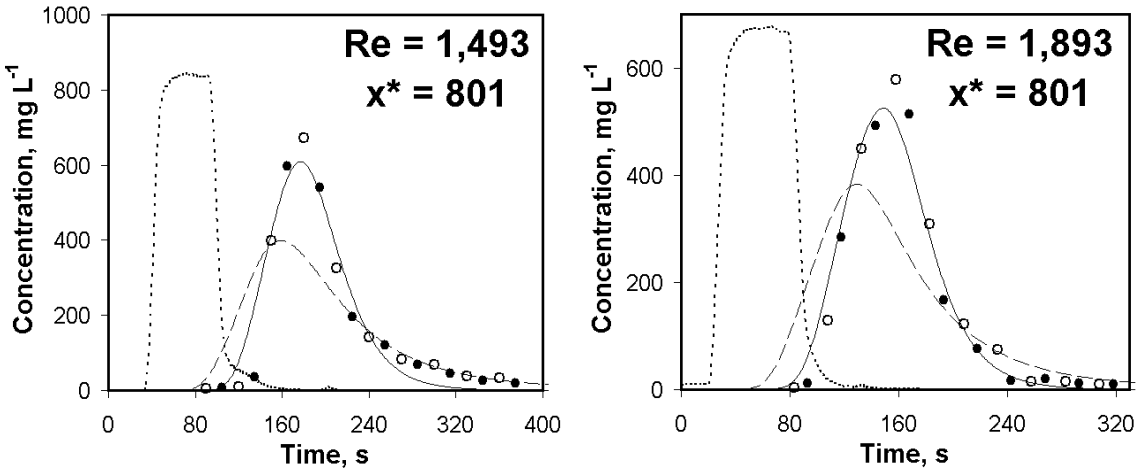

Figure 9. Experimental verification of the developed axial dispersion coefficient model at two Reynolds numbers with long injection pulses (1 min). The inlet concentration pulse (dotted line, ·····) gives rise to downstream concentration vs. time curves at x* = 801 by several approaches: 1D-ADR with dispersion rates developed in the present study (continuous line, —), 1D-ADR with dispersion rates by Lee (2004) (dashed line, – – –), and experimental measurements at L = 12.5 m (1st run, ●; 2nd run, ○).

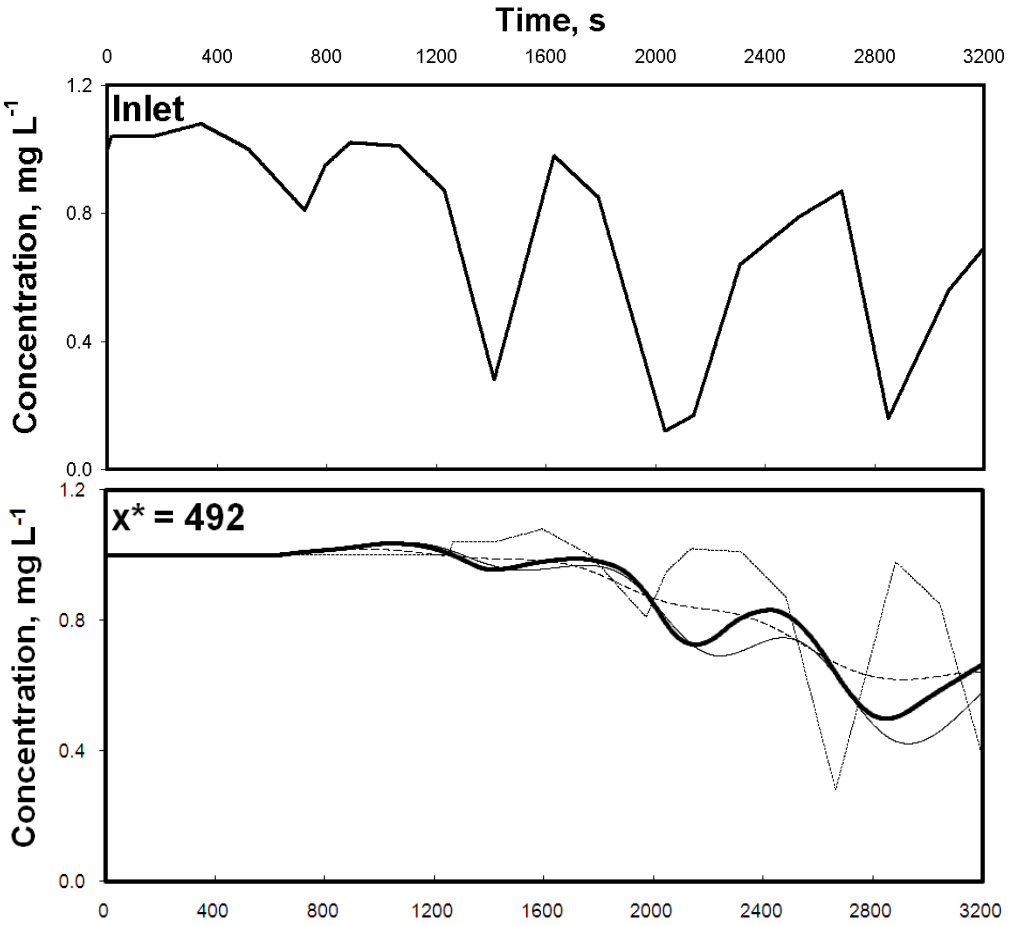

Figure 10. Verification of the developed axial dispersion coefficient model upon a continuous injection of chlorine (D_{AB} = 1.38 x 10^{-9} m^2 s^{-1}) traveling at Re = 1,011 in a 5.08 cm-diameter (2 in) pipe. The inlet solute concentration profile gives rise to downstream concentration vs. time curves at x* = 492 by several approaches: CFD (bold line, ▬), only-advection model (dotted line, ·····), 1D-ADR with dispersion rates developed in the present study (continuous line, —), and 1D-ADR with dispersion rates by Lee (2004) (dashed line, – –)

APPENDIX C

IMPACT OF AN INCOMPLETE SOLUTE MIXING MODEL ON SENSOR NETWORK DESIGN

Pedro Romero-Gomez[1], Kevin E. Lansey[2] and Christopher Y. Choi[3]

Submitted to the Journal of Hydroinformatics

[1] Graduate Research Assistant, Department of Agricultural and Biosystems Engineering, The University of Arizona, Tucson, AZ, 85721 U.S.A. E-mail: pedromer@email.arizona.edu
[2] Professor, Department of Civil Engineering and Engineering Mechanics, The University of Arizona, Tucson, AZ, 85721 U.S.A. E-mail: lansey@email.arizona.edu
[3] Professor, Department of Agricultural and Biosystems Engineering, The University of Arizona, Tucson, AZ, 85721 U.S.A. E-mail: cchoi@arizona.edu

Abstract

Incomplete mixing models have recently been shown to better represent solute transport at junctions of pressurized water systems, compared to a complete mixing assumption. The present work incorporated an incomplete solute mixing model into Ostfeld et al's (2004) methodology for sensor network design. Water quality simulations conducted using both mixing models were carried out to generate pollution matrices that provided the input data for the set covering optimization formulation. Multiple contamination and detection scenarios were simulated by considering both a minimum hazard level of the contaminant and a maximum volume of contaminated water consumed. Examination and comparison of outcomes demonstrated that the water quality solver used may impact sensor network designs in three ways by altering: (i) the minimum number of monitoring stations required for full detection coverage, (ii) the optimal layout of stations over the water network and (iii) the detection domain of some stations.

Keywords: contamination, optimization, sensor, solute mixing, water system.

Introduction

Early warning monitoring systems deployed in municipal water networks seek to protect the public health and to reduce the effects of contamination incidents. Because each water system is unique, a persistent problem relates to locating water quality monitoring stations in such a way that they will provide large spatial detection coverage, detect contaminant intrusions promptly, and minimize the system's vulnerability. Potential health effects have spurred research on the technical guidelines for designing sensor networks, i.e., finding a set of locations that can provide, with the highest possible certainty, information on the water quality status over the entire piping system.

The starting point of most Sensor Network Design (SND) methodologies is the definition of contamination scenarios characterized by timing and location of pollutant intrusions. Their resulting impacts are evaluated by hydraulic and water quality (WQ) simulations. Optimal sensor locations can then be determined to detect these intrusions based on one or more objective functions. Core assumptions in these methodologies are that the scenarios are representative of possible events and that the simulation models are representative of the system. Here, we examine the impact of an incomplete mixing model on SNDs.

Approaches to SND have evolved along with the capabilities of the computational solvers used to predict hydraulic variables (e.g., water demand, pressure, tank level, etc.) and water quality variables (e.g., water age, tracer, chlorine concentration, etc.). In an early SND study, Lee and Deininger (1992) analyzed the flow pathways using hydraulic simulations and maximized the percentage of the total water demand that was actually covered or monitored by a set of stations using integer programming. In a subsequent study, Kumar et al. (1997) eliminated the need for integer programming by performing hydraulic simulations that produced a means of ranking nodes according to the demand covered and selected the locations with highest rank as monitoring stations. They also demonstrated that the optimal sensor location lay on the node with the lowest water quality (or with the lowest chlorine concentration as predicted by simulations) thus recognizing the role of water quality behavior in SND.

Kessler et al. (1998) fully employed the results of their water quality simulations as the primary input data for optimal placement of monitoring stations capable of detecting accidental contaminations in water networks. Their optimal locations were a function of the volume of contaminated water consumed prior to detection defined as the Level of Service, LOS. A small LOS prevented the pollutant from further propagating to other zones of the network at the expense of more monitoring stations. A binary pollution matrix summarized the contamination status for each contemplated scenario and was the basis for formulating a set covering optimization problem. In the similar fashion, Ostfeld et al. (2004) implemented a Minimum Hazard Level (MHL) within the optimization procedure in order to examine the impact of dilution in the water network. Additionally, the sensing capacity of monitoring stations (Minimum Detection Level, MDL) was taken into account as SND parameters.

Research efforts subsequent to these have dealt with solving multi-objective formulations, reducing the computational time required when the method was applied to real-world water networks, and more realistically considering water utility needs. Despite advances in SND methodologies, a research gap remains with respect to the integration and evaluation of more accurate water quality solvers. Using a WQ model that assumed incomplete mixing at cross junctions, Romero-Gomez et al. (2008a) produced steady-state-based designs. They found that making such a mixing assumption had significant effects on the layout of sensor over a small network as well as over a highly-interconnected piping system with multiple cross junctions.

The present study thoroughly examines the impact of water quality solvers on sensor network designs intended for transient networks with multiple types of 4-way junctions. Ostfeld et al's SND formulation (2004) is used as the optimization model and the improved WQ model, AZRED, is used to evaluate alternative contamination events under the incomplete mixing assumption. These scenarios are used when optimizing sensor locations that are then compared against designs that are based on the conventional complete mixing assumption.

Incomplete solute mixing at junctions

Water quality solvers are mathematical models that describe the underlying transport mechanisms of constituents in piping networks. These solvers have been developed on the basis of the convenient but potentially erroneous assumption that solute mixing is complete and instantaneous at the pipe junctions. As Fowler and Jones (1991) first pointed out, completely mixed conditions can differ greatly from measurements obtained directly during laboratory and field observations. By making preliminary computational and experimental comparisons of impinging flows with different qualities, van Bloemen Waanders et al. (2005) found that the assumption of complete mixing failed to represent the mass transport at cross junctions. Romero-Gomez et al. (2006), Ho et al. (2006), Romero-Gomez et al. (2008b) and Austin et al. (2008) examined tracer mixing at cross and double-T junctions involving two adjacent inflows and two adjacent outflows, all came to the general conclusion that the expected complete mixing does not take place under most flow configurations. Instead, the limited spatio-temporal interaction that occurs between the two inflows actually produces a rather incomplete tracer mixing, with most of the incoming tracer deflected to the adjacent outlet and only a small amount crossed the junction to the opposite outlet.

In an effort to improve on solvers that rely on the perfect mixing assumption, researchers at the University of Arizona recently developed a WQ engine that incorporates incomplete mixing at junctions. Named AZRED ("AZ" refers to the University of Arizona and "RED" means "network" in Spanish), this solver integrated experimental data sets of tracer mixing at single cross, double-T, and wye junctions (as shown in Figure 1) under multiple flow configurations (Austin et al. 2008).

The experimental databases summarized the level of mixing as a function of (i) the ratio of incoming flow rates, (ii) the ratio of outgoing flow rates, and (iii) the type of junction. These databases, along with functions designed to retrieve and to process the data, were incorporated into the EPANET C/C++ code. EPANET performs extended period simulations of the hydraulics and water quality of pressurized water systems (Rossman, 2000). Thus, AZRED takes advantage of most of EPANET's built-in

functions in order to implement incomplete mixing at the junctions types depicted in Figure 1. The performance of AZRED on a laboratory-scale water network has been experimentally examined and validated (Song et al., 2009) and applied to a large scale network (Choi et al., 2008). The present study uses AZRED as the WQ modeling tool for providing the input data needed to carry out sensor network designs over two exemplary water networks.

Procedure

Pollution matrix

As the first step of the Ostfeld et al methodology (2004), a pollution matrix is constructed. This pollution matrix has binary elements in which the *i*-th row lists all nodes contaminated when an intrusion at node *i* occurs, and, consequently, its *j*-th column lists all pollution nodes that contaminate the *j*-th node. Two parameters are defined to establish the criteria for determining whether a node becomes contaminated or not. First, a node is considered contaminated when its concentration becomes greater than a Minimum Hazard Level (MHL). Second, it is assumed that a contaminant continues to propagate throughout the water network until a volume of contaminated water (the Level of Exposure, LOE) is consumed.

Once these two parameters have been established, then the pollution matrix can be constructed in the following manner. Here, we assume that the set of intrusion scenarios are that each network node will be impacted individually at the simulation's starting time. The Ostfeld's procedure is general and allows for any contamination location and timing.

1. Set all the elements ($\lambda_{i,j}$) of the pollution matrix equal to zero
2. Introduce a contaminant intrusion at the *i-th* node of the water network at time zero
3. Carry out an extended-period WQ simulation (EPS) with EPANET. At each quality time step, calculate the total volume of contaminated water consumed

(withdrawn from the network) up to that time at nodes in which concentration is greater than the MHL. Enter $\lambda_{i,j} = 1$ if the concentration at the j-th node is greater than the MHL

4. If the total contaminated water volume consumed is equal or greater than LOE, stop the simulation; otherwise, continue until the end of the simulation
5. Reinitialize the network and return to Step 2 to set the intrusion at the *(i+1)-th* node
6. Repeat Step 2 through 5 for the *N* nodes considered to be potential intrusion locations
7. Repeat Step 1 through 6, using AZRED instead of EPANET to carry out the WQ EPS in Step 3.

Mathematical formulation

After the pollution matrix is constructed, the next step is to find the location of the minimum number of sensors that detect a defined proportion of all of the intrusions within the water network (here, 100% coverage). This problem type, known as a Set Covering Problem (SCP), has wide application and has been the subject of numerous studies (e.g., Beasley, 1987; Beasley and Jørnsten, 1992). The SND formulation seeks to find the minimal set of columns (sensor locations) that include at least one value of 1 in all the rows of the pollution matrix (i.e., nodes impacted by each intrusion). The decision variable representing the sensor location at node *j* is a binary variable, X_j. If the *j*-th column (a sensor is installed at node *j*) is part of the solution, X_j is equal to 1; otherwise X_j is equal to 0. Mathematically, the problem can be defined as follows:

$$\text{Minimize} \quad \sum_{j=1}^{N} C_j X_j$$

$$\text{Subject to} \quad \sum_{j=1}^{N} \lambda_{i,j} X_j \geq 1 \qquad i = 1 \ldots N$$

$$X_j \in (0,1), \qquad j = 1 \ldots N$$

According to Ostfeld et al (2004), in order to maximize the overlapping of sensor coverage (so that a contaminant intrusion will be detected by more than one sensor, if possible), a cost C_j can be assigned to each column by using the following formula:

$$C_j = G - \sum_{i=1}^{N} \lambda_{i,j} \qquad \text{where } G >> N$$

This minimization problem is solved by using the software Premium Solver for Excel (Frontline Systems, Inc., Incline Village, NV, U.S.A.).

Modeling modifications to account for incomplete mixing

Conventionally, junctions in hydraulic models are represented as single nodes at which links of different diameter may connect. However, to account for incomplete mixing a junction's configuration must be modified. First, the base demand at the junction node is set to zero. Next, four nodes, all at the same elevation and also having no water demand are added around the junction. These dummy nodes connect to the junction node through short links (relative to the overall network size) with diameters that fall between the smallest and largest diameters of the links that are physically connected to the junction. These features ensure that the network's hydraulic behavior will not be affected by WQ modification. These changes are consistent with the physical conditions in the field in which demands are not located at nodes but rather along a pipe and the experimental conditions applied in the incomplete mixing studies.

In AZRED's GUI, the added pipes are drawn to resemble the junction type that they represent, i.e., an N-type arrangement (as shown in Figure 1b) should follow a straight line from which two nearly-perpendicular links branch out in opposite directions. The combination of angles formed by the links directs AZRED to search for the level of mixing in the correct database according to the junction type.

Illustrative examples

A simple network configuration

Net1 of the EPANET Examples consists of 12 pipes, 9 nodes (only 8 with base demands), a water source, a pump, and an elevated tank. The base demands are subject to a transient pattern throughout a simulation period of 24 hours. The remaining characteristics are readily accessible for downloading from the EPANET software package and are fully described as the "Application Example 1" by Ostfeld et al. (2004). A few of the original network's features were modified. The initial quality at all nodes was set equal to zero so that only the injected pollutant had an effect on nodal concentrations. Node 22 was modified to conform to the AZRED requirements for 4-way junctions. Since the remaining junctions connected two or three pipes, they were not changed. Eight nodes are defined as possible contaminant sources. The resulting network configuration is shown in Figure 2.

Pollution matrices were generated for MHL values of (in mg L^{-1}): 0.5, 1, 1.5, 2, 3, and 4 and LOE values (in m^3) equal to 100, 200, 500, 1000, and 2000. Thus, pollutions matrices were prepared and optimal SND were determined for thirty MHL-LOE combinations (six MHL values by five LOE values). Each intrusion was represented by a constant injection mass rate of 10,000 mg min^{-1} over the entire simulation period, starting from time zero for all intrusion scenarios.

Comparing EPANET and AZRED results showed that the designs differed following one of three cases: (i) the minimum number of sensors is different, (ii) the minimum number of sensors is the same but some locations are different, and (iii) the minimum number of sensors and the optimal locations are the same but some sensors have different detection domains.

Of the thirty designs that were obtained for Net1, five (indicated as MHL-LOE combinations A, B, C, D and F in Figure 3) required a different number of sensors owing to the WQ solver used, whereas one design (Combination E) required the same number of sensors but they were placed at different locations. In the former 5 results, EPANET-based designs required more sensors than AZRED-based designs, with the greatest

difference (2 stations) resulting from combination A (MHL = 1.5 mg L^{-1}, LOE = 1000 m^3). Such a difference was deemed significantly large with respect to the maximum number of sensors possible for this network (8 possible stations). Under incomplete mixing, the presence of the cross junction at node 22 produced a tendency for the contaminant to be concentrated at one of the two downstream nodes (nodes 23 and 32). Greater levels of mixing (as produced by EPANET) will cause the contaminant to spread more widely at lower concentrations, making detection more difficult and require more monitoring stations.

This network is simple enough to allow for a detailed observation of the contaminant pathways. For example, when contamination is introduced at node 21 (Figure 2), the complete mixing outcome was that clear (or non-contaminated) water from node 12 reduced the contaminant concentration in the pipes leaving node 22, dispersing the contaminant but at low concentrations. In contrast, in the incomplete mixing analysis in AZRED most of the contaminant entering node 22 was deflected towards node 32 with little mixing. The transient concentration patterns at node 32, as obtained using both WQ solvers, are shown in Figure 4. The node 32's AZRED concentration exceeds the MHL value of 2 mg L^{-1} established for combination C while the complete mixing model does not. Consequently, this difference was reflected in the pollution matrices generated by both WQ solvers, as indicated in Table 1. A value of 0 is set in the source row for node 21 and column (detection location) for node 32 in Table 1a. On the other hand, the same matrix element in Table 1b, generated by AZRED, is set to 1. The other elements remained the same regardless of the WQ solver.

Despite the minor difference between the two pollution matrices, the optimal SNDs were different (Figure 5a and 5b). Based on the EPANET WQ predictions, a minimum of four stations is required in order to detect intrusions from any of the eight source nodes (Figure 5a). On the other hand, the AZRED-based design for this combination of parameters (combination C, Figure 3) requires only three monitoring stations in order to achieve full detection coverage (Figure 5b). In a broader context, such a difference directly increases the cost of the network. Detection domains in Figure 5

show which nodes are covered by each station; for instance, injections at nodes 11 and 12 will be detected by the station placed at node 11 for both EPANET and AZRED-based designs.

Figures 5c and 5d depict conditions (combination E: MHL = 2 mg L^{-1}, LOE = 2,000 m^3) under which the number of required stations remained the same but their locations were different due to the mixing assumption. To provide full coverage under this combination, the monitoring station that was placed at node 11 using the EPANET results was shifted to node 21 based on AZRED outcomes. In addition to providing full coverage, a monitoring station at node 21 increases sensor overlap as compared to the optimal design that included a sensor at node 11. A monitoring system's ability to detect contaminant intrusions at more than one station is particularly desirable when the probability of sensor failure is taken into consideration as part of the SND methodology.

Figures 5e and 5f present the EPANET- and AZRED-based designs, respectively, for MHL = 1 mg L^{-1} and LOE = 500 m^3, in which the number and location of stations are the same but the detection domains are different. Although the EPANET based design maximized sensor overlap (Figure 5e), injections at node 21 undergo incomplete mixing at the cross that prevents the contaminant concentrations at node 23 from reaching the MHL. Consequently, the detection domain of a station at node 23 is reduced (Figure 5f).

In assessing the effect of refining the water quality predictions, the quality time step for EPS simulations was found to have only a slight affect on the SND. Concentration spikes, due to sudden changes in the hydraulic conditions, occur at the nodes closest to the tank (the tank fills up during the initial hours and drains during later times). During short simulation time steps, these spikes instantaneously exceed MHL values that are not attained during long time steps. Consequently, these SNDs require fewer stations to achieve full coverage of the water network. However, this effect is relatively minor with the number of sensors differing by at most one between long and short water quality time steps.

Net3 from EPANET Examples

Net3 is available with the EPANET download and consists of 117 links, 92 nodes, 3 elevated tanks, and 2 pumps that connect to 2 reservoirs (a lake and a river). Eight nodes from the network are 4-way junctions (Table 2) and were modified to each of the four alternative AZRED junction types (Figure 1). The location and characteristics of the modified junctions are listed in Table 2. Contamination scenarios were developed with each of the eighty four nodes being equally likely as the contamination source. The quality time step and parameter setting were set at 2 min and "Chemical", respectively. The injection mass rate was set equal to 20,000 mg min^{-1} for all the scenarios. The settings for the MHL value (in mg L^{-1}) were 1, 2, 5, 10, 20, 50 and 100, and the LOE settings (in m^3) were 50, 100, 200, 500, 1000, 2000 and 5000. Pollution matrices were thus developed for all 49 MHL-LOE combinations.

The tradeoff between the level of exposure and the number of monitoring stations for MHL = 1 mg L^{-1} is presented in Figure 6a. The LOE level indirectly implies the time till a contamination event is detected. Higher LOE values allow for more consumption (or usage) of contaminated water and, consequently, longer times to detection and further pollutant propagation. Thus, fewer stations are needed and, as seen in Figure 6a, the number of stations decreases monotonically with increasing LOE. This decreasing trend is consistent with Ostfeld et al. (2004) and occurred for all sensor arrangements regardless of the mixing model applied. However, AZRED simulations generally required one more station for most LOE values. Therefore, if complete mixing at junctions is applied, some nodes will not be covered by any of the sensors.

Figure 6b illustrates the tradeoff between the Minimum Hazard Level (MHL) and the number of monitoring stations for LOE = 100 m^3. Lower MHLs will result with more sensitive sensors that can detect at lower concentrations Thus, more dilute contaminations could be identified and fewer stations are likely necessary for the same protection. On the other end of the spectrum (MHL > 20 mg L^{-1} in this exemplary case), few nodes become contaminated and monitoring stations are only needed at those locations.

Comparing SNDs for the alternative WQ modeling assumptions for the 49 MHL-LOE combinations, differences in designs occurred primarily for conservative parameter sets i.e. when detection capacity was enhanced (MHL $\leq$ 10 mg L^{-1}) or when the propagation of polluted water was restricted (LOE $\leq$ 200 m^3) (Table 3). No specific trend was identified in relation to the minimum number of sensors needed for either WQ solver.

To understand the spatial differences in SND, the frequencies that a node was selected by both water quality model based SNDs were computed and compared for the 49 MHL-LOE combinations. It was found that nodes with the highest frequency corresponded to the locations that were more sensitive to the solute mixing model used to generate the pollution matrices. Figure 7 shows that sensitive nodes generally lie near 4-way junctions, a finding that suggests the effect will be stronger at locations in close proximity to a junction and weaker further downstream from 4-way junctions. Circle sizes in Figure 7 represent the magnitude of the difference in frequencies; the small circles indicate the node was selected one more time by one of the models, and the larger circles are differences greater than one. This analysis also reveals that certain patterns will occur according to the water quality model used. For instance nodes 211 and 213 were consistently interchangeable (as were nodes 247 and 251) due to the influence of a YU-type junction (node 255) and the elevated tank (tank 2) that produced highly dynamic hydraulics in this region.

Conclusions

This study incorporated a newly-developed, incomplete solute mixing model in an optimal sensor network design. We analyzed various contamination and detection scenarios over two exemplary networks. The first example system allowed for detailed descriptions of the contaminant pathway and its ultimate impact on each design while the second exemplary network provided the global trends of the impact on the sensor configurations due to the WQ solvers. Application results demonstrated that while the quantitative impact of incomplete mixing varies, EPANET-based designs did not provide

the desired level of protection under incomplete mixing conditions. For example, several AZRED-based designs allocated more monitoring stations than EPANET based design; this strongly implies that an EPANET-based sensor arrangement will fail to detect some contaminant intrusions.

Overall, these results demonstrate that water quality modeling tools and their accuracy play a central role in SND. Developing and implementing SND approaches should necessarily entail a continuous re-examination in view of the new advances in water quality modeling in pressurized piping systems. More accurate solute transport predictions will make SNDs account for a better representation of the water quality behavior of a network. This in turn should increase the effectiveness and reliability of early warning monitoring systems as well as the likelihood that intentional or accidental contamination events can be detected early enough to initiate countermeasures that can protect water customers.

References

Austin, R. G., van Bloemen Waanders, B., McKenna, S., and Choi, C. Y. 2008. Mixing at cross junctions in water distribution systems. II: Experimental study. *J. Water Resour. Plann. Manage.*, 134(3), 295-302.

Beasley, J.E. 1987. An algorithm for set covering problem. *Eur. J. Operational Res.*, 31, 85-93.

Beasley, J.E. and Jørnsten, K. 1992. Enhancing an algorithm for set covering problems. *Eur. J. Operational Res.*, 58, 293-300.

Choi, C.Y., Shen, J. Y., Austin, R. G. 2008. Development of a comprehensive solute mixing model (AZRED) for double-tee, cross, and wye junctions. *Proc. 10th Annual Water Distribution System Analysis Symp.*, Kruger Park, South Africa. Also, note the website http://cals.arizona.edu/~cchoi/AZRED.

Fowler, A. G., and Jones, P. 1991. Simulation of water quality in water distribution systems. *Proc. Water Quality Modeling in Distribution Systems*, AwwaRF/EPA, Cincinnati.

Ho, C. K., Orear, L., Wright, J. L., and McKenna, S. A. 2006. Contaminant mixing at pipe joints: comparison between laboratory flow experiments and computational fluid dynamics models. *Proc,. 8th Annual Water Distribution System Analysis Symp.*, Cincinnati, OH.

Kessler, A., Ostfeld, A., and Sinai, G. 1998. Detecting accidental contaminations in municipal water networks. *J. Water Resour. Plann. Manage.*, 124(4), 192-198.

Kumar, A., Kansal, M.L., and Arora, G. 1997. Identification of monitoring stations in water distribution system. *J. Environ. Eng.*, 123(8), 746-752.

Lee, B.H. and Deininger R.A. 1992. Optimal locations of monitoring stations in water distribution system. *J. Environ. Eng.*, 118(1), 4-16.

Ostfeld, A., Kessler, A., and Goldberg, I. 2004. A contaminant detection system for early warning in water distribution networks. *Eng. Optim.*, 36(5), 525-538.

Romero-Gomez, P., C. Y. Choi, Lansey, K. E., Preis, A., Ostfeld, A. 2008a. Sensor network design with improved water quality models at cross junctions. *10th Annual Water Distribution Systems Analysis Symposium*, Kruger National Park, South Africa.

Romero-Gomez, P., Ho, C.K., and Choi, C.Y. 2008b. Mixing at cross junctions in water distribution systems. I: Numerical study. *J. Water Resour. Plann. Manage.*, 134(3), 285-294.

Romero-Gomez, P. Choi, C. Y., van Bloemen Waanders, B., and McKenna, S. A. 2006. Transport phenomena at intersections of pressurized pipe systems. *Proc. 8th Annual Water Distribution System Analysis Symp.*, Cincinnati, OH.

Rossman, L. 2000. *EPANET user's manual*, USEPA, Cincinnati, OH.

Song, I., Romero-Gomez, P., and Choi, C.Y. 2009. Experimental verification of incomplete solute mixing in a pressurized pipe network with multiple cross junctions. *J. Hydraul. Eng.*, 135(11), 1005-1011.

van Bloemen Waanders, B., Hammond, G., Shadid, J., Collis, S., and Murray, R. 2005. A comparison of Navier-Stokes and network models to predict chemical transport in municipal water distribution systems. *Proc., World Water and Environmental Resources Congress*, Anchorage, Alaska.

Tables

Table 1. Pollution matrix resulting from MHL-LOE combination C, based on (a) EPANET, and (b) AZRED

a)

		Contaminated node							
		10	**11**	**12**	**13**	**21**	**23**	**31**	**32**
Injection node	**10**	0	0	0	0	0	0	0	0
	11	0	1	0	0	1	0	1	0
	12	0	1	1	1	0	0	0	0
	13	0	0	0	1	0	1	0	0
	21	0	0	0	0	1	0	1	0
	23	0	0	0	0	0	1	0	0
	31	0	0	0	0	0	0	1	1
	32	0	0	0	0	0	0	0	1

b)

		Contaminated node							
		10	**11**	**12**	**13**	**21**	**23**	**31**	**32**
Injection node	**10**	0	0	0	0	0	0	0	0
	11	0	1	0	0	1	0	1	0
	12	0	1	1	1	0	0	0	0
	13	0	0	0	1	0	1	0	0
	21	0	0	0	0	1	0	1	1
	23	0	0	0	0	0	1	0	0
	31	0	0	0	0	0	0	1	1
	32	0	0	0	0	0	0	0	1

Table 2. Modifications on Net3 example from EPANET package

Node ID	Type	Junction diameter (D)	Dimensionless distance (L/D)
121	YN	24	2.0
120	N	10	1.0
119	X	20	N/A
115	YN	10	3.0
193	N	12	2.5
189	X	12	N/A
255	YU	10	1.0
111	YN	12	2.0

Table 3. Summary of number of sensor based on AZRED vs. EPANET simulations

		Minimum Hazard Level, mg/L						
		1	2	5	10	20	50	100
Level of Exposure, m^3	50							
	100							
	200							
	500							
	1000							
	2000							
	5000							

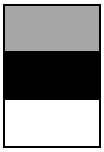

One more sensor under AZRED

One more sensor under EPANET

Same number of sensors

Figures

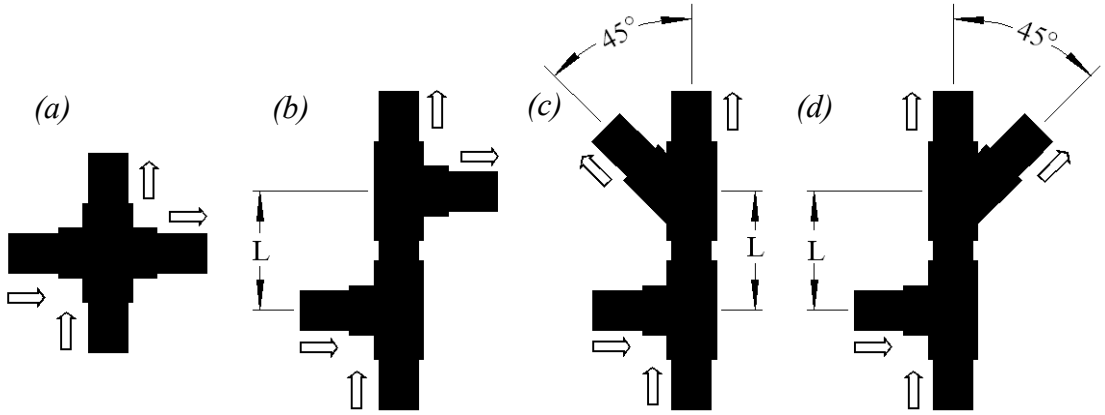

Figure 1. Junctions and flow configurations at which AZRED applies incomplete mixing of constituents. (a) cross (X), (b) double-T (N), (c) tee and wye junctions in U-shape (YU), and (d) tee and wye junctions in N-shape (YN). Length (L) indicates the distance between junctions

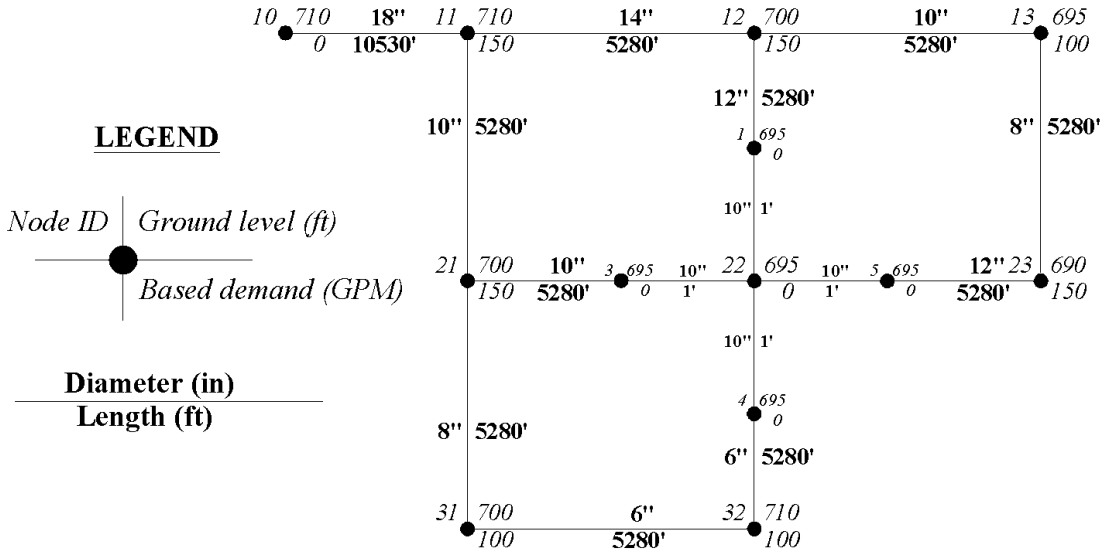

Figure 2. Example network 1 (Modified Net1.net from EPANET examples)

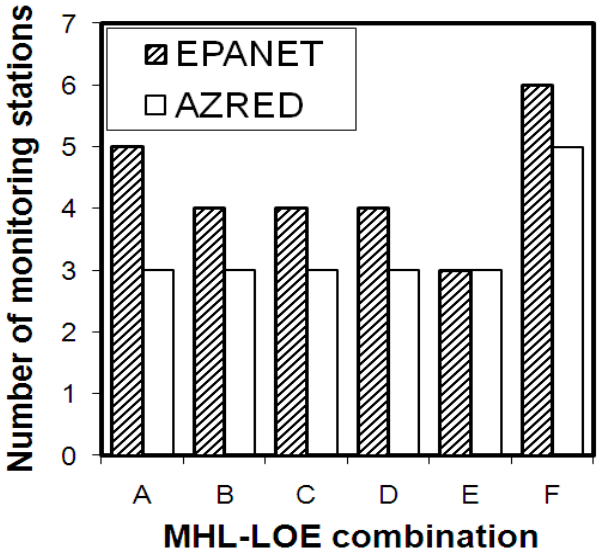

Figure 3. Number of stations based on EPANET and AZRED at different MHL-LOE combinations , (A) MHL = 1.5 mg L^{-1}, LOE = 1,000 m^3, (B) MHL = 1.5 mg L^{-1}, LOE = 2,000 m^3, (C) MHL = 2 mg L^{-1}, LOE = 500 m^3, (D) MHL = 2 mg L^{-1}, LOE = 1,000 m^3, (E) MHL = 2 mg L^{-1}, LOE = 2,000 m^3, (F) MHL = 3 mg L^{-1}, LOE = 100 m^3

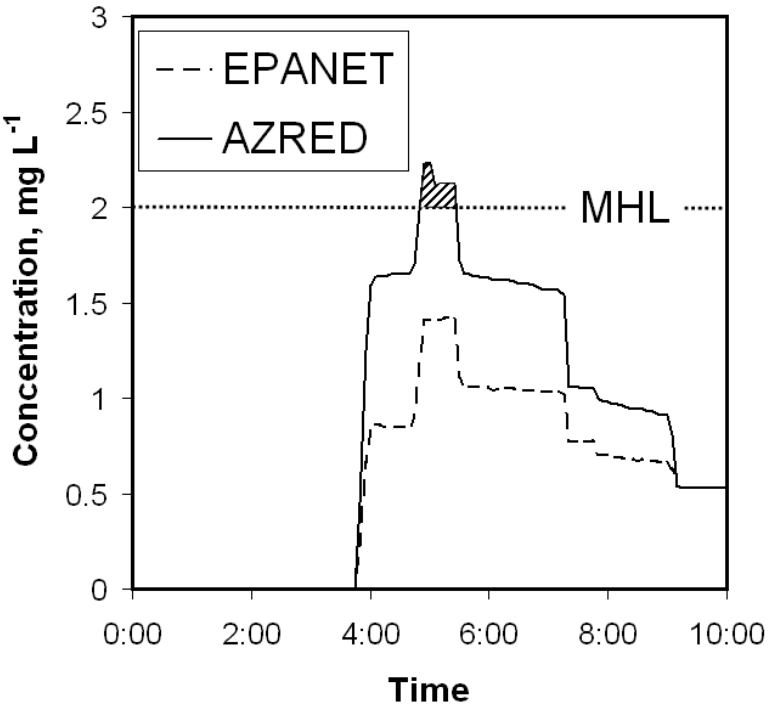

Figure 4. EPS contaminant concentration at node 32, based on EPANET and AZRED solvers. Shaded area indicates concentrations higher than 2 mg L^{-1} (dotted horizontal line, MHL setting for combination C)

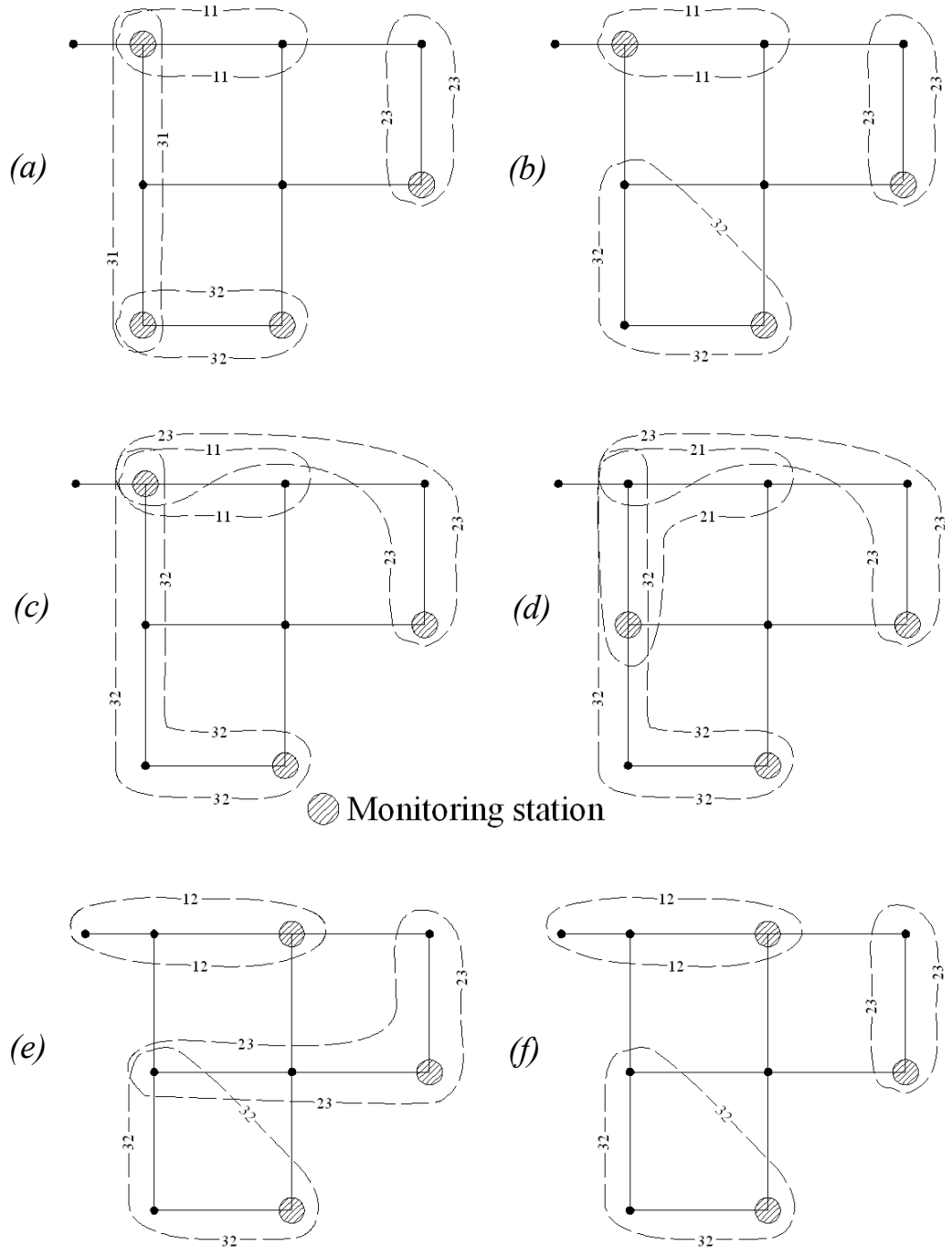

Figure 5. Sensor Network Designs based on *(a)* EPANET, and *(b)* AZRED for combination C (MHL = 2 mg L^{-1}, LOE = 500 m^3); *(c)* EPANET, and *(d)* AZRED for combination E (MHL = 2 mg L^{-1}, LOE = 2,000 m^3); and *(e)* EPANET, and *(f)* AZRED for combination MHL = 1 mg L^{-1} and LOE = 500 m^3. Dashed lines indicate the coverage domain of each monitoring station.

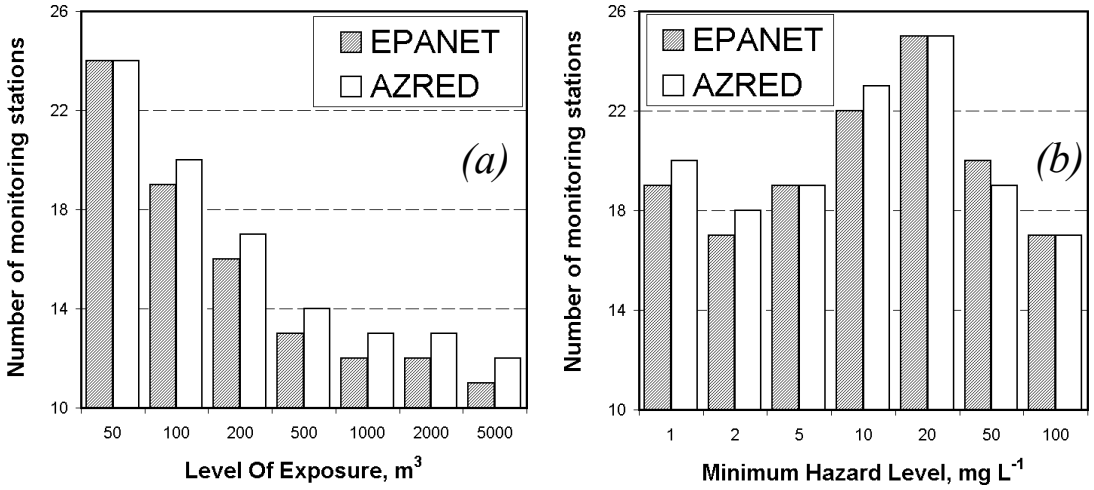

Figure 6. Number of monitoring stations as a function of (a) the Level Of Exposure (LOE) for MHL = 1 mg L^{-1}, and (b) the Minimum Hazard Level (MHL) for LOE = 100 m^3

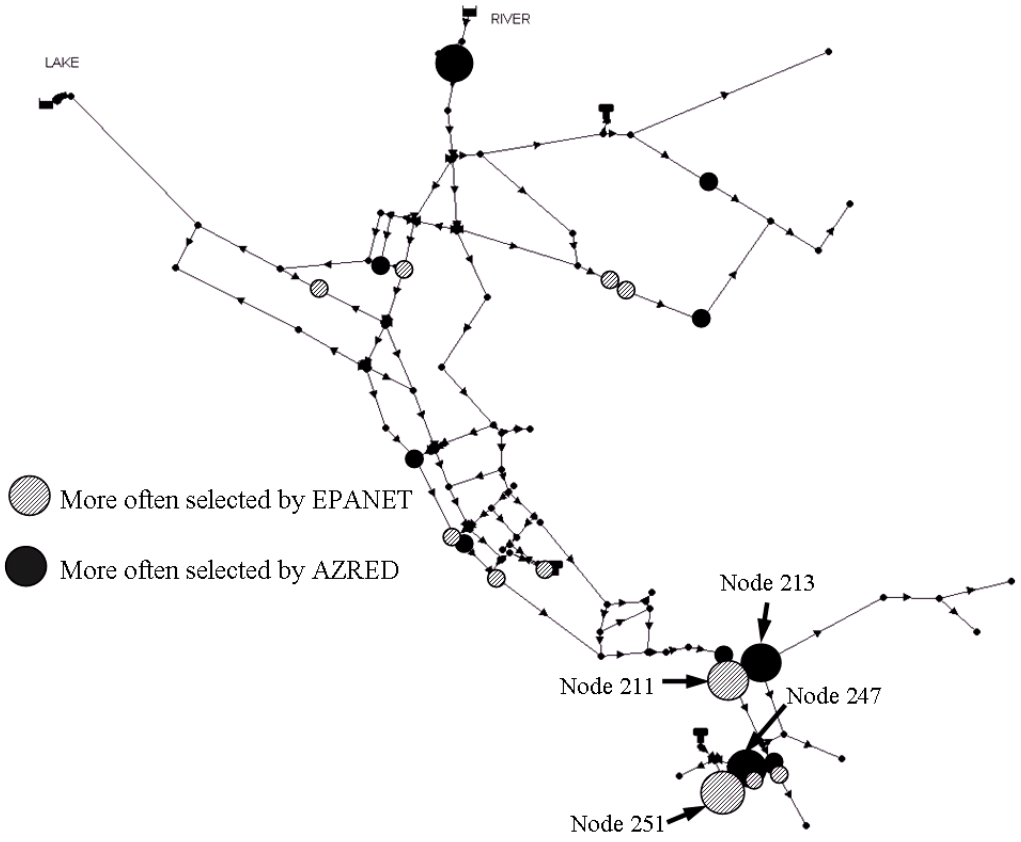

Figure 7. Nodes that were more often selected as optimal sensor locations based on EPANET or on AZRED WQ simulations. Circle sizes indicate higher sensitivity to solute mixing model